The Role of Theta- / Gamma-Coupling in Working Memory Dysfunction in Schizophrenia

A Dissertation
SUBMITTED TO THE FACULTY OF THE
UNIVERSITY OF MINNESOTA
BY

Peter A. Lynn, M.A.

IN PARTIAL FULFILLMENT OF THE REQUIREMENTS
FOR THE DEGREE OF
DOCTOR OF PHILOSOPHY

Advisor: William G. Iacono, Ph.D.
Co-Advisor: Scott R. Sponheim, Ph.D.

April 2019

Acknowledgements

Many people have helped me along the journey that this document brings to close—perhaps innumerable, but I will do my best to mention those that I can, and beg forgiveness of those I may omit.

First and foremost, I would very literally not be where I am today were it not for Dr. Scott Sponheim. Scott invited me into his lab as a volunteer, was supportive of my desire to transition to EEG analysis, endorsed me wholeheartedly in my application to the University for graduate school, and was my tireless advocate, advisor, counselor and dare I say friend through the tumultuous years in CSPR. I can likely never accurately express the gratitude I feel towards him, but I will again try, and hope he knows how verily and fully I appreciate everything he has done for me.

I also owe a debt of gratitude to Dr. Bill Iacono. Though our scientific collaborations were relatively short-lived in the program, he remained a kind and straightforward advisor, who helped me navigate difficult times by providing thoughtful guidance with never a reprimand (even when I perhaps deserved it). I wish we had worked together more, but I am grateful for the time we shared and the aid he provided me.

To the rest of the CSPR faculty, I thank you for your instruction, but also your support in helping me and allowing me to make it through. Thank you for your patience and your faith.

I am also immensely grateful to Dr. Seung Suk-Kang, who mentored me through the demanding and often confusing world of EEG collection, processing and analysis. His guidance has been instrumental in my coming to understand what I understand about EEG and the nuances of transforming it into a comprehensible and meaningful measure of the brain. I am honored to have worked with him, and learned from him a great deal.

Let me not forget the many other members of the CAB Lab I worked with over the years; I will not name them individually as I would most certainly omit some, but I am sure those who were particularly close to me know who they are, and each and every one of them made work a truly enjoyable place to be.

Next I must acknowledge my classmates: Craig Marquardt, Sam Abram, Merav Silverman, Amanda (née) Wenzel, Adrienne VanZomeren, Jenalee Doom, Rowena Ng, and Julia (née) Longenecker. Our field is quick to disperse us such that the time we spent together was relatively brief, but I look back fondly on it, and derived from you all not only in many cases very concrete assistance, but also a sense of comradery and friendship that was instrumental in getting me through those early years in particular. I wish you all the very best, and look forward to seeing your many successes.

I feel it also important to mention my many positive supports during my clinical internship at Canvas Health. My supervisors there, namely Jim Wojcik, Dan Johnson, and Kim Carter (official or not!), were beyond compare; they taught me about clinical practice, but also lent emotional and professional support without which the intense

demands of that placement would have been markedly more difficult. And God forbid I fail to mention my fellow interns, Stephanie Jasper and Jessica Miller. Truly, each of you is one of a kind, and I cannot imagine having endured internship with anyone else. I hope you consider me as good a friend as I consider the both of you, and I thank you immensely for the friendship, entertainment and support you gave me over that year. I swear we'll get together one of these days. All in all, I would never trade that clinical year for any other, and believe it—and the people within it—contributed tremendously to my education and my growth as a professional and a person.

I am further grateful to have had such wonderful clinical supervisors pre-internship, especially Drs. Tasha Nienow, Michael Fuhrman, Jim Ayers, and Aimee Murray. You taught me how to practice psychology, and prepared me exceptionally well for my clinical year and the years to come. I am honored to have been mentored by each of you.

I would also like thank my mother-in-law, Johanna Gallagher, for her endless willingness to lend aid when needed. She has countless times been the solution when there seemed to be no other, and I hope she knows how much she has been appreciated.

I am grateful to my sister and brother-in-law, Kristen and Tom Jeffers, for their renewed patience, understanding and support. I look forward to having much more time to spend with them in the years to come.

To my mother and father, Nancy and Andrew Lynn: I will never be able to repay the selfless support and assistance they gave to me over these past seven years. Time and time again, they have shown me what it means to love unconditionally, and they have been unequivocally instrumental in encouraging me and allowing me to make it through my graduate studies. Though I will forever try, I cannot thank you both enough for everything you have done and continue to do for me and my family. From the sincerest place in my heart, I thank you and love you immensely.

To my wonderful children, Michael and Charlie: from the days of your birth, you boys have been the lights of my life, and it has been a privilege and a lesson in love to watch you grow into the remarkable people you are today. Thank you for tolerating long work nights without me, nights when dad dozed off mid-bedtime-story, and times when my many demands may have made me less pleasant than I might have otherwise been. Know that I love you more than anything, that I always will, and that I will do my best to be the best father to you I can be.

Finally, to my wife, Brenna: it goes without saying that this journey has not been easy for us, but here we are. I hope you know that I absolutely could not have done this without you; I know I often fail to express my appreciation for your support and sacrifice over these past years, but truly I could have never made it through without you and everything you do. I look forward to entering this next chapter of our lives, side-by-side, to meet both the teardrops and laughter together as we always have. Thank you so much for everything; this achievement is as much yours as it is mine. I am grateful to have you as my wife, as an unparalleled mother to our sons, and as a friend. I love you very much.

Dedication

For my wife, Brenna,
whose support and sacrifice
made this all possible,

And for my children,
Michael and Charlie,
who continue to teach me
about joy, love, and the purpose of life

Abstract

Background: Prominent working memory (WM) deficits have been repeatedly observed in people with schizophrenia (PSZ) and their unaffected relatives (REL), including in the spatial domain. Given the apparent association between spatial WM dysfunction and genetic liability for schizophrenia, spatial WM deficits have been proposed as a potential endophenotype for the disorder. Deficits in the neural correlates of WM performance have likewise been observed in PSZ and REL. Lisman and Idiart (1995) offered a model delineating a mechanism for the representation of multiple stimuli in WM through systematic interactions between activity in the theta- and gamma- frequency ranges, and much experimental evidence in support of this model has been obtained since. Activity in these frequency ranges has also been proposed as a potential underlying factor in WM dysfunction in PSZ and REL, especially in light of documented deficits in the theta- and gamma- bands independently.

Methods: Theta- and gamma-band oscillatory activity recorded during a spatial WM task was examined through time-frequency analyses in PSZ, REL, and CTRL. Indices of power, phase-synchrony, cross-frequency coupling and their relationships to task performance were explored.

Results: PSZ demonstrated abnormalities in measures of both theta- and gamma-band power as compared to CTRL and REL, whereas deviance in power measures were limited to gamma-activity in REL. Both PSZ and REL showed reduced phase-synchrony across examined frequencies for electrodes where synchrony was observed in CTRL. Theta-gamma coupling increased significantly in response to WM stimuli, though

minimal differences were observed across diagnostic groupings. Behavioral performance was generally predicted by measures of low frequency power and high-frequency phase synchrony, though the predictive ability of focused measures of gamma-band power, synchrony and phase-amplitude coupling was increased for PSZ as compared to CTRL and REL.

Discussion: Disturbances in various measures of theta- and gamma-band oscillatory activity was observed in PSZ and to a lesser extent in REL. PSZ showed unique predictive relationships between certain neural indices (including limited indices of cross-frequency coupling) and behavioral performance, even in measures where no group differences were observed, suggesting PSZ are more impaired by normal variability in neural processes related to these measures than CTRL and REL. These findings, in light of preserved WM performance in REL, may further support the presence of a compensatory mechanism in REL that insulates them from deficits in performance. Cross-frequency coupling appears to have some predictive utility regarding WM ability, though further work in determining particular frequency pairs of relevance is needed.

Table of Contents

List of Tables

List of Figures

Visuospatial working memory (WM), comprised by the coordination of processing, maintaining, manipulating, and retrieving spatial and visual information within the brain (De Beni, Pazzaglia, Gyselinck, & Meneghetti, 2005), has been implicated in a variety of tasks necessary for the navigation of day-to-day life, including wayfinding (Meilinger, Knauff, & Bülthoff, 2008) and visuomotor learning (Anguera, Reuter-Lorenz, Willingham, & Seidler, 2010; Uresti-Cabrera, Diaz, Vaca-Palomares, & Fernandez-Ruiz, 2015). Prominent WM deficits have been demonstrated across multiple sensory modalities in people with schizophrenia, including in the visuospatial realm (Conklin, Curtis, Calkins, & Iacono, 2005; J. Lee & Park, 2005). Furthermore, better visuospatial WM function in people with schizophrenia has been shown to predict better functional and social outcomes (Goghari et al., 2014; H. Takahashi et al., 2005). Spatial WM deficits are likewise observed in unaffected first-degree relatives of people with schizophrenia (Bachman et al., 2009; S. Park, Holzman, & Goldman-Rakic, 1995; Pirkola et al., 2005), suggesting they may represent genetic liability for schizophrenia and thus constitute a potential endophenotype for the disorder (A. J. Allen, Griss, Folley, Hawkins, & Pearlson, 2009; Glahn et al., 2003; Gottesman & Gould, 2003; Snitz, MacDonald, & Carter, 2006).

Electroencephalography (EEG) has been widely used to investigate the neural underpinnings of WM processes, traditionally in the form of event-related potential

(ERP) studies (reviewed in Perez, Vogel, Luck, & Kappenman, 2012). People with schizophrenia have been found to demonstrate deficits in ERPs elicited from WM tasks (Dias, Butler, Hoptman, & Javitt, 2011; Haenschel et al., 2007; Zhao et al., 2011) and tasks probing sustained attention (Davenport, Sponheim, & Stanwyck, 2006; Ergen, Marbach, Brand, Başar-Eroğlu, & Demiralp, 2008; S. Y. Lee, Namkoong, Cho, Song, & An, 2010; Oribe et al., 2013; reviewed in Yeap et al., 2008), among others; similar deficits have been observed in first-degree relatives of people with the disorder (S. Y. Lee et al., 2010; Sponheim, McGuire, & Stanwyck, 2006; Yeap et al., 2006). More recently, EEG research has examined oscillatory activity in the brain associated with WM. Oscillatory activity in the brain, which arises from the rhythmic activation of large number of synapses (Spellman & Gordon, 2015), is crucial to coordinated activity in the normally functioning brain (Uhlhaas & Singer, 2010). People with schizophrenia demonstrate many abnormalities in oscillatory activity, which interfere with efficient integration of activity within the brain and may contribute to the prominent cognitive and functional deficits observed in the disorder (Haenschel et al., 2009; Spellman & Gordon, 2015; Uhlhaas & Singer, 2010).

Generally speaking, high frequency oscillations are associated with synchronization in local cortical networks, and lower frequency oscillations with synchronization between brain structures / across greater distances (Uhlhaas & Singer, 2010). Oscillations in the gamma-band (25-100 Hz) and the theta-band (4-8 Hz) in particular have been widely implicated in episodic memory and WM alike (reviewed in Nyhus & Curran, 2010). Furthermore, the synchronized superimposition of gamma

cycles on oscillatory theta activity has been proposed as a mechanism for the representation of multiple items in WM, a mechanism termed the "theta/gamma code" (Lisman & Jensen, 2013, p. 1002). Multi-item WM has been associated with phase-phase coupling between theta and gamma frequencies in healthy people (e.g., Sauseng et al., 2009). In addition, theta-gamma phase-amplitude coupling, in which the amplitude of gamma activity is strongly correlated with the phase shift of simultaneous theta activity, has been observed in the hippocampus (Axmacher et al., 2010; Chaieb et al., 2015) as well as from scalp EEG (J. Y. Park, Jhung, Lee, & An, 2013; J. Y. Park, Lee, & Lee, 2011) in healthy humans and, in both cases, has been predictive of WM performance (Axmacher et al., 2010; Chaieb et al., 2015; J. Y. Park et al., 2013, 2011). Given these findings, abnormal theta-gamma coupling has been proposed as a mechanism for impaired WM function in people with schizophrenia (Moran & Hong, 2011), and recent work has shown disturbances in theta-gamma coupling in people with schizophrenia during performance of a WM task (described below; Barr et al., 2017).

Much research has already shown abnormalities in the gamma- and theta- bands in people with schizophrenia, suggesting dysfunction in neural integration on local and global scales. These gamma and theta abnormalities in people with schizophrenia are herein considered in the context of the theta/gamma neural code. Though investigation of the theta/gamma code in schizophrenia has been limited to date, the mechanism and hypothesized utility of the superimposition of gamma cycles on theta cycles in relation to WM in healthy people is herein reviewed. Subsequently, this review will recount observed abnormalities in people with schizophrenia for activity in the gamma-band,

theta-band, and interactions between the two, discussing how such abnormalities may interfere with efficient theta/gamma coding in schizophrenia. Finally, though literature on oscillatory abnormalities in relatives of people with the disorder is sparse, instances where relatives demonstrate deficits in neural oscillations similar to people with schizophrenia are detailed. Through integration of present knowledge regarding abnormalities in gamma- and theta-band oscillations in schizophrenia, the present review will attempt to elucidate the potential implications of these abnormalities in the context of the theta/gamma neural code.

The Superimposition of Gamma-Band Oscillations on Theta Oscillations: The Theta/Gamma Neural Code

The theta/gamma code, or the theory that short-term memories are serially processed via the superimposition of high-frequency gamma-band oscillations on low-frequency theta-band oscillations, was first posited by Lisman and Idiart (1995). The neuromodulators acetylcholine and serotonin have been shown to be released in the brain during periods of oscillatory activity (Bland, 1986; Steriade, Dossi, Pare, & Oakson, 1991). In the presence of these neuromodulators, firing of neuronal cells induces a period of membrane afterdepolarization (ADP) rather than the typical afterhyperpolarization, leading to a transient increase in cell excitability (Andrade, 1991; Storm, 1989; Caeser, Brown, Gähwiler, & Knöpfel, 1993). Building off these findings, the authors used computer simulations to show that the duration of ADP was on the time scale of oscillations in the alpha-theta range (5 to 12 Hz), and that such ADP could be propagated for many cycles. Thus, a single excitatory input could lead to sustained firing on

subsequent oscillatory cycles, potentially serving a storage function (Figure 1a; Lisman & Idiart, 1995). Furthermore, the authors noted that in Sternberg's (1966) classic work on serial scanning in WM, the addition of each additional stimulus to the string of stimuli to be recalled resulted in an increase in reaction time of roughly 38 ms—an increase corresponding to the cycle of a neural oscillation in the beta-gamma range. Jensen and Lisman (1998) elaborated on this observation, showing that the theta-gamma code model could effectively account for reaction time data and serial position effects reported by Sternberg (1964; 1966). Roughly seven cycles in the beta-gamma range could be superimposed on a lower frequency cycle in the alpha-theta range—such as those cycles induced by the ADP—which Lisman and Idiart (1995) emphasized corresponded to the canonical average capacity of WM determined by Miller (1956). Finally, Lisman and Idiart (1995) demonstrated through simulation how differing, non-overlapping stimuli or "memories" (p. 1515) could be stored through systematic variation in the phases of the different high-frequency subcycles, with each stimulus being represented by different groups of cells that maintain the stimulus by firing simultaneously at a particular high-frequency subcycle within the nesting lower frequency cycle (Figure 1c). Thus, particular stimuli or memories are represented by the particular spatial pattern of a group of cells, or neural ensemble (Lisman & Buzsáki, 2008), these memories are propagated or maintained through interactions between oscillatory activity in the theta and gamma frequencies, and sequential information regarding these memories are linked to the particular gamma subcycle within the nesting theta cycle a given memory's neural ensemble produces (or perhaps more accurately, the phase offset between the neural

ensemble's gamma cycle and the nesting theta cycle; Lisman & Idiart, 1995; Lisman & Buzsáki, 2008).

Koene and Hasselmo (2007) elaborated the original theta-gamma code model to provide a mechanism for the ordered displacement of items in a first-in-first-out (FIFO) manner, as Lisman and Idiart (1995) originally proposed. The FIFO principle is a plausible and frequently assumed method of replacement in WM that posits that when a new stimulus or memory is added to a "full" WM buffer, the oldest item in temporary storage is lost (Atikinson & Shriffin, 1968; Phillips, Atkinson & Shriffin, 1967). In addition to providing an explanation as to how the theta-gamma neural code would replace information in this manner, the authors' simulation incorporated a "leaky integrate-and-fire" neural model that could better account for experimental data showing an asymmetric distribution of spiking activity across the different theta cycles (e.g., the fact that different stimuli are represented by different numbers of simultaneous spikes; Koene & Hasselmo, 2007).

The theta-gamma neural code as proposed by Lisman and Idiart (1995) and further elaborated by Koene and Hasselmo (2007) represents a theoretical framework which, at its inception, integrated a number of experimental findings to provide a plausible model for the storage of multiple items in WM. This framework has served as the basis for a substantial body of experimentation over the past twenty years, the vast majority of which has produced results supporting the Lisman and Idiart (1995) model. A brief review of this sizeable body of literature follows.

Empirical Support for the Theta-Gamma Neural Code

The experimental support for Lisman and Idiart's (1995) model of the theta-gamma neural code is now widespread. In their original proposal, the authors cited classic examples of induced repetitive, low-frequency activity after brief sensory stimulation (namely, responses to brief electrical clicks from both thalamic and cortical surface recordings of electrical activity in cats; Chang, 1950). Such observations are consistent with the model prediction that memory patterns repeat on each low-frequency oscillation. In addition, the model predicted that single cells, when artificially excited, should continue to fire on subsequent oscillations (Lisman & Idiart, 1995); such a finding had been recently reported in recordings from monkeys during performance of a simple visual WM task (Nakamura, Mikami, & Kubota, 1992). They likewise pointed to then recent observations that approximately seven high frequency oscillatory subcycles were found to be nested in lower frequency cycles in the human dream state (Llinas & Ribary, 1993) as well as in the hippocampus of the rat (Bragin et al., 1995; Soltesz & Deschenes, 1993). In addition, though the notion that the phase of oscillatory cell firing could be used to distinguish different patterns of activity, and thus stimuli, was not new (Singer, 1993; Von der Malsburg & Schneider, 1986), the authors note that the emphasis in their model on different stimuli being represented not only by phase differences but also entirely distinct neural ensembles would predict that particular cells would not necessarily fire on sequential high-frequency subcycles (Lisman & Idiart, 1995). While single cell firing on multiple sequential high-frequency subcycles has been observed, such observations are the minority (Koch & Crick, 1994), and direct experimentation had recently shown that sequential gamma subcycles corresponded to differing rather than

identical auditory stimuli (Joliot, Ribary, & Llinas, 1994).

Perhaps the most significant early support for the theta-gamma neural code model came from the work of O'Keefe and Recce (1993), as well as clarifying work by Skaggs, McNaughton, Wilson, and Barnes (1996). These researchers examined pyramidal cells from the hippocampus of rats known as place cells, which fire bursts of spikes as the animal moves through a particular area in its environment termed the place field of that cell (O'Keefe & Recce, 1993). Concurrent to these bursts of neural activity, theta-band activity increases in the hippocampal EEG as a rat relocates itself in its environment. Though phase correlations between firing of hippocampal cells and theta activity had then been well-established (Buzsáki, Leung, & Vanderwolf, 1983; Fox, Wolfson, & Ranck Jr, 1986; Otto, Eichenbaum, Wible, & Wiener, 1991; Sinclair, Seto, & Bland, 1982), the nature of the relationship was not well clarified. Using a combination of single unit and EEG recordings from hippocampal CA1 and CA3 place cells, O'Keefe and Recce (1993) showed that for a single run through the field of a given place cell on a linear track, the cell fired bursts of spikes at progressively earlier parts of the of the concomitant theta cycle, a phenomenon termed "phase precession" (Skaggs, McNaughton, Wilson, & Barnes, 1996, p. 149; Figure 2). This finding was taken to indicate that the hippocampus may use a neural code in which theta phase conveys important information (Lisman & Jensen, 2013)—namely, the theta-gamma neural code that Lisman and Idiart (1995) proposed. Skaggs and colleagues (1996) replicated and elaborated this finding to demonstrate that the phase precession effect was indeed robust throughout the rat hippocampus, and observed as animals moved through two-

dimensional in addition to one-dimensional space. More significantly, the researchers emphasize the support their findings lend to the notion that the theta phase-offset at which a place cell fires carries important spatial information (Skaggs et al., 1996). Bieri, Bobbitt, and Colgin (2014) similarly observed theta-gamma phase precession in rat CA1 hippocampal cells and suggested differential relationships between coupling between high- and low-gamma signals. Phase precession has likewise been observed in entorhinal grid cells (De Almeida, Idiart, Villavicencio, & Lisman, 2012), supporting the organization of multi-item WM by way of theta- and gamma- cycles as by Lisman and Idiart's (1995) model and its elaborations. Phase-precession is further reviewed in Lisman and Redish (2009).

Much subsequent experimentation has added to the support for Lisman and Idiart's (1995) model, demonstrating systematic relationships between theta- and gamma-oscillatory activity. These relationships are most frequently presented in one of two forms: phase-phase coupling (also called phase-synchrony, or simply phase-coupling), in which the phase of ongoing theta-activity is systematically related to the phase of concurrent gamma-activity; and phase-amplitude coupling, in which the amplitude of gamma activity is modulated by the phase of concurrent theta-oscillations (Figure 3). Findings of both types of coupling are discussed below.

Theta-Gamma Phase-Phase Coupling

Phase-phase coupling, or phase synchronization, between oscillations in the theta- and gamma- bands during WM processes has been widely observed in animal and human brains alike. Theta-gamma phase-coupling has been repeatedly observed in the

entorhinal-hippocampal system of rats. Chrobak and Buzsáki (1998) reported nesting of gamma oscillations within theta oscillations in the entorhinal cortex and hippocampus of rats during exploratory behavior, as well as neuronal spiking in layers II and III of the entorhinal cortex that was in phase with the local, nested gamma oscillations. They further found (delayed) synchronization between theta-gamma rhythms in the entorhinal cortex and the dentate hilar region of the hippocampus, leading the authors to propose that the systematic phase-locking of gamma oscillations to nesting theta oscillations is necessary for such synchronization (and presumably, communication[1]) within the perforant pathway (Chrobak & Buzsáki, 1998). Phase-phase coupling has likewise been observed between hippocampal theta rhythms and gamma oscillations in multiple regions of neocortex (including prefrontal cortex and primary sensory areas) in active, sleeping and anesthetized rats (Sirota et al., 2008), as well as in CA1 pyramidal cells in the rat hippocampus (Belluscio, Mizuseki, Schmidt, Kempter, & Buzsáki, 2012; De Almeida et al., 2012). Combined with the well-accepted phenomenon of phase-precession in rats, these findings lend support to the prominence of theta-gamma phase-coupling during environmental navigation, as well as to the ongoing presence of theta-gamma interactions outside of conscious activity.

Phase-phase coupling has likewise been observed in the human brain. Intracranial human recordings have afforded local recordings of the strong temporal relationship between theta- and gamma-activity. Intracranial EEG recorded during the encoding

[1] The importance of theta- and gamma-band oscillations in the synchronization of activity between brain regions has been further reviewed in Lisman and Jensen (2013), and Benchenane, Tiesinga, and Battaglia (2011).

phase of a word memorization task likewise showed phase-phase coupling between theta- and gamma- activity across the rhinal cortex and hippocampus in humans; this relationship was observed only for words successfully recalled, thus supporting the role of theta-gamma synchrony in memory formation (Fell et al., 2003). Chaieb and colleagues (2015) likewise observed phase-phase coupling between theta- and gamma-activity using intracranial EEG recorded from human hippocampus during the maintenance period of a serial Sternberg-like WM task; coupling was observed for multiple stimulus loads but not for single-item trials, suggesting the importance of theta-gamma interactions for multi-item WM. Furthermore, changes in measures of coupling across loads predicted individual WM capacities (Chaieb et al., 2015). Thus, theta-gamma phase-synchrony recording intracranially has shown a strong relationship to memory function in humans.

Phase-phase coupling has similarly been reported using EEG recorded from the human scalp. Schack, Vath, Petsche, Geissler, and Möller (2002) found theta-gamma synchrony over prefrontal areas in scalp EEG recorded during performance of the Sternberg (1964; 1966) task, thereby lending support to Lisman and Idiart's (1995) initial suggestion that the frequency of gamma cycles could account for increases in reaction time with the addition of stimuli, and that the interaction of theta- and gamma-activity is crucial to maintaining these stimuli in WM. Theta-gamma phase synchronization has elsewhere been shown to be enhanced during WM tasks in electrodes over prefrontal areas in humans (J. Y. Park et al., 2013, 2011), and synchronization in the same area has been found to predict WM performance (J. Y. Park et al., 2011). Similarly, phase

synchrony between theta and gamma frequencies recorded from scalp EEG has been associated with visual WM performance in healthy people, with greater theta-gamma phase synchronization at posterior parietal sites predicting greater visual WM capacity (Sauseng et al., 2009). Y. Lee and Yang (2014) likewise found that the extent to which the phases of theta- and gamma- activity recorded from scalp EEG in healthy people were synchronized predicted spatial working memory ability. Scalp EEG recorded from humans has also shown increased phase-synchrony between theta- and gamma- activity in parieto-occipital areas during a visuospatial delayed match-to-sample task, supporting the importance of phase-phase coupling between theta- and gamma-oscillations to visuospatial WM (Holz, Glennon, Prendergast, & Sauseng, 2010). Sauseng, Klimesch, Gruber, and Birbaumer, (2008) similarly observed increased synchrony during a cued visual attention task between theta- and gamma- bands in posterior signal sources derived from scalp EEG recordings, which the authors took to reflect processes of matching incoming visual input to information stored in memory. Thus, recordings from scalp-level EEG and intracranial EEG alike demonstrate a prominent relationship between theta-gamma coupling and WM processes.

Theta-Gamma Phase-Amplitude Coupling

Though Lisman and Idiart's (1995) model emphasized coherence between theta- and gamma-band activity in the context of phase-phase coupling, frequently reported is a relationship between the relative phase shift of theta- activity and the amplitude of gamma-activity, known as phase-amplitude coupling. As with phase-phase coupling, many reports of phase-amplitude coupling come from the animal literature. Phase-

amplitude coupling between theta- and gamma-activity has been observed in the hippocampus (Buzsáki et al., 2003; Hentschke, Perkins, Pearce, & Banks, 2007; Wulff et al., 2009; Yamamoto, Suh, Takeuchi, & Tonegawa, 2014; Tamura et al., 2017), medial prefrontal cortex (Tamura et al., 2017) and entorhinal cortex (Yamamoto et al., 2014) of mice. Tamura and colleagues (2017) found increased theta-gamma coupling in the medial prefrontal cortex of *Zdhhc8*$^{+/-}$ mice, typically used as an animal model of cognitive dysfunction, during correct performance of a spatial WM task. They also found increased theta-gamma coupling *between* medial prefrontal cortex and the ventral hippocampus with correct performance. Finally, increased theta-gamma coupling was observed in long-delay trials as compared to short-delay trials in wild-type mice. The authors suggest that these findings implicate theta-gamma coupling as a potential compensatory mechanism in maintain spatial WM in the performance of particularly difficult tasks, and that theta-gamma coupling within the hippocampal-prefrontal circuit may especially contribute to this behavioral advantage. Conversely, Zhang and colleagues (2017) found concurrent decreases in memory performance and theta-gamma coupling in the hippocampus after long-term exposure to a magnetic field, further supporting a connection between these two indices. Goutagny and colleagues (2013) examined theta-gamma phase-amplitude coupling in TgCRND8 mice, a strain which at three months of age develops amyloid-beta plaques typical of Alzheimer's disease in humans and accompanied by similar cognitive decline. The authors found that hippocampal theta-gamma phase-amplitude coupling was disrupted in these mice prior to the accumulation of plaques or the appearance of cognitive impairment, suggesting that

the disruption of phase-amplitude coupling may be linked to precursors of amyloid-beta plaques and associated cognitive impairments, most notably memory loss (Goutagny et al., 2013). Using implanted electrodes, Siegle and Wilson (2014) stimulated interneurons in the mouse hippocampus, and found improvements in spatial WM performance with stimulation time-locked to particular phases of theta-oscillations in the local field potential; improvement in encoding and retrieval came with stimulation at different relative phase shifts, suggesting the importance of relative theta-phase to the timing of activity bursts. Differences in the frequency of the gamma-activity coupled to theta have been observed in mice CA1 place cells depending on the memory strategy (environmentally anchored or allocentric versus egocentric) used by the animals to navigate a pentagonal maze (Cabral et al., 2014). Thus, mice models support the role of theta-gamma coupling in successful WM performance.

Theta-gamma phase-amplitude coupling has been similarly reported in the rat hippocampus (Buzsáki et al., 1983; Csicsvari, Jamieson, Wise, & Buzsáki, 2003; Quilichini, Sirota, & Buzsáki, 2010; Tort et al., 2008; Tort, Komorowski, Manns, Kopell, & Eichenbaum, 2009) as well as rat entorhinal cortex in vivo (Chrobak & Buzsáki, 1998; Chrobak, Lörincz, & Buzsáki, 2000; Quilichini et al., 2010) and in isolation (Cunningham, Davies, Buhl, Kopell, & Whittington, 2003), and rat striatum (Tort et al., 2008). Trimper, Stefanescu, and Manns, (2014) reported theta-gamma phase-amplitude coupling in the hippocampi of rats exploring novel objects, but also gamma-gamma phase synchrony between CA3 and CA1 LFPs that varied with relative theta- phase and was greatest for objects subsequently remembered. Schomburg and colleagues (2014)

found similarly found phase-amplitude coupling between theta- and gamma- activity in the hippocampus and entorhinal cortex of rats, with differences in preferred theta phase and frequency of gamma occurring across hippocampal layers and dependent upon the cells from which they received input. M. Takahashi, Nishida, Redish, and Lauwereyns, (2014) found that gamma-amplitudes in CA1 cells from rat hippocampus were similarly phase-locked to theta during a "fixation" period prior to completing a memory-guided spatial alternation task. Furthermore, preferred theta-phase differed between high- (60-90 Hz) and low- (30-45 Hz) gamma activity, and low-gamma activity increased with a concurrent decrease in high-gamma activity towards the end of the fixation period, which the authors took to indicate that high-gamma activity was associated with externally cued information processing and low-gamma with internally generated information processing (M. Takahashi et al., 2014). In addition, modulation of gamma-activity by theta phase was found to be strengthened overall from the beginning to the end of the session in the same paradigm (Nishida, Takahashi, & Lauwereyns, 2014). Especially relevant to theta-gamma coupling in schizophrenia, Michaels and colleagues (2018) found that ketamine administration to Long Evans rats, a frequently employed animal model for schizophrenia, altered theta-gamma coupling in the CA1 hippocampus, supporting the potential role of coupling in the pathophysiology of schizophrenia. Similarly, Kalweit and colleagues (2017) found decreased theta-gamma coupling in the hippocampus of rats treated with MK801, an animal model of first episode psychosis, suggesting the potential for similar declines in the onset of schizophrenia. Thus, experimentation with rats further supports the role of theta-gamma coupling in memory function, as well as its potential

relevance to observed WM dysfunction in schizophrenia.

Siegel, Warden, and Miller (2009) reported both phase-phase and phase-amplitude coupling for activity in the delta- and beta-bands—frequency bands comparable to theta- and gamma- —recorded from electrodes implanted in the prefrontal cortices of macaque monkeys during a visual WM task, supporting the importance of nested high-frequency signal in lower frequency activity to WM processes. Theta-gamma phase-amplitude coupling was similarly observed between various sites in the anterior cingulate cortex and prefrontal cortex of macaque monkeys during a visual attention task, suggesting a role for theta-gamma coupling in organizing internally generated information that facilitates attentional control (Voloh, Valiante, Everling, & Womelsdorf, 2015). In addition, gamma- amplitudes have been found to be coupled to theta-phase—and theta-amplitudes subsequently coupled to delta-phase—in the auditory cortex of macaque monkeys during simple stimulus processing (Lakatos et al., 2005). Taken together, these latter findings suggest that theta-gamma coupling plays a role in cognitive processes closely related to memory function but not memory per se. Overall, the widespread prominence of theta-gamma phase-amplitude coupling in the animal literature suggests that systematic interactions between these frequency bands are central features to WM function and related processes.

Reports of phase-amplitude coupling between theta- and gamma- activity are similarly widespread in experimentation with human subjects. Recent work has focused on the relationship between WM performance and theta-gamma coupling through manipulation of brain rhythms through via stimulation. Alekseichuk and colleagues

(2016) used precisely timed transcranial alternating current stimulation to demonstrate that high-gamma (80-100hz) stimulation at particular phase-shifts of concurrent theta activity selectively improved WM function, which they assert as evidence supporting a causal role of theta-gamma coupling in WM performance. Similarly, Reinhart and Nguyen (2019) observed a predictive relationship between theta-gamma phase-amplitude coupling in young adults but not older adults (aged 60-76), where coupling was markedly less prominent. However, frontotemporal transcranial alternating-current stimulation both restored phase-amplitude coupling and improved WM function for an hour or more in the older adults. These remarkable studies strongly support a causal role for theta-gamma coupling in the human brain, and represent promising avenues for potential future treatment.

These exceptional results build off a strong body of correlational analyses supporting the role of theta-gamma coupling in WM. Intracranial recordings have demonstrated prominent theta-gamma phase-amplitude coupling during WM processes in the rhinal-hippocampal complex. In intracranial EEG recorded from humans during a word recognition WM paradigm, Mormann and colleagues (2005) reported modulation of gamma- amplitude by theta- phase in both the rhinal cortex and the hippocampus. As rhinal modulation was greatest for correct rejections—which necessarily requires the encoding of a new item—and hippocampal modulation greatest for hits, the authors speculate that phase-amplitude coupling may underlie encoding processes in rhinal cortex and retrieval processes in the hippocampus. Axmacher and colleagues (2010) likewise found modulation of gamma-amplitude by theta-phase using intracranial EEG recorded

from human hippocampus during performance of a visual analogue of the Sternberg task; this phase-amplitude coupling was most pronounced during WM maintenance. Furthermore, more precise coupling (that is, a narrower modulation width for the gamma-peak) was associated with better performance, as measured by faster reaction times (Axmacher et al., 2010). These observations of theta-gamma coupling in human rhinal cortex and hippocampus mirror observations reported in the animal literature, and echo the importance of systematic theta-gamma interactions to WM in the human brain.

Theta-gamma phase-amplitude coupling during tasks probing WM has been similarly observed in intracranial recordings from humans using sensors spread throughout the brain's four lobes. Bahramisharif and colleagues (2018) used electrocorticogram recordings from patients with epilepsy during performance of a WM task to show that bursts of gamma activity for different sequential items preferred different phases of concurrent theta activity, providing strong support for the original formulation of the theta-gamma code. Canolty and colleagues (2006) similarly found that the power of high gamma-band activity was modulated by the phase of theta in subdural human electrocorticogram recordings from left frontotemporal regions during various cognitive tasks including a verbal WM task, with the strongest gamma-activity occurring at a preferred phase of theta (within the "trough" of the cycle). Also using electrocorticogram, Maris, van Vugt, and Kahana (2011) found phase-amplitude coupling that was widely distributed across frequency as well as locations including frontal, temporal and parietal sites during a Sternberg task, with theta-gamma coupling being most prominent in within-electrode analyses, and van der Meij, Kahana, and Maris

(2012) demonstrated widespread phase-amplitude coupling across distances greater than 10 cm between sensors spread throughout parietal, occipital and temporal regions during a Sternberg WM task. Moreover, reports of theta-gamma coupling in humans are not exclusive to WM processes. Electrocortigram analysis in humans has also showed prominent phase-amplitude coupling across multiple frequency bands, including theta- and gamma-, for similarly widespread sensor locations during wakefulness and slow-wave sleep (He, Zempel, Snyder, & Raichle, 2010), visual search tasks (Miller et al., 2010; Voytek et al., 2010), and other assorted tasks including self-referential descriptive categorization and verbal phoneme / word repetition / target detection (Voytek et al., 2010).

Theta-gamma phase-amplitude coupling has also been observed in humans utilizing scalp-level recordings, as in Goodman and colleagues' (2018) study of coupling in people with Alzheimer's dementia, mild cognitive impairment and healthy controls. They found decreasing theta-gamma coupling at frontal sites from controls to participants with mild cognitive impairment to Alzheimer's patients; furthermore, coupling was the strongest predictor of performance on the 2-back task performed during EEG collection for all participants. Such results further support the link between theta-gamma phase-amplitude coupling and WM performance. Also using scalp-level EEG, Rajji and colleagues (2017) observed a selective increase in frontal theta-gamma phase-amplitude coupling during *N*-back trials that required ordering of information versus those that did not, leading them to posit a special role for theta-gamma coupling in such WM-related ordering of information. Scalp recordings in humans were also used to detect phase-

amplitude coupling between theta- and gamma-activity during a visual object recognition task (Demiralp et al., 2007), demonstrating the extension of interaction between the two frequency bands beyond WM. Thus, theta-gamma phase-amplitude coupling plays an important role in human WM; furthermore, the observation of theta-gamma interactions outside of WM again supports the notion that the neural code comprised by the two frequency bands is not exclusively circumscribed to communications regarding memory.

Though reports of phase-amplitude coupling most often emphasize only the phase of the theta-activity, the relative phase-shift between the theta- and gamma- waves is essential to the gamma-amplitude modulation in such coupling. Canolty and colleagues (2006) acknowledged that the high-gamma amplitude modulation they observed is greatly tied to the phase offset of the gamma cycles relative to the theta cycle. Furthermore, Belluscio and colleagues (2012) assert that phase-phase and phase-amplitude coupling occur in most reports of phase-amplitude coupling alone and "may reflect two aspects of a single mechanism" (p. 433). The authors further speculate that phase-phase coupling is rarely reported due to methodological limitations, namely researchers' lack of appropriate for estimating the phase of nonharmonic oscillations as well as for proper separation of frequency bands (Belluscio et al., 2012). Still, both phase-amplitude and phase-phase coupling of theta- and gamma- activity were reported in rat entorhinal cortex (Chrobak & Buzsáki, 1998), and Schack and colleagues (2002) indicate that modulation of gamma amplitudes by theta phase may explain the increased coherence they observed in scalp recordings over prefrontal sites in humans during the Sternberg task. Pastoll, Solanka, van Rossum, and Nolan (2013) similarly report both

phase-phase coupling and phase-amplitude coupling between theta- and gamma- activity recorded from medial entorhinal cortex in mice. Thus, certain research examined and reported simultaneous phase-amplitude and phase-phase coupling. In those studies that did not, we should err on the side of conceptualizing phase-phase and phase-amplitude coupling as two forms of the same phenomenon, rather than two distinct processes with potentially different meanings and mechanisms of function.

Criticisms of the Lisman and Idiart Model

Certain experimental evidence has been difficult to reconcile with Lisman and Idiart's (1995) model. Sederberg, Kahana, Howard, Donner, and Madsen (2003) found that gamma- and theta- oscillations recorded intracranially from human patients during the encoding phase of a verbal WM task predicted subsequent recall; however, the gamma- and theta- activity was not significantly correlated, leading the authors to conclude activity in the two bands had differing origins. This result is challenging to incorporate into the theta-gamma neural code model and its supporting literature. However, as it is very much in the minority, further demonstrations of unrelated theta- and gamma- activity must be made to leverage a significant argument against Lisman and Idiart's (1995) model. In addition, Demiralp and colleagues (2007) point out that Lisman and Idiart's (1995) observation that roughly seven cycles of gamma can be superimposed on a single theta, which the authors emphasized due to its correspondence to the classic capacity of WM determined by Miller (1956), is not groundbreaking, as the division of the two frequency bands will produce a number close to seven simply by virtue of their definition. If individual WM capacity is indeed determined by the number of gamma

cycles that can "fit" within a single theta cycle, then people with slower theta cycles or faster gamma cycles should have greater WM capacity, and this has yet to be determined. While true, several papers have demonstrated correlations between measures of theta-gamma coupling and WM performance, thus lending credibility to the proposal that the two indices are related. In general, criticisms of the Lisman and Idiart (1995) model and its elaborations are few, with most researchers performing related work indicating that their results fit well with the model.

The Role of Abnormal Theta- / Gamma- Oscillations in Schizophrenia

Given the well-documented importance of theta-gamma modulations to memory processes in animal and human studies alike, abnormal interactions between theta- and gamma-oscillations have been proposed to explain the prominent WM deficits observed in people with schizophrenia (Lisman & Buzsáki, 2008; Moran & Hong, 2011). Formal investigation of this proposal has been scarce to date, though recent work has supported this theory (described below; Barr et al., 2017). As such, in addition to the few direct examinations of theta- / gamma- coupling in people with schizophrenia, demonstrated abnormalities in theta- and gamma- oscillations independently are likewise reported, and their potential relevance to interactions between the two frequency bands discussed.

Theta-Gamma Coupling in People with Schizophrenia

Few studies have directly examined interactions between theta- and gamma-activity in people with schizophrenia. Most notably, Barr and colleagues (2017) investigated theta (4-7hz) to gamma (30-50hz) coupling in people with schizophrenia

during performance of a verbal *N*-back task, and found reduced coupling in frontal sites during correct target trials for people with schizophrenia as compared to controls. Coupling was also observed over occipital regions, but no statistical analyses for this activity were reported. Measures of coupling were further found to predict task performance in controls but not relatives. Such findings represent the first direct support for the notion that theta-gamma coupling is reduced in people with schizophrenia, though measures of coupling were not predictive of WM performance.

Outside of the realm of WM, E. A. Allen and colleagues (2011) examined phase-amplitude coupling between low- and high- frequencies using independent component analysis of EEG recorded from people with schizophrenia during performance of an auditory oddball task. Overall coupling between low-frequency phase and high-frequency amplitude across the entire scalp was decreased in people with schizophrenia compared to healthy controls, and people with schizophrenia showed stronger modulation of high frequency amplitude by low frequency phase than controls at frontotemporal sites; this latter modulation included a negative relationship between the phase of frequencies ≤ 4 hz and various frequencies > 98 hz (that is, decreased high-frequency amplitude at preferred low frequency phases) and a positive relationship between the phase of frequencies ≥ 8 hz and the amplitude of most frequency bands ≥ 64 hz (that is, increased high-frequency amplitude at preferred phases). Strong theta-gamma coupling was observed over occipital-parietal areas, but no difference was observed between groups. First-degree relatives of people with the disorder were included in this study and showed coupling intermediate to that of people with schizophrenia and healthy controls,

though their data were not tested statistically due to power limitations. The authors interpret their results to indicate that abnormal cross-frequency coupling may represent an endophenotype for schizophrenia, particularly in light of genetic associations they report for genotypes for certain genes and loading parameters for various independent components in people with schizophrenia; however, theta-gamma coupling may not be significantly altered in the disorder, at least in the context of novelty detection. No correlations between measures of cross-frequency coupling and performance were observed (E. A. Allen et al., 2011). Thus, preserved theta-gamma phase-amplitude coupling has been observed in people with schizophrenia; however, given the minimal role WM processes play in the oddball paradigm used herein, the processes that theta-gamma interactions underlie in this study may be distinct from those related to WM.

Other published work examining theta-gamma cross-frequency interactions in people with schizophrenia focus on 40-hz steady state auditory stimuli. Used scalp EEG recorded during presentation of 40-hz steady state auditory stimuli, Kirihara, Rissling, Swerdlow, Braff, and Light (2012) found reduced intertrial phase coherence, increased theta amplitude, and undisturbed theta-gamma phase-amplitude coupling in people with schizophrenia relative to healthy controls. The authors interpret these findings to indicate a preserved hierarchical organization of theta and gamma activity in people with schizophrenia despite abnormalities in theta- and gamma- activity independently (Kirihara et al., 2012). These findings are largely replicated in the work of Hirano and colleagues (2018), who similarly found preserved theta-gamma coupling in people with schizophrenia in response to 40-hz auditory steady-state stimulation as compared to

controls; both groups showed increased coupling during stimulation. Notably, however, the simple auditory processing task used in this study does not tap memory processes, for which theta-gamma interactions have been shown to be essential and greatly impaired in people with schizophrenia; thus, the intact theta-gamma coupling they report should not be interpreted as indicative of preserved coupling at large. Thus, disturbances in theta-gamma coupling in people with schizophrenia seem circumscribed to WM related tasks, supporting the relationship between cross-frequency coupling in these bands and WM function.

Despite relatively limited investigations of theta-gamma coupling in schizophrenia, preliminary works suggests it may prove useful as an electrophysiological marker for schizophrenia. Won and colleagues (2018) examined a variety of EEG measures from 90 neuroleptic-naïve people with schizophrenia and 90 healthy controls to determine which were most useful in blindly identifying those with the disorder. Phase-amplitude coupling between theta- and gamma- outperformed measures all other examined measures (primarily power measures across a wide range of frequencies), returning an overall classification accuracy of 92.5%. This finding both supports the relevance of theta-gamma coupling to schizophrenia and suggests a potentially useful diagnostic function for coupling measures in the future.

Theta-Band Abnormalities in People with Schizophrenia

Though research on theta-gamma coupling in schizophrenia is sparse, findings from the individual bands support the notion of WM impairments in people with

schizophrenia stemming from aberrant theta-gamma interactions. Abnormalities in theta-activity have been reported in people with schizophrenia. Examinations of theta-theta phase-synchrony, or the extent to which phase-offsets in theta-cycles recorded from different locations remains constant, have revealed prominent deficits in people with schizophrenia in comparison with healthy controls. Using MEG, Kang and colleagues (2018) found decreased theta-band event-related synchrony during encoding in dorsolateral prefrontal and orbital frontal regions during of a visual object construction WM task, as well as a failure to modulate this response with increased task demands. Deficits in theta synchrony were also observed during retrieval in anterior and posterior areas related to visual processing. The authors advanced that these findings in conjunction with other observed synchrony deficits may represent underlying neural mechanisms for a variety of cognitive deficits in schizophrenia, WM included. Using scalp EEG, Griesmayr and colleagues (2014) found reduced phase-synchronization in theta-activity in people with schizophrenia during a delayed-match-to-sample task. The reduced phase-synchrony stemmed primarily from reductions in synchrony between frontal and posterior regions, but reduced synchrony was also observed in posterior areas during high WM load. As theta- has been posited to be central to integrative functions within the brain (e.g., Sauseng, Griesmayr, Freunberger, & Klimesch, 2010), the authors interpret deficient phase-synchrony in theta-oscillations to represent difficulties with binding in people with schizophrenia (Griesmayr et al., 2014). Kustermann and colleagues (2018) found abnormal theta synchrony between temporal and posterior regions in people with schizophrenia during a verbal working memory task, which they

took to reflect abnormalities in neuronal communication in the disorder. Similarly, Ryman and colleagues (2018) found reduced midline theta synchrony as well as power in people with schizophrenia relative to controls using EEG recorded during a cognitive control paradigm, which the authors suggested may reflect a failure in people with schizophrenia to recruit cognitive control processes. Berger and colleagues (2016) used analyzed source-space EEG collected during a delayed-match-to-sample paradigm that suggested disrupted theta-synchrony between the anterior cingulate cortex and the right posterior parietal cortex, which they interpreted to reflect deficits in long-term neural communication. Additionally, König and colleagues (2001) found reduced global field synchronization, a measure of functional connectivity which examines the phase synchronization in a given frequency across all electrode locations, in the theta-band in people with schizophrenia relative to healthy controls during resting EEG recorded from the scalp. Though participants did not perform any task during these recordings, the authors suggested this reduced connectivity in people with schizophrenia underlies their prominent memory dysfunction nonetheless, given previous reports of correlations between resting theta-activity and memory performance. Deficits in theta-phase-synchrony have also been observed in basic visual processes in people with schizophrenia. Martínez and colleagues (2015) examined oscillatory responses in EEG to visual sinusoidal gratings and found reduced phase-locking in occipital theta responses to stimuli of low spatial frequency in people with schizophrenia relative to controls, indicating a lack of consistency in theta activity across trials. The authors take these results to support the notion of a preferential visual processing deficit in the

magnocellular/dorsal pathway that is activated by stimuli of low spatial frequency in people with schizophrenia (Martínez et al., 2015); if such a deficit is associated with inconsistencies in the temporal anchoring of theta-activity, it may contribute to deficits in visuospatial WM processes, namely the coordination of theta- and gamma- nesting observed in healthy people, involving stimuli that preferentially activate the magnocellular system. Thus, deficits in within-band synchronization of theta activity seems to be associated with schizophrenia. Impairments in theta-theta synchrony are presumably disruptive to communication within the brain, and inconsistencies in theta phase-locking could certainly interfere with the formation of neural messages coded by interactions between theta- and gamma- activities.

Though less directly related to the theta-gamma neural code as outlined by Lisman and Idiart (1995), several studies have shown abnormalities in theta-amplitudes in people with schizophrenia. Visual WM paradigms have revealed theta-amplitude deficits in people with schizophrenia across encoding, maintenance and retrieval processes. Schmiedt, Brand, Hildebrandt, and Başar-Eroğlu (2005) found in people with schizophrenia widespread reduced amplitude compared to healthy controls of theta-oscillations recorded using scalp EEG during performance a variable load visual N-back task, with the exception of enhanced theta-amplitudes at left temporal locations in the first 250 ms after stimulus presentation; people with schizophrenia also failed to modulate theta amplitudes with task-related changes. Increased theta-amplitude in frontal-temporal areas has been previously observed in people with schizophrenia, including during auditory hallucinations (Ishii et al., 2000) but also in those with

prominent negative symptoms (Begić, Hotujac, & Jokić-Begić, 2000). As such, increased frontotemporal theta has been generally interpreted as reflecting pathological processes in people with schizophrenia in frontal and temporal regions (Schmiedt et al., 2005). Similarly, the authors took the observed overall reductions in theta-enhancement during the N-back WM task to indicate deficits in theta-modulated control of various executive functions closely related to WM processes (Schmiedt et al., 2005). In their recent investigation of theta-gamma coupling in people with schizophrenia, Barr and colleagues (2017) also observed reduced theta amplitude as compared to controls over frontal areas; furthermore, people with schizophrenia failed to modulate theta for the highest WM load (3-back) in contrast to controls, though modulation did occur for 0 through 2-back conditions. In additions to reports of theta-amplitude reductions in people with schizophrenia, increased theta-amplitudes in frontal areas for manipulation processes as compared to retention processes have likewise been observed in people with schizophrenia during a delayed-match-to-sample task, whereas controls showed no differences in theta-amplitude associated with manipulation versus retention (Griesmayr et al., 2014). These findings have led Griesmayr and colleagues (2014) to propose that frontal theta activity may be more related to an allocation of cognitive resources rather than reflective of memory processes, as has been proposed in light of modulation of theta with by WM load in healthy individuals (e.g., Jensen & Tesche, 2002). However, elsewhere people with schizophrenia have shown no modulation of theta activity with WM load (Missonnier et al., 2012). Here, people with schizophrenia showed increased sustained theta amplitudes in frontal areas for the retention period of 0-back and 1-back

trials in a visual N-back paradigm, thought to indicate atypical neural responses associated with item retention and manipulation (Missonnier et al., 2012). Reductions in the EEG amplitude of theta-activity in people with schizophrenia have been likewise reported during WM encoding and retrieval during performance a visual WM paradigm; evoked theta activity decreased with WM load in controls, but not people with schizophrenia (Haenschel et al., 2009). Furthermore, evoked anterior theta amplitude during encoding was predictive of WM performance in healthy controls but not people with schizophrenia. The authors posit that reduced evoked activity during encoding may be reflective of impaired stimulus-induced phase resetting, and reductions during retrieval may reflect a failure in people with schizophrenia to recognize previously encountered stimuli, for which theta-responses are increased in healthy individuals (Haenschel et al., 2009). Notably, Kustermann and colleagues (2018) found no deficits in midline theta power during a verbal working memory task (2018), which is largely undiscussed by the authors but may reflect insufficient power due to a relatively high-functioning sample of people with schizophrenia. However, in most studies, theta-activity during working memory processes have been reported to be abnormal in people with schizophrenia; though there are discrepancies in the types of abnormalities demonstrated from study-to-study, these discrepancies may stem from the differences between the tasks used in each study.

Abnormal theta-power in people with schizophrenia has likewise been observed in non-WM paradigms. Reduced amplitudes of scalp-wide evoked theta-activity have been observed in people with schizophrenia using EEG recorded during an auditory

oddball task, which the authors posit to be related to generalized cognitive impairments, and specifically executive functions, in people with schizophrenia (Doege et al., 2009). Reduced theta activity has also been observed in people with schizophrenia in Go-No Go paradigms (see Simmonite, Bates, Groom, Hollis, & Liddle, 2015), which has been generally interpreted to reflect dysfunctional connectivity in the brains of people with schizophrenia. Abnormalities in the spatial distribution of theta-activity in people with schizophrenia have also been reported. Başar-Eroğlu, Schmiedt-Fehr, Marbach, Brand, and Mathes (2008) found differences between people with schizophrenia and healthy controls in the scalp distributions of EEG recorded during simple viewing of visual stimuli; people with schizophrenia showed maximal theta-activity at frontal locations compared to controls' maximums over occipital electrode sites. This anterior shift in theta-activity in people with schizophrenia suggests inefficient stimulus processing as compared to controls (Başar-Eroğlu et al., 2008). Given these results, the dysfunctions associated with aberrant theta-activity in people with schizophrenia may extend outside the realm of memory.

Theta-Band Abnormalities in Relatives of People with Schizophrenia

The examination of oscillatory abnormalities in relatives of people with schizophrenia has been limited to date. However, Hong and colleagues (2008) found that reductions in theta-activity over central cortex may underlie impaired sensory gating in relatives of people with the disorder. Furthermore, reduction in parietal evoked theta-power and reductions in theta-synchronization over fronto-central sites have been observed in first-degree adolescent relatives of people with schizophrenia using EEG

recorded during a visual oddball task (Donkers et al., 2011). As theta- activity is associated with attentional and detection processes in the healthy brain (Başar-Eroğlu, Başar, Demiralp, & Schürmann, 1992) and may stem from cortico-hippocampal loops that affect processing in frontal cortex, stimulus evaluation processes may be impaired in relatives of people with schizophrenia, and frontotemporal connectivity abnormalities may represent a biomarker for schizophrenia liability. Thus, relatives of people with schizophrenia demonstrate abnormalities in the theta-band akin to their disordered relatives.

Gamma-Band Abnormalities in People with Schizophrenia

Abnormalities in the gamma-frequency range have been more extensively documented in people with schizophrenia than those in the theta-band. Visual WM paradigms have demonstrated abnormalities in gamma-power in people with schizophrenia as compared to healthy controls. Using EEG recorded during a visual N-back paradigm, Barr and colleagues (2010) found increased evoked gamma-power over frontal sites as well as a failure to modulate gamma-power with increasing WM load as compared to healthy controls, potentially indicating an inefficient allocation of attentional resources. These results are consistent with those of Başar-Eroğlu and colleagues (2007), who found a trend towards increased gamma-power across the scalp in people with schizophrenia relative to controls in a visual N-back task; controls showed a gradual increase in gamma during maintenance, while people with schizophrenia showed increased gamma amplitudes pre- and post-stimuli. In addition, people with schizophrenia showed a failure to modulate gamma-responses with WM load, in contrast

to controls (Başar-Eroğlu et al., 2007).

In contrast to these reports of increased gamma-power, reductions in gamma-power in people with schizophrenia during performance of WM tasks has also been reported. Haenschel and colleagues (2009) found reduced induced gamma-power during visual WM retrieval using EEG over both anterior and posterior sites in people with schizophrenia as compared to healthy controls. The authors posit that this suggests difficulties in the ability of people with schizophrenia to retrieve stimulus representations effectively. Frontal gamma amplitudes were likewise found to be reduced in people with schizophrenia in a Sternberg WM paradigm, and gamma-amplitudes correlated with the duration of illness in people with schizophrenia; these gamma-deficits were taken to indicate impaired inter-regional connections involving the frontal lobe (Chen et al., 2014). Berger and colleagues (2016) observed reduced gamma-band power in the anterior cingulate cortex through source-space EEG analysis for a group of people with primarily negative symptoms of schizophrenia as compared to those with primarily positive symptoms, which they posit may reflect particularly important activity for differentiating these symptoms profiles within the disorder. Kang and colleagues (2018) also observed reduced gamma-band synchrony in premotor and parietal cortices using MEG during manipulation and retrieval portions of a visual object construction WM task, which the authors posited to reflect deficiencies in spatial localization, computation and manipulation of memory stimuli. Using MEG recorded during performance of a mental arithmetic task, Kissler, Müller, Fehr, Rockstroh and Elbert (2000) found increases in controls in frontotemporal gamma-activity during arithmetic; people with schizophrenia

failed to show such increases, and rather demonstrated reduced gamma-amplitudes at temporal and occipital areas independent of the task. Thus, gamma-power in people with schizophrenia has been variably reported to be both increased and decreased during WM relative to healthy controls, whereas gamma-synchrony appears to be deficient in people with schizophrenia.

Further gamma-band abnormalities in people with schizophrenia have been observed in processes related to, but not purely, WM. Here, deficits in people with schizophrenia related to gamma-activity seem to underlie dysfunctional communication between brain regions. The auditory oddball task in particular has been frequently used to examine gamma activity in people with schizophrenia. Haig and colleagues (2000) found reductions relative to healthy controls in gamma-band activity across the scalp for people with schizophrenia during an auditory oddball task, in addition to increased gamma-power in response to targets over right hemisphere sites, particularly in parieto-occipital areas. Given gamma's posited role in binding or integrating the various parts of a complex stimulus, the authors suggest the observed deficits support the notion that schizophrenia is disorder of disconnection—that is, a failure of communication between various regions of the brain (Haig et al., 2000). (Topographical differences in these results are consistent with previous studies reporting left hemisphere deficits and right hemisphere compensation; see Roemer & Shagass, 1990; Shenton et al., 1989.) The prospect of impaired communication between brain regions in people with schizophrenia is further supported by the work of Symond, Harris, Gordon, and Williams (2005), who found decreased gamma-synchrony both globally and in anterior regions in people with

schizophrenia as compared to controls during performance of an auditory oddball task; peak gamma amplitudes over anterior electrode sites were likewise reduced in people with schizophrenia relative to healthy controls. Williams and colleagues (2009) thereafter found disturbed laterality of early gamma activity in people with schizophrenia, as well as globally reduced synchrony in later gamma activity during performance of an auditory oddball task. Reduced gamma-synchrony in people with schizophrenia during the auditory oddball task has been similarly reported by Slewa-Younan and colleagues (2004), who further found this reduction was more pronounced in female participants. Gamma abnormalities in people with schizophrenia during an auditory oddball paradigm over anterior and posterior regions have also been reported by Başar-Eroğlu, Mathes, Brand, and Schmiedt-Fehr, (2011), though they found increased gamma-activity at a single-trial level as compared to healthy controls. These authors likewise suggest that these abnormalities in gamma-band activity reflect irrelevant neural signals that underlie impaired communication within the schizophrenic brain (Başar-Eroğlu et al., 2011). Thus, disruptions in gamma-power and phase-synchrony in the gamma-band observed in people with schizophrenia may reflect impaired communication within the brain.

Correlations between measures of gamma-activity and behavioral as well as clinical measures have been examined in people with schizophrenia. Dysfunctional communication within the schizophrenic brain as indexed by gamma-synchrony has been shown to relate to symptoms of the disorder. Fujimoto and colleagues (2013) examined the relationship between various clinical measures of schizophrenia and the coherence of gamma-activity between various brain regions during an auditory oddball task using

combined EEG and MEG. Multiple significant correlations were found for all subjects: coherence between left occipital and right prefrontal areas predicted PANSS scores, conceptual disorganization, and social avoidance scores; coherence between left occipital and right frontoparietal areas predicted hallucination measures; and coherence between right temporal and left prefrontal areas predicted delusions. For all cases, coherence was reduced in people with schizophrenia relative to healthy controls (Fujimoto et al., 2013). Behaviorally, people with schizophrenia show aberrant relationships between behavioral measures and gamma-activity. Prestimulus gamma-power in an auditory oddball paradigm was found to predict reaction time in healthy controls, but not people with schizophrenia (Reinhart, Mathalon, Roach, & Ford, 2011); the researchers interpreted said finding as indicative of a breakdown in the brains of people with schizophrenia as they prepare for stimulus processing and subsequent motor action, again consistent with notions of impaired neuronal communication in people with schizophrenia. Thus, correlational analysis reveals that gamma-activity relates to clinical measures in people with schizophrenia rather than behavioral measures, as it does in healthy controls.

Abnormal gamma-responses in people with schizophrenia have also been demonstrated in visual discrimination tasks. Başar-Eroğlu and colleagues (2011; 2008) examined EEG recorded from visual as well as auditory oddball tasks, and found reduced phase-synchrony in the gamma-band for people with schizophrenia as compared to controls over occipital sites in the visual task alone; no differences between groups were observed for amplitude nor synchrony measures in the auditory task. Taken together with the previous finding of reduced gamma-synchrony in a visual Gestalt paradigm

(discussed below; Spencer et al., 2008), the researchers conclude that deficits in gamma-synchrony related to visual processing may represent a general, task-independent phenomenon in people with schizophrenia. Thus, deficits in gamma-activity in people with schizophrenia suggest dysfunctional interregional communication within the brain, even outside of WM processes.

Cognitive control paradigms have likewise been used to investigate gamma oscillations in people with schizophrenia. Frontal gamma band responses have been found to be reduced in people with schizophrenia during performance of a cognitive control task; here, gamma-band activity was predictive of task performance for controls but not people with schizophrenia, while gamma-band activity correlated with disorganization symptoms in people with schizophrenia (Cho, Konecky, & Carter, 2006). These results further support a notion that aberrant gamma-oscillations underlie deficits in executive processes in people with schizophrenia. Minzenberg and colleagues (2010) obtained similar results, reporting gamma-band reductions over frontal areas in people with schizophrenia compared to healthy controls associated with cognitive control demands. EEG recorded from an auditory reaction paradigm revealed reduced gamma-band activity over central areas as well as reduced phase-locking in people with schizophrenia compared to healthy controls. Combining these results with source analysis techniques, the authors concluded that the observed deficits in people with schizophrenia could be attributed to impaired functional interaction facilitated by gamma activity between the anterior cingulate cortex and auditory cortex (Leicht et al., 2010). Thus, gamma-activity is disturbed in people with schizophrenia in association with

stimulus evaluation and cognitive control, functions that may feature in a variety of WM tasks.

Gamma-activity has been found to be similarly disturbed in people with schizophrenia using paradigms less justifiably related to WM. Clementz, Blumenfeld, and Cobb (1997) investigated the role of gamma band responses in P50 responses to paired click stimuli, a well-established paradigm which elicits the P50 ERP component. People with schizophrenia demonstrate a failure to suppress P50 responses to the second of these two stimuli, presented in rapid succession (Boutros et al., 1991; Freedman et al., 1983). Clementz and colleagues (1997) found a lack of suppression in MEG gamma-band responses to second stimuli and suggested that these deficits in gamma-band activity could explain P50 sensory gating deficits. However, they were unable to replicate their findings, later finding no group differences in the gamma-band response (Clementz & Blumenfeld, 2001). Kwon and colleagues (1999) found reduced gamma-power as well as delayed gamma-band synchronization and desynchronization in people with schizophrenia over frontal electrode sites in response to auditory click trains. Wilson and colleagues (2008) suggested similar reductions of gamma-power in response to click trains in people with early-onset schizophrenia were indicative of disturbed local and long-range auditory circuitry in the disorder. Using a visual Gestalt task, Spencer and colleagues (2003) found abnormally distributed anterior gamma-responses, a lack of a posterior gamma-response in people with schizophrenia, and reduced / abnormal phase-coherence between hemispheres as compared to healthy controls, supporting the notion that the efficiency and organization of neural networks in general are impaired in people

with schizophrenia due to deficient gamma-synchrony. This notion is supported by the work of Yeragani, Cashmere, Miewald, Tancer, and Keshavan (2006), who found decreased gamma-synchrony in people with schizophrenia as compared to controls between central and frontal areas using scalp EEG measured during resting wakefulness, non-REM and REM sleep. Observation of abnormalities in gamma-band activity independent of any exogenous stimuli supports the idea that these abnormalities may be a core feature of the disorder itself. In contrast, Spencer and colleagues (2004) found evoked gamma-activity phase locked to reaction time over occipital and parietal areas in response to visual Gestalt stimuli in both people with schizophrenia and healthy controls, but the frequency of gamma was lower in people with schizophrenia than in healthy controls; again, this discrepancy was thought to be indicative of impaired support for high-frequency synchronization in the brains of people with schizophrenia. Furthermore, the degree of phase-locking in this sample predicted the presence of visual hallucinations, symptoms of disorganization, and symptoms of thought disorder in people with schizophrenia (Spencer et al., 2004). Visual backwards-masking tasks have also been used to demonstrate a lack of typical hemispheric lateralization as well as reduced gamma-power in people with schizophrenia as compared to healthy controls (Wynn, Light, Breitmeyer, Nuechterlein, & Green, 2005). These results, together with those indicative of impaired gamma-activity in cognitive control and stimulus evaluation / novelty detection, support the notion that gamma-band dysfunction in people with schizophrenia may be representative of a dysfunctional organization of neural networks on a scale greater than memory processes alone.

Gamma-Band Abnormalities in Relatives of People with Schizophrenia

Though studies on gamma-band abnormalities in relatives of people with schizophrenia are scarce, deficiencies have been reported. Leicht and colleagues (2011) found reduced phase locking and evoked gamma-band amplitudes over central areas in people with schizophrenia and their first-degree relatives during performance of an auditory reaction paradigm, suggesting that such gamma-band deficits may represent an endophenotype for the disorder. Thus, relatives of people with schizophrenia may exhibit deficiencies in gamma-band activity similar to people diagnosed with the disorder.

Relevance of Abnormalities in Theta- and Gamma- Activity in People with Schizophrenia

Numerous abnormalities in theta- and gamma- band activity have been reported in people with schizophrenia, including disturbances in phase synchrony and amplitude measures in WM paradigms and elsewhere. Though these studies did not examine coupling between theta- and gamma- activities, the ramifications of deficiencies within each of these bands independently on their interaction are easily ascertained. Inconsistencies in phase-information, as indexed by abnormal phase synchrony measures, would interfere significantly in any meaningful coordination between signals of varying frequencies. Similarly, deficiencies in amplitude measures suggest abnormal generation of neural oscillations, be it through activation of fewer cells or impaired coordination of cellular assemblies that would function more cohesively in the healthy brain. Regardless, less reliable generators of oscillatory activity will find it more difficult to function in the

unitary manner necessary for the coordination of signals necessary for a meaningful theta-gamma neural code. Although abnormal coupling between theta- and gamma-activity in people with schizophrenia has not yet been observed, the few examinations of interactions between these bands in people with schizophrenia have not involved WM directly. Though theta-gamma coupling has been observed during other processes in healthy people, the bulk of the literature ties it to memory processes; thus, further investigation is needed to clarify whether theta-gamma interactions are indeed abnormal during WM processes in people with schizophrenia, and whether those abnormalities explain behavioral performance deficits.

The Theta-Gamma Neural Code and Visuospatial WM in Schizophrenia

Lisman and Idiart's (1995) model positing a theta / gamma neural code as a means for representing multiple items in WM has generated a significant body of literature, and has been implicated in an even greater collection of research. A considerable amount of evidence has been accumulated and overwhelmingly supports the notions advanced by the model, namely that the interaction between theta- and gamma-oscillations communicate meaningful information within the brain in terms of memory and potentially other cognitive processes. However extensive the reach of the theta / gamma code within the brain, it is difficult to dispute the notion that theta-gamma interactions are central features of WM processes, in human and animal brains alike. Furthermore, measures of the strength of coupling between the two bands have repeatedly shown to predict WM performance, supporting the notion that theta- / gamma-interaction and memory are causally linked.

Much of the evidence supporting the theta / gamma code comes from examinations of spatial WM processes in both rodents and humans. Given the well documented deficits in spatial WM in people with schizophrenia (J. Lee & Park, 2005) and their relatives (Bachman et al., 2009; S. Park et al., 1995; Pirkola et al., 2005), the idea that interactions between theta- and gamma-activity within their brains may be abnormal is more than defensible; indeed, such abnormalities may explain the deficits in visuospatial WM and WM at large, and may represent an endophenotype for the disorder. This idea becomes even more plausible in light of the considerable body of literature demonstrating abnormalities in theta- and gamma-bands individually within the disorder, including in connection with WM. Though theta-gamma coupling during WM in people with schizophrenia has been examined to a limited extent (Barr et al., 2017), additional investigation is necessary to replicate reported deficits, elaborate their extent, and better understand their relationship to WM performance. Furthermore, better understanding of how neural oscillations factor into visuospatial WM deficits in the disorder could help inform interventions for improving memory performance, particularly in light of continually developing techniques of neuromodulation that have been shown to improve cognitive function using oscillatory stimulation (e.g., Reinhart & Nguyen, 2019; Alekseichuk et al., 2016; D. J. Lee et al., 2013).

Lisman and Idiart's (1995) theta-gamma neural code provides a framework from which specific, testable hypotheses can be derived regarding potential dysfunction in people with schizophrenia. Using the Lisman and Idiart (1995) model as a guide, we might expect to find generally reduced phase-phase coupling between theta- and gamma-

activity during performance of tasks probing WM in people with schizophrenia. Theta-gamma coupling in healthy people has been observed prominently over prefrontal and posterior regions in scalp level recordings (Holz et al., 2010; J. Y. Park et al., 2013, 2011; Sauseng et al., 2009, 2008; Schack et al., 2002). Thus, deficits in synchrony between the two bands observed over anterior and posterior regions in scalp recordings, as well as in theta-gamma synchrony between the two areas, would particularly support the notion that deficits in the temporal alignment of theta- and gamma- activities are inextricably linked to WM function in the disorder. Furthermore, such synchrony deficits would mirror reports of inefficiencies in prefrontal areas (Potkin et al., 2009) as well as deficient functional connectivity between prefrontal and posterior areas associated with WM processes observed in people with schizophrenia using functional MRI (Kang, Sponheim, Chafee, & MacDonald, 2011; Poppe, Carter, Minzenberg, & MacDonald, 2015), and may represent the same dysfunction. Theta-gamma interactions may likewise be disrupted in the hippocampus in people with schizophrenia, given the predominance of reported theta-gamma coupling during WM processes in animals (Cabral et al., 2014; Chrobak & Buzsáki, 1998; De Almeida et al., 2012; Nishida et al., 2014; Schomburg et al., 2014; Siegle & Wilson, 2014; Sirota et al., 2008; H. Takahashi et al., 2005; Trimper et al., 2014) and healthy people (Axmacher et al., 2010; Canolty et al., 2006; Chaieb et al., 2015; Fell et al., 2003; Maris et al., 2011; Mormann et al., 2005; van der Meij et al., 2012) and observations that structural abnormalities in the hippocampus are prominent in schizophrenia (MacDonald & Schulz, 2009) and are observed even in cases of early-onset (White et al., 2008). Though it is difficult to assess hippocampal function using

scalp EEG (see Mormann et al., 2005), any observed abnormalities therein may support and inform future efforts at such exploration.

Thus, EEG data collected during a WM task featuring the sequential presentation of stimuli were utilized to examine theta- and gamma-band indices in people with schizophrenia (PSZ) and their first-degree unaffected relatives (REL) in comparison with healthy controls (CTRL). It was hypothesized that PSZ would show deficits in theta-gamma-coupling, and that indices of coupling in PSZ would predict WM performance on the analyzed task. It was further hypothesized that PSZ would show deficiencies in analyses of theta- and gamma-band activity independent of their interaction. REL were also expected to show EEG abnormalities as compared to CTRL, though potentially different from those observed in PSZ on the basis of past research and preserved performance on the WM task (Lynn, Kang & Sponheim, 2016).

Methods

Participants

Participants (n=87) were comprised by 22 PSZ, 29 first-degree biological relatives of PSZ (REL), and 36 healthy controls (CTRL; Table 1). Participants had enrolled in a family study of severe psychopathology based out of the Minneapolis Veterans Affairs Medical Center. PSZ were recruited through the site's mental health clinic, past research rosters, other current studies of severe psychopathology, as well as referrals from physicians, community-based mental health facilities and the greater medical center. REL were recruited using contact information provided by their probands relatives, and CTRL were recruited primarily through advertisement in the medical center and community, in addition to past research rosters. Enrolled participants underwent clinical assessments that included the Structured Interview for DSM-IV-TR, Patient Edition (SCID; First, Spitzer, Gibbon, & Williams, 2002), the Scale for the Assessment of Positive Symptoms and Scale for the Assessment of Negative Symptoms (SAPS and SANS; Andreasen, 1984a, 1984b), and the Brief Psychotic Rating Scale (BPRS; Overall & Gorham, 1962) with all measures being administered by a trained and supervised B.A. or M.A. level research assistant or M.A. or Ph.D. level clinicians. The results of these assessments were subjected to a consensus diagnosis process in which two or more Ph.D. clinicians or advanced doctoral students reviewed participants' study materials to form jointly agreed upon diagnoses.

To be included as a schizophrenia proband, participants were required to have a diagnosis of schizophrenia or schizoaffective disorder, depressed type as determined by

SCID diagnosis confirmed by consensus review. Exclusion criteria for schizophrenia probands included being over 60 years old, lacking first-degree biological relatives, being an adoptee, IQ < 70, substance dependence in the past 6 months, substance abuse in the two weeks prior to study participation, or more than three substantial uses of inhalants. Probands were further excluded for a past skull fracture or loss of consciousness of 30 minutes or more, past electroconvulsive therapy, a current or past diagnosis of epilepsy, a history of multiple seizures in adulthood, a documented seizure in the 6 months prior to participation, a history of strokes, other neurological conditions, possessing non-removable hearing aids, legal blindness, having an uncorrected lazy eye, compromised visual acuity unable to be corrected to normal, other visual conditions that compromise vision, and other general medical conditions that made participation impossible and/or substantially affected brain functioning. Controls had all the same exclusion criteria as schizophrenia probands, except that controls could participate without first-degree relatives; in addition, a past or current diagnosis of schizophrenia, schizoaffective disorder, any other psychotic disorder, bipolar affective disorder (I or II), learning disability, a past or current depressive episode, and/or a family history of psychotic symptoms or bipolar disorder precluded participation as a control. The only exclusion criteria for participation as a first-degree relative of a person with schizophrenia were visual conditions / acuity that could not be corrected to normal and/or general medical conditions that prevented participation.

SPAM Task

The EEG data analyzed were recorded from participants during performance of the Spatial Working Memory (SPAM) task (Figure 4), adapted from a delayed response task administered to people with schizophrenia by Park (1997). In the SPAM task, either two or three memory stimuli were presented in sequence at one of sixteen possible locations configured circularly around a central fixation. These memory stimuli were either "targets" (black circles) or "distractors" (black squares). After all memory stimuli were presented, a probe stimulus (green circle) appeared at one of the sixteen possible locations, and participants were asked to indicate whether or not the probe appeared in the position of a previous target stimulus. It was emphasized that if the probe appeared in the position of a previous distractor stimulus, "no" was the correct response. The task included 2 two-stimulus blocks and 6 three-stimulus blocks of 36 trials each, presented in a pseudo-randomized order. Participants who performed at less than 60% accuracy on two-stimulus trials were excluded from behavioral and ERP analyses. See Figure 4 for information regarding stimulus timing and duration.

EEG Recording and Preprocessing

EEG was recorded using a BioSemi Active-Two *AgCl* electrode system (BioSemi Inc., Amsterdam, The Netherlands). Recordings were made using a 128-channel, full scalp dense array sampled at 1024hz. Recordings were down-sampled offline to 512hz, high-pass filtered at 0.5hz, and transformed to a linked earlobe reference.

Data were preprocessed using a custom independent component analysis (ICA) based method for ocular, muscular and cardiac artifact removal. Data were visually inspected and bad electrodes and time segments judged to contain significant signal noise

other than brain activity were excluded. Continuous recordings were epoched into 1000ms stimulus-locked epochs (150ms pre-stimulus, 850ms post-stimulus). The epoched data were transformed into the frequency domain and plotted highlighting low-frequency and high-frequency signal in sequence, with extreme epochs being removed based on visual inspection. Data were retransformed into the time domain, and final ICs were identified as either primarily brain or artifact based on visual inspection; the denoised signal was reconstituted using those ICs dominated by brain signal. Participants for whom greater than 35% of their EEG data were contaminated by artifact were excluded from further analyses.

Laplacian Current Source Density Transformation

In order to minimize the effects of volume conduction, which may produce spuriously high synchronization values for nearby electrode sites and potentially distort power computations, a Laplacian current source density (CSD) transformation was applied to the filtered data prior to time-frequency decomposition (see Trujillo, Peterson, Kaszniak, & Allen, 2005).

Time-Frequency Decomposition

EEG were analyzed using time-frequency decomposition methods, which extract both power and phase information for various frequencies of oscillatory activity that comprise "raw" EEG data. The EEG data underwent analyses focused on time-frequency power data, time-frequency phase data, and a combination of the two in analyses related to phase-amplitude coupling. Though these techniques will be detailed below, the time-frequency decomposition methods utilized varied dependent upon the particular analysis.

For analyses of time-frequency power information alone, a discrete time-frequency decomposition of the CSD transformed data using a binomial kernel for convolution was utilized to extract power information. For the extraction of phase synchrony information (see below), Morlet wavelets were convolved with the CSD transformed data, where the number of cycles comprising the wavelet varied depending upon the target frequency for convolution. Morlet wavelet convolution was also used for the extraction of information necessary to compute phase-amplitude coupling (e.g., both power and phase information). All time-frequency decomposition was performed in MATLAB (http://www.mathworks.com/). Given the emphasis of the Lisman and Idiart (1995) model on encoding stimuli into memory, all analyses focused on oscillatory responses to memory stimuli (e.g., the encoding phase of working memory).

Principal Components Analysis

In order to determine relevant frequency and time windows for further analysis, time-frequency power surfaces were subject to principal components analysis (PCA) in accordance with methods employed by Bernat, Williams and Gehring (2005). In order to accomplish PCA utilizing multiple two-dimensional time-frequency energy surfaces, the rows of a given surface (e.g., different 1hz frequency bands in these data) were concatenated together into one long row containing all time samples for all frequencies. This procedure was repeated for all energy surfaces for all electrodes for all subjects, and the resulting rows were stacked to create one large matrix representing all data for all frequencies and electrodes across all subjects. This matrix was then subjected to traditional PCA, after which the resulting principal components (PCs) were rearranged

into time *x* frequency surfaces by effectively reversing the procedure above. This method is possible and valid on account of the fact that the decomposition process is not affected by the structured reordering of the data by row-long units (Bernat, Williams & Gehring, 2005).

Separate PCAs were conducted for the induced and evoked power data (see below). For each dataset, multiple PCA solutions were examined in sequence, beginning with the simplest (1 PC) solution and progressing until PCs emerged with activity focused in theta- and gamma-band windows. A final solution was chosen by selecting the simplest solution (e.g., fewest PCs) that provided clean cut definitions of target time *x* frequency windows in the bands of interest. PCs from these solutions with focused theta- and gamma-band activity were then used to define both windows for computing median values for statistical analysis as well as to reduce the number of electrodes used in subsequent analyses by determining which electrode sites loaded most strongly onto the relevant PCs. In selecting windows of interest, preference was given to windows that encompassed activity over multiple frequency bands within theta and gamma-frequencies so as to avoid focusing too narrowly without significant a priori justification. For determining theta-band target windows, activity from all frequencies (1-30hz) was submitted to PCA. For the determination of gamma-band windows, only activity above 30hz was submitted to PCA due to the high variance accounted for by lower frequency activity.

Theta- and delta-band induced power / phase synchrony windows of interest. The chosen PCA solution used in determining a target theta-band window for induced

power analyses is depicted in Figure 5. On the basis of PCs 1 and 2 from this solution, a window of 150-300ms from 4-8hz was selected for time-frequency power and phase analyses of theta activity. However, examination of the PCs also suggested prominent activity in lower frequencies. As such, supported again by PCs 1 and 2, an additional delta window of 1-3hz from 150-600ms was also used in power and phase analyses. A union of those electrodes that had positive loadings exceeding one standard deviation of all loadings for each respective PC, comprised by Fp1, F8, C4, Pz, T6/P8, Oz, and O2, were examined in subsequent induced power and phase synchrony analyses of theta- and delta-band activity to increase statistical power and limit multiple comparisons.

Upon examination of time-frequency surfaces for induced power in the theta- and delta-frequencies, the initial PCA-informed time-frequency windows were slightly adjusted to better capture apparent areas of interest. The theta-band window was adjusted to 4 to 8hz, 100-250ms post-stimulus, and the delta-band window was adjusted to 1 to 2hz, 100-300ms post-stimulus (see Figures 17 through 21).

Gamma- band induced power / phase synchrony windows of interest. Two PCA solutions were utilized in determining target gamma-band windows for induced power analyses. The first 12 PC solution is depicted in Figure 6. On the basis of PC 5 from this solution, windows of 36-56hz from 425-775ms post-stimulus, 64-81hz from 425-775ms post-stimulus, and 71-81hz from 100-400ms post-stimulus were selected for time-frequency power and phase analyses. The second 13 PC solution is depicted in Figure 7. On the basis of PC 3 from this solution, an additional window of 86-126hz from 100-400ms post-stimulus was added, while previous windows of 36-56hz and 64-

81hz from 425-775ms post-stimulus were supported. Just as was done with the lower frequency data, a union of those electrodes with loadings on each of the relevant PCs exceeding one standard deviation of all loadings, which was comprised by electrodes Cz, Pz, P4, T4/T8, T5/P7, T6/P8, and O1, was utilized in induced power and phase synchrony analyses of gamma-band activity.

Theta- and delta-band evoked power windows of interest. Separate PCAs were run for evoked power data. The chosen PCA solution for the lower frequencies is depicted in Figure 8. Here, the two PCs together suggested one theta window and two delta windows for analysis: a 4-8hz, 150-300ms post-stimulus window for theta (PCs 1 and 2), a 2-4hz, 150-400ms post-stimulus for delta (PC 1), and another 1-2hz, 200-700ms post-stimulus window for delta (PC 2); these windows were used for evoked power analyses. Once more, a union of those electrodes whose loadings exceeded more than one standard deviation for a given PC were used to determine electrodes for subsequent analysis; here, this union set was comprised by electrodes F3, C3, C4, Pz, P4, and T6/P8.

Gamma-band evoked power window of interest. In the gamma PCA, the windows determined in the induced power solution were not observed in any of the solutions examined. The PCA solution chosen for the evoked power gamma-activity is depicted in Figure 9. On the basis of PC 6 from this solution, a window of 73-93hz from 150-775ms post-stimulus was selected for gamma-band evoked power analyses. Electrodes F8, Fp1, Cz, C3, Pz, P3, T3/T7, T4/T8, and T5/P7 had positive loadings on this component and were thus the focus of the evoked gamma-power analyses.

Time-Frequency Power Analyses

In time-frequency analysis, it is possible and prudent to investigate two types of changes in power elicited by stimulus events: evoked power and induced power. Evoked power is akin to the ERP in broadband time-series analyses, in that evoked power is computed by averaging all trials in the time domain and subsequently performing time-frequency decomposition on the time-averaged data to calculate the power response in a specified time window from said average. Induced power, in contrast, is calculated through time-frequency decomposition of each individual trial and subsequently averaging the time-frequency surfaces for each trial; such a procedure captures changes in power that are not strictly time-locked to stimulus events, but elicited by task stimuli nonetheless (Roach & Mathalon, 2008).

Both evoked and induced power in response to the sequentially presented stimuli in the SPAM task were examined for the delta-, theta- and gamma-band windows of interest. For both evoked and induced power transformations, a discrete time-frequency decomposition with a binomial kernel was applied to the time domain data to extract power information in the time-frequency domain. To extract evoked power information, the transformation was applied to each subject's condition-level average ERP. To extract induced power information, the time-frequency decomposition was applied to each individual stimulus / trial for each subject, and these surfaces were subsequently averaged to produce mean time-frequency surfaces for each relevant condition.

To examine differential changes in power with increasing working memory load, evoked and induced power were examined separately for stimuli presented first, second and third in sequence. To examine the modulation of power in response to stimulus relevance, evoked and induced power were examined separately for target stimuli versus distractor stimuli.

Baseline Correction

Examination of time-frequency surfaces revealed notable "edge effects" in the data, well-known artifacts in time-frequency decomposition that often occur at the beginning and end of analyzed data epochs (Roach & Mathalon, 2008). Ideally, time-frequency decomposition methods would be applied to a notably longer epoch than the time window intended to be analyzed, such that the excess (including any derived edge effects) may be trimmed off prior to analysis. However, in the SPAM task, relevant stimuli were presented once every second, such that extending the epoch beyond the 1000ms utilized herein would have led to potential contamination from preceding and / or subsequent stimuli. To avoid baseline contamination from both edge effects and preceding stimuli, a baseline period of 0 to 50ms *post*-stimulus was used, as visual inspection of the data suggested this period was free from distortion related to edge effects and could still be reasonably assumed to contain minimal brain activity related to the memory processes this analysis intended to target.

Data were baseline corrected by subtracting the median value for the 50ms immediately following the stimulus from each subsequent data point and subsequently

dividing by the standard deviation of the baseline for each 1-hz frequency band. For the power analyses, the resulting unitless measure represents a standardized magnitude of change in power, either evoked or induced, as compared to the baseline period. For phase synchrony analyses, this measure represents a change in synchrony as compared to the baseline period. Similarly, for cross-frequency-coupling measures, relevant indices of cross-frequency coupling (PAC for phase-amplitude coupling or PPC for phase-phase coupling) were divided by corresponding values in the 50ms time sample that contained the same baseline period used in the power and phase analyses. Thus, analyzed PAC and PPC measures represented a change in these metrics from the baseline period.

Statistical Analysis: Evoked and Induced Power

Differences in measures of evoked and induced power between PSZ, REL, and CTRL were assessed using mixed model, repeated measures ANOVA, with evoked and induced power analyzed separately. For each analysis, fixed factors of diagnostic group (PSZ versus REL versus CTRL), order of stimulus presentation (first versus second versus third), and electrode site were included. Subject was included as a random factor in all ANOVAs. Examined conditions found to violate assumptions of sphericity were corrected using the Greenhouse-Geisser procedure, and subsequently adjusted degrees of freedom are reported where appropriate.

Time-Frequency Phase Synchrony Analyses

Phase-synchrony measures were also computed for the delta-, theta- and gamma-band windows of interest derived from the PCA of the power data. To reduce multiple

comparisons and increase statistical power, phase-synchrony for a given time-frequency window was computed for all possible electrode pairings for all electrodes utilized in either the induced or evoked power analyses (see above for listings). Phase-synchrony was quantified in accordance with Cohen's (2014) procedure; though he called his measure intersite phase clustering (ISPC), it is identical to Lachaux, Rodriguez, Martinerie, and Varela's (1999) phase-locking value (PLV), as it is more frequently termed:

$$\mathrm{ISPC}_f = \left| n^{-1} \sum_{t=1}^{n} e^{i(\emptyset_{xt} - \emptyset_{yt})} \right|,$$

in which n represents the number of time points t over which synchrony was examined, and ϕ_x and ϕ_y are the phase angles from electrodes x and y for frequency f. Phase angles for the electrodes to be compared were extracted via the convolution of Morlet wavelets with the time-domain data, where the number of cycles comprising the wavelet varied depending upon the target frequency for convolution.

$ISPC_f$ was computed for individual stimuli in each appropriate electrode pairing within trials in sliding time segments over the post-stimulus period to produce post-stimulus $ISPC_f$ values associated with each individual stimulus. To determine whether phase-synchrony was differentially affected by stimulus type, $ISPC_f$ stimulus values were subsequently averaged for target versus distractor stimuli to produce $ISPC_f$ values for each type of stimulus. $ISPC_f$ was similarly computed for the 0-50ms post-stimulus baseline period for each-electrode pairing, subject, and group.

To assess group differences in $ISPC_f$, $ISPC_f$ values for a given electrode pair and

time-frequency window of interest were submitted to one-sample *t*-tests to determine whether values differed from those at baseline. For those pairs that showed increases in $ISPC_f$ from the baseline period, analysis of variance was conducted for each electrode pairing to determine whether $ISPC_f$ differed between groups at said electrode pair. Again, examined effects that violated assumptions of sphericity were corrected using the Greenhouse-Geisser procedure, and subsequently adjusted degrees of freedom are reported where appropriate.

Phase-Amplitude Coupling

Examination of cross-frequency coupling was pioneered by Canolty and colleagues (2006), and their methods have come to represent analytical standards (Cohen, 2014). As such, their methods were utilized for analysis of theta-gamma coupling in the SPAM task. The strength of phase-amplitude coupling between the phase of a (typically low) frequency f_1 and the amplitude of a (typically higher) frequency f_2 is quantified through first constructing a composite complex signal $z(t)$ through the combination of the phase-angle time series of f_1 (ϕ_{f1}) with the amplitude time series of f_2 (A_{f2}):

$$z(t) = A_{f2}(t) * e^{i\emptyset_{f1}(t)},$$

where t represents the time point at which instantaneous amplitude and phase angle are extracted. Each complex value of $z(t)$, when plotted in complex space, can be thought to represent the endpoint of a vector extending from the origin (see Figure 10A-E). The length of this vector represents the magnitude of f_2 amplitude at time point t, and the angle formed by the x-axis and the vector is equivalent to the phase angle of f_2 at said

time point (Canolty et al., 2006; Cohen, 2014). As such, the mean (M) of z(t) provides an index of overall phase-amplitude coupling, PAC, in the length of the mean vector as well as the phase of f_1 that is associated with the largest amplitudes for f_2.

PAC was computed within subjects for all individual stimuli at a subset of electrodes selected again on the basis of their loadings on their respective relevant principal components. Those electrodes with loadings that exceeded one standard deviation of all loadings taken together *and* that were used in both theta- and gamma-band analyses (e.g., an intersection set between theta- and gamma- electrodes) were initially selected. This intersection set was comprised by C3, Cz, Pz, P4, and O1. In order to analyze mirror sites in each hemisphere, this set was adjusted to C3, C4, P3, P4, O1, and O2. Phase and power data were both extracted via convolution with separate Morlet wavelets for lower (phase) and higher (amplitude) frequencies. 1hz frequency bands from 4-8hz were used as the lower (phase) frequencies. Upper frequencies (amplitude) ranged from 32.5hz to 58.5hz in 2hz increments; these half-hertz points were used to ease computational demands in these highly exploratory analyses as convolution with a wavelet built for these frequencies may be reasonably assumed to resemble integer frequencies both immediately above and below the center frequency. PAC was calculated from 100ms to 600ms post-stimulus and divided by the baseline PAC value at 50ms, again selected to avoid potential contamination from edge effects. Thus, reported PAC values, akin to the reported IPSC values for phase-synchrony, represent change in PAC as compared to baseline.

Principal components and statistical analysis. As with the time-frequency energy data, the PAC surfaces were submitted to PCA in an effort to isolate the most relevant frequency pairings, time samples, and electrode sites for statistical analysis. In light of four relevant factors (low- / phase-frequency, high- / power-frequency, time sample, and electrode site), high-frequency by time-sample surfaces for a given electrode site at a given low-frequency were tiled to represent all data in a single surface prior to restructuring for PCA as described above. The resulting PCs were then interpreted according to this structural layout, with regions of interest being identified in most cases according to identified high-frequency bands with prominent activity in PCs comprising the utilized solution(s) (see Figure 11).

Guided by examination of scree plots and visual inspection of solutions to determine the number of PCs to be selected for analysis, an 8 PC solution was chosen for PAC analysis (Figure 11). On the basis of this solution, various low-frequency to high-frequency pairings at particular electrode sites were selected for analysis: 4hz and 52.5hz at O2, 5hz and 34.5hz at O2, 5hz and 42.5hz at O1, 7hz and 32.5hz at C4, 7hz and 36.5hz at O2, 7hz and 40.5hz at P4 and C3, 7hz and 42.5hz at C4, 7hz and 44.5hz at C3, 7hz and 46.5hz at O2, 7hz and 48.5hz at O2, 7hz and 50.5hz at C4, and 7hz and 54.5hz at C3. PAC values for CTRL associated with each of these low-frequency band / high-frequency band / electrode sites were first subjected one sample *t*-tests to determine whether PAC increased meaningfully from baseline. If so, PAC values for all participants were subjected to subsequent repeated measures ANOVA with fixed-factors of diagnostic grouping and time sample; a random factor of subject was also included in each

ANOVA. The Greenhouse-Geisser correction for violations of sphericity assumptions were again utilized and reported appropriately.

Phase-Phase Coupling

Phase-phase coupling was computed by extracting phase values from both theta- and gamma-band frequencies and computing phase-synchrony between the activity in the different frequency bands (e.g., Mormann et al., 2005). This measure, termed the synchronization index (SI; Cohen, 2008), is essentially ISPC between phase-angles of differing frequencies rather than different electrodes:

$$\mathrm{SI} = \left| n^{-1} \sum_{t=1}^{n} e^{i(\emptyset_{lt} - \emptyset_{ut})} \right|,$$

where ϕ_{lt} represents the phase-angle of the lower frequency at time t, and ϕ_{ut} that of the higher-frequency.

As with the phase-amplitude analysis, SI was computed for the same subset of electrodes whose loadings exceeded one standard deviation for both theta- and gamma-band principal components that was utilized for PAC_z. Again, lower frequencies ranged from 4-8hz, with 1hz frequency bands, while limited upper frequency bands ranging from 32.5hz to 58.5 incremented by 2hz were used to compute SI. SI was computed for individual stimuli at each individual electrode site for each combination of low-frequency and high-frequency activity, and averaged thereafter across all stimuli within each subject. PPC values for 100ms through 600ms were divided by PPC at baseline (50ms)

to extract a value representing change in phase-phase coupling from baseline, which was used for subsequent analyses.

As with the PAC analyses, scree plots and various PCA solutions were visually inspected to determine the number of PCs to be selected for analysis. The 8 PC solution chosen is depicted in Figure 12. On the basis of this solution, various low-frequency to high-frequency pairings at particular electrode sites were selected for analysis: 4hz and 40.5hz at C4, 4hz and 44.5hz at O1, 4hz and 48.5hz at C4, 4hz and 52.5hz at O1, 4hz and 54.5hz at O2, 4hz and 56.6hz at P4, 6hz and 34.5hz at O1, 6hz and 36.5hz at C4, 6hz and 40.5hz at O1, 6hz and 42.5hz at P4, 6hz and 44.5hz at C3 *and* P3, 6hz and 48.5hz at O1 *and* O2, 6hz and 52.5hz at O1, 6hz and 54.5hz at O1, 6hz and 56.5hz at O2, 6hz and 58.5hz at O1, 7hz and 46.5hz at C4, 8hz and 34.5hz at C3, and 8hz and 38.5hz at P4. PPC values for CTRL associated with each of these low-frequency and high-frequency bands were first averaged across time and electrode site and subsequently subjected to single-sample *t*-tests to determine whether PPC values differed from baseline. PPC values were thereafter subjected to individual repeated measures ANOVA for each low-to-high-frequency pairing with fixed-factors of diagnostic grouping, time sample, and electrode site. A random factor of subject was also included in each ANOVA. Once more, the Greenhouse-Geisser correction for violations of sphericity assumptions were again utilized and reported appropriately.

Predicting WM Task Performance[2]

To determine which examined variables were most effective predictors of participants' performance on the WM task, ridge regression was used to first identify a subset of variables that may potentially have the most predictive utility. Ridge regression, a type of penalized regression, is an extension of ordinary least squares regression that adds a "shrinkage" penalty equal to the sum of the squared regression coefficients scaled by a tuning parameter λ. This tuning parameter, ranging from 0 to infinity, is meant to control the size of the coefficients. Of several options for penalized regression, ridge regression was ultimately selected as it is the least stringent of available options and is preferable in cases of highly correlated predictors, which is often the case in psychophysiological analyses such as those employed here. To identify ideal values for the tuning parameter λ, the *glmnet* package (Friedman et al., 2010) for the R programming language was utilized to employ *k*-fold cross-validation for selecting the optimal value for λ. In accordance with procedures described by Abram and colleagues (2016), *k*-fold cross-validation was applied to each of 5000 bootstrap samples of the full dataset to obtain bootstrap distributions for each of the predictors submitted to the ridge regression. The 95% confidence intervals derived from each of these bootstrap distributions were subsequently examined, and a given predictor was selected for inclusion in subsequent modeling if its respective confidence interval did not contain

[2] This entire section and the procedures therein described are strongly informed by Abram et al., 2016. Code provided in the supplementary materials for this publication was adapted for use with the present data.

zero. Thereafter, predictors identified by the bootstrapped ridge regression procedure were submitted to ordinary least squares regression.

In an effort to tease out potentially unique effects related to distractor stimuli, three separate analyses were run: one predicting overall WM task performance, one predicting performance on target only trials, and one predicting performance on trials featuring distractors. In all cases, all variables which demonstrated a main or interaction effect in previous analyses were submitted to ridge regression, with the exception of diagnostic status; no interaction effects were included in the ridge regression procedure. Predictors and WM task performance outcome measures were verified to sufficiently meet assumptions of normality and homoscedasticity, and thereafter standardized. Bootstrapped ridge regression and subsequent evaluation of confidence intervals for each coefficient's bootstrap distribution identified several relevant predictors for each of the models. These identified predictors were then submitted to ordinary least squares regression to produce typical regression models for each WM performance outcome.

Results

Working Memory Task

Performance on the WM task was extensively analyzed by Lynn, Kang and Sponheim (2016) for a slightly larger sample (three subjects were removed from the original sample due to EEG data unsuitable for time-frequency analyses). Performance on the task was reanalyzed for the current sample, and a summary of performance as well as related group effects are presented in Table 2. All relevant effects described previously persist in the present sample.

Evoked Power

Theta-band (4-8hz).

Time-frequency energy – order of stimulus presentation. Time-frequency energy surfaces were computed for stimuli based on the sequential order in which they were presented, and median energy in the theta window of interest (4-8hz, 100-250ms), was computed to determine whether it varied with stimulus presentation order. ANOVA did indeed reveal a main effect of presentation order on elicited theta energy, $F(2,162)=35.00$, $p<.001$. Here, energy increases from baseline were different for each ordered stimuli, with 2nd stimuli showed the greatest increases (2nd stimulus > 3rd stimulus > 1st stimulus, *ps*<.001; see Figure 13). Thus, evoked theta energy in the target window differed for each stimulus by order of presentation, with second stimuli eliciting the greatest energy increases.

Time-frequency energy – stimulus type. Time-frequency energy surfaces were likewise computed for stimuli based on the type of stimulus (target versus distractor), and median theta energy in the target window was computed to determine whether it varied with type. Here, ANOVA did reveal a main effect of type on evoked theta energy, $F(1,81)=5.66$, $p=.02$, where energy in response to target stimuli was greater than that to distractors ($p=.02$; Figure 14). Thus, targets elicited more evoked energy in the examined theta window than did distractors.

Delta-band (2-4hz).

Time-frequency energy – order of stimulus presentation. As described above, PCA of time-frequency evoked power showed significant variance in frequencies even lower than theta. As such, median energy in a delta-band window of interest (2-4hz, 150-400ms), was computed to determine whether power in this time-frequency window varied by stimulus presentation order. A main effect of order was indeed observed for this window, $F(2,162)=6.59$, $p=.004$. Here, energy increases in response to 2nd stimuli were greater than those to 1st ($p=.009$), as were those to 3rd ($p=.05$; Figure 15). Thus, evoked delta (2-4hz) power varied with stimulus presentation order.

Time-frequency energy – stimulus type. Median delta energy in the 2-4hz target window was also subjected to ANOVA to determine whether it varied with type. Here, ANOVA showed only a marginal effect of electrode site, $F(5,405)=2.20$, $p=.07$; here, evoked energy increases at Pz were greater than those at C4 ($p=.04$). Thus, energy increases in the target delta window did not vary between target and distractor stimuli.

Delta-band (1-2hz).

Time-frequency energy – order of stimulus presentation. Median energy in a lower delta window of interest (1-2hz, 200-700ms), was also computed on the basis of the low-frequency evoked energy PCA. ANOVA again revealed a main effect of presentation order on evoked delta energy, $F(2,162)=3.27$, $p=.046$. Here, energy increases to 2nd stimuli were greater than those to first stimuli ($p=.04$; see Figure 16). Thus, increases in low evoked delta energy in the target window were greater in response to second and third stimuli than in response to first stimuli.

Time-frequency energy – stimulus type. As with the 2-3hz delta window, ANOVA on the 1-2hz medians showed only an effect of electrode site, $F(5,405)=3.19$, $p=.01$; as with the presentation order analyses, increases at Pz were marginally greater than those at C4 ($p=.09$). Thus, energy increases in the target delta window did not vary between target and distractor stimuli.

Gamma-band (73-93hz).

Time-frequency energy – order of stimulus presentation and stimulus type. No main or interaction effects were observed for median evoked energy values in the 73hz-93hz window identified by principal components analysis. Thus, evoked energy in this gamma range was not affected by stimulus presentation order or stimulus type.

Induced Power

Theta-band (4-8hz).

Time-frequency energy – order of stimulus presentation. Time-frequency energy surfaces were computed for stimuli based on the sequential order in which they were presented, and median energy in the theta window of interest (4-8hz, 100-250ms), was computed to determine whether it varied with stimulus presentation order. Type II ANOVA revealed a main effect of order of stimulus presentation, $F(2,162)=3.40$, $p=.045$, where increased power in response to third stimuli was greater than decreased power elicited by first stimuli ($p=.04$; Figure 17). A marginal effect of diagnostic grouping was also observed, $F(2,81)=2.58$, $p=.08$, where energy increases for REL differed marginally from energy decreases observed in PSZ ($p=.09$) and CTRL fell in between (see Figure 18 and the next section for the same effect when medians are calculated according to stimulus type). Thus, changes in response to third stimuli differed from those in response to first stimuli, and theta energy in the target window was marginally greater in REL than in PSZ.

Time-frequency energy – stimulus type. Time-frequency energy surfaces were likewise computed for stimuli based on the type of stimulus (target versus distractor), and median theta energy in the target window was computed to determine whether it varied with type. Here, Type II ANOVA revealed a main effect of diagnostic grouping, $F(2,81)=3.19$, $p=.047$, where REL again demonstrated greater theta energy than PSZ ($p=.04$) and CTRL fell in between (Figure 18; note that this is similar to the effect reported in the previous section, except here it achieves statistical significance with different collapsing of variables). Thus, energy changes observed in REL again differed from those observed in PSZ.

Delta-band (1-3hz).

Time-frequency energy – order of stimulus presentation. On the basis of PCA analyses, a delta window of interest (1-3hz, 150-600ms) was also added to analysis of induced energy values. This window was adjusted upon examination of the surfaces to 1-2hz, 100-300ms post-stimulus to better capture apparent activity in the data. Median induced energy in this window was also examined to determine whether it varied with stimulus presentation order. ANOVA indeed revealed a main effect of presentation order on induced delta energy, $F(2,162)=3.79$, $p=.04$. Here, energy increases to 3rd stimuli were greater than those to 1st stimuli ($p = .03$), and increases to 2nd stimuli were marginally greater than those to 1st ($p=.08$; see Figure 19). Furthermore, a marginal interaction effect between diagnostic grouping and presentation order was observed, $F(4,162)=2.41$, $p=.07$ (Figure 20). Here, REL showed a strong effect of stimulus order, $F(2,54)=5.45$, $p=.007$, where energy increases to 3rd stimuli were greater than those to 1st ($p=.005$). CTRL showed a lesser effect, $F(2,68)=2.90$, $p=.08$, in which increases to 3rd stimuli were slightly greater than those to 1st ($p=.06$). No effect of presentation order was observed for PSZ, $F(2,40)=1.42$, $p=.25$. Thus, induced delta energy in the target window was greater in response to third stimuli than first stimuli; this pattern of differences was observed for CTRL and REL, but not PSZ.

Time-frequency energy – stimulus type. Median delta energy in the target window was also subjected to ANOVA to determine whether it varied with type. A strong effect of type was indeed observed, $F(1,81)=13.86$, $p<.001$, where energy elicited by distractor stimuli was greater than that in response to targets ($p<.001$; Figure 21).

Thus, delta-band energy was greater in response to distractor stimuli than to target stimuli.

Gamma-band.

Time-frequency energy in three separate gamma-band time by frequency windows was computed to determine whether these quantities varied with stimulus presentation order and stimulus type.

Time-frequency energy – order of stimulus presentation.

36-56hz, 425-775ms. No main or interaction effects were observed for median induced energy values in the 36-56hz window.

64-81hz, 425-775ms. For the 64-81hz, 425-775ms post-stimulus window, ANOVA revealed a three-way interaction between diagnostic grouping, presentation order and electrode site, $F(24,972)=1.96$, $p=.01$ (Figure 22). Here, an interaction between order and electrode site was observed for REL, $F(12,324)=2.10$, $p=.045$. Herein, an effect of order was observed at T4/T8, $F(2,54)=5.62$, $p=.006$ ($2^{nd} > 1^{st}$, $p=.004$; $3^{rd} > 1^{st}$, $p=.07$), as well as a marginal effect at Pz, $F(2,54)=2.7$, $p=.08$ ($1^{st} > 2^{nd}$, $p=.08$). CTRL showed a marginal interaction effect for order and electrode site, $F(12,408)=1.87$, $p=.07$. Herein, marginal effects of order were observed at O1, $F(2,68)=2.79$, $p=.08$ ($2^{nd} > 1^{st}$, $p=.07$); and Pz, $F(2,68)=2.60$, $p=.09$ ($2^{nd} > 1^{st}$, $p=.09$). No interaction was observed for PSZ, $F(12,240)=1.42$, $p=.22$. Thus, CTRL and REL showed effects of stimulus order in the 64-81hz gamma window at certain electrode sites, whereas PSZ did not.

71-81hz, 100-400ms. For the 71-81hz, 100-400ms post-stimulus window, a marginal interaction effect between diagnostic grouping and presentation order was observed, $F(4,162)=2.41$, $p=.07$ (Figure 23). Here, CTRL showed a marginal effect of presentation order, $F(2,68)=2.83$, $p=.08$, wherein energy increases elicited by first stimuli differed from decreases to third, $p=.06$. REL also showed a marginal effect of order, $F(2,54)=3.29$, $p=.06$, in which increases to 3rd stimuli differed from decreases to 1st, $p=.05$. PSZ showed no effect of presentation order, $F(2,40)=0.89$, $p=.39$. Thus, CTRL and REL demonstrated effects of presentation order on energy changes in the 71-81hz window, while PSZ did not.

86-126hz, 100-400ms. In the 86hz to 126hz, 100-400ms post-stimulus window, an interaction between diagnostic grouping and presentation order was observed, $F(4,162)=3.58$, $p=.02$. However, though the strength of the effect of order varied slightly between diagnostic grouping, no group showed a significant main effect of presentation order (CTRL, $F(2,68)=1.79$, $p=.19$; PSZ, $F(2,40)=1.80$, $p=.19$; REL, $F(2,54)=2.11$, $p=.15$).

Time-frequency energy – stimulus type.

36-56hz, 425-775ms. No main effects or interaction effects were observed for median induced energy values grouped by type in the 36-56hz gamma window.

64-81hz, 425-775ms. For the 64-81hz gamma window, ANOVA revealed a marginal interaction between diagnostic grouping and stimulus type, $F(2,81)=2.52$, $p=.09$. Here, CTRL showed a marginal effect of stimulus type, $F(1,34)=3.78$, $p=.06$,

where increases to targets exceed those to distractors (p=.06). No effect of stimulus type was observed for the 64-81hz window in PSZ, F(1,20)=0.23, p=.64, or REL, F(1,27)=1.60, p=.22. Thus, a slight effect of stimulus type was observed for CTRL but not for PSZ or REL.*71-81hz, 100-400ms.* For the 71-81hz, 100ms-400ms post-stimulus window, an interaction effect between diagnostic grouping and stimulus type was observed, F(2,81)=3.33, p=.04 (Figure 24). Here, CTRL showed an effect of stimulus type, F(1,34)=4.89, p=.03, in which energy increases to targets differed from decreases to distractors (p=.03). No effect of stimulus type was observed for PSZ, F(1,20)=1.01, p=.33, or REL, F(1,27)=0.46, p=.51. Thus, stimulus type had an effect on energy changes from baseline in the 71-81hz window for CTRL but not PSZ or REL.

86-126hz, 100-400ms. For median energy change values in the 86-126hz, 100-400ms post-stimulus window, ANOVA revealed an interaction effect for diagnostic grouping and electrode site, F(2,81)=1.58, p=.048. Here, PSZ showed an effect of electrode site, F(6,120)=3.02, p=.03, where changes at P4 differed from those at O1 (p=.04) and T4/T8 (p=.02); changes at T5/P7 were also marginally different from those at T4/T8 (p=.09). REL showed a marginal effect of electrode site, F(6,162)=2.17, p=.08. Here, though values differed superficially across electrodes, post-hoc tests revealed no meaningful differences. No effect of electrode site was observed for CTRL, F(6,204)=0.94, p=.45. Thus, PSZ showed meaningful differences in the 86-126hz gamma window from electrode to electrode, while CTRL and REL did not.

Intersite Phase Clustering (Phase Locking Value)

Median intersite phase clustering coefficients (e.g., phase locking values) were calculated within the various windows of interest determined by PCA for each possible pairing of electrodes associated with the principal component of interest. CTRL values for each electrode pair were subjected to one-sample *t*-tests to determine those electrode pairs that showed significant intersite phase synchrony (e.g., values different from zero) in the respective target windows.

Theta-band (4-8hz).

ISPC, 4-8hz, 100-250ms. One-sample *t*-tests on median intersite phase clustering coefficients (e.g., phase locking values) in CTRL for the target theta window (4-8hz, 100-250ms post-stimulus) revealed several electrode pairs demonstrating synchrony changes compared to baseline at an alpha level of .10 in response to target stimuli (Figure 25a): a decrease between C3 and T6/P8, $t(35)=-3.83$, $p<.001$; a decrease between Oz and T6/P8, $t(35)=-3.02$, $p=.005$; an increase between F3 and O2, $t(35)=2.99$, $p=.005$; an increase between Fp1 and Pz, $t(35)=1.93$, $p=.06$; an increase between C4 and O2, $t(35)=1.80$, $p=.08$; a decrease between Fp1 and O2, $t(35)=-1.80$, $p=.08$; and an increase between F3 and Oz, $t(35)=1.74$, $p=.09$. Phase synchrony values within these pairs differed between groups for C3 and T6/P8, $F(2,84)=8.47$, $p<.001$; here, decreases in CTRL differed from changes observed in PSZ and REL (ps < .03). Marginal group differences were also observed for T6/P8 and Oz, $F(2,84)=2.76$, $p=.07$ (CTRL < PSZ, $p=.06$); and F3 and O2, $F(2,84)=3.07$, $p=.05$ (CTRL > PSZ, $p=.06$); No group differences were found for Fp1 and Pz, $F(2,84)=0.61$, $p=.55$; C4 and O2 $F(2,84)=1.17$, $p=.32$; Fp1 and O2, $F(2,84)=0.53$, $p=.59$, or F3 and Oz, $F(2,84)=0.75$, $p=.47$. Notably, PSZ showed meaningful phase

synchrony changes for only one pair, namely an increase from baseline between C3 and T6/P8, $t(21)=3.23$, $p=.004$ (Figure 25c). REL showed no significant changes from baseline in phase synchrony for these pairs in the theta window ($ps > .74$). Thus, PSZ showed theta-band phase synchrony changes in only one electrode pair for which CTRL showed changes, while REL showed no changes any of these pairs.

CTRL additionally showed phase synchrony changes in the target theta window in response to distractors in three electrode pairs (Figure 25b): an increase between Fp1 and Oz, $t(35)=2.75$, $p=.01$; a decrease between F3 and P4, $t(35)=-2.44$, $p=.03$; and an increase between Fp1 and T6/P8, $t(35)=1.94$, $p=.07$. Neither PSZ nor REL ($ps>.40$) showed any meaningful synchrony changes from baseline in the theta window in response to distractor stimuli. However, ANOVA also revealed that group differences for these pairs did not achieve statistical significance ($ps>.76$). Thus, while CTRL alone did show synchrony changes in the target theta window as compared to baseline, these changes did not differ meaningfully from those observed in PSZ and REL.

Gamma-band.

ISPC, 36-56hz, 425-775ms. One sample *t*-tests on IPSC values in CTRL for the 36-56hz, 425-775ms post-stimulus gamma window showed many electrode pairs demonstrating synchrony changes at an alpha level of .10 in response to target stimuli (Figure 26a): an increase between T4/T8 and T6/P8, $t(35)=2.65$, $p=.01$; an increase between C3 and T4/T8, $t(35)=2.39$, $p=.02$; an increase between F8 and Pz, $t(35)=2.37$, $p=.02$; a *decrease* between T3/T7 and T5/P7, $t(35)=-2.03$, $p=.05$; and an increase between

T4/T8 and T5/P7, $t(35)=1.95$, $p=.06$. PSZ showed no synchrony changes in any of these pairs; REL showed synchrony changes to target stimuli in the 36-56hz gamma window for only one of these electrode pairs, namely an increase between C3 and T4/T8, $t(29)=2.26$, $p=.03$ (Figure 26e). However, ANOVA revealed no meaningful group differences for these electrode pairs ($ps>.12$) Thus, in response to target stimuli, REL showed synchrony increases in the 36-56hz window in a single electrode pair where CTRL showed changes, while PSZ showed no synchrony changes for these pairs; however, the groups did not meaningfully differ for any of these sites within the 36-56hz gamma window.

CTRL also showed several electrode pairs demonstrating synchrony changes in the 36-56hz window in response to distractor stimuli (Figure 26b): a decrease between Fp1 and P3, $t(35)=-3.64$, $p=.002$; an increase between T4/T8 and T5/P7, $t(35)=3.29$, $p=.004$; an increase between Pz and T5/P7, $t(35)=2.89$, $p=.01$; an increase between Pz and T4/T8, $t(35)=2.68$, $p=.02$; a decrease between Fp1 and T6/P8, $t(35)=-2.37$, $p=.03$; a decrease between Fp1 and T5/P7, $t(35)=-2.11$, $p=.049$; a decrease between Fp1 and Cz, $t(35)=-2.05$, $p=.06$; a decrease between Fp1 and T3/T7, $t(35)=-1.87$, $p=.08$; a decrease between C3 and T6/P8, $t(35)=-1.79$, $p=.09$; and a decrease between T5/P7 and T6/P8, $t(35)=-1.74$, $p=.099$. PSZ again showed synchrony changes in the 36-56hz gamma window in response to distractors for only one these electrode pairs, namely an increase between Fp1 and Cz, $t(21)=2.43$, $p=.02$ (Figure 26d). REL also showed synchrony changes in only one of these pairs, namely an increase between Fp1 and T3/T7, $t(29)=2.42$, $p=.02$ (Figure 26f).

Several group differences were observed for phase synchrony in the 36-56hz gamma window in response to distractor stimuli (Figure 27): between T4/T8 and T5/P7, $F(2,84)=3.51$, $p=.03$, where increases in CTRL differed from minimal changes observed REL ($p=.03$); between Fp1 and T5/P7, $F(2,84)=3.34$, $p=.04$, where decreases in CTRL differed slightly from slight increases in REL ($p=.06$); between Fp1 and Cz, where decreases in CTRL differed from increases in PSZ ($p=.004$); and between Fp1 and T3/T7, $F(2,84)=5.58$, $p=.005$, where decreases in CTRL differed from increases in REL ($p=.004$). Marginal effects of group were observed for Fp1 and P3, $F(2,84)=3.01$, $p=.06$, in which decreases in CTRL differed from minimal change in REL, $p=.04$; and for Pz and T4/T8, $F(2,84)=3.05$, $p=.05$, where increases in CTRL were greater than slight decreases in REL ($p=.08$). No group differences were observed for the other electrode pairs ($ps>.31$). Thus, PSZ and REL showed synchrony changes from baseline in different single electrode pairs where changes were observed for CTRL in response to distractors for the 36-56z gamma window; furthermore, group differences in synchrony changes were observed for a variety of different electrode pairs, many of which included a frontoparietal sensor.

ISPC, 64-81hz, 425-775ms. One-sample *t*-tests on median IPSC coefficients (e.g., phase locking values) in CTRL for the 64-81hz, 425-775ms post-stimulus gamma window revealed no electrode pairs demonstrating changes in phase synchrony in response to target stimuli for the CTRL (alpha = .10). However, CTRL showed several electrode pairs demonstrating synchrony changes in response to distractor stimuli: an increase between T6/P8 and O1, $t(35)=2.23$, $p=.04$; an increase between C3 and T4/T8,

t(35)=2.03, *p*=.06; a *decrease* between C3 and P4, *t*(35)=-1.90, *p*=.07; an increase between F8 and Pz, *t*(35)=1.90, *p*=.07; and an increase between P4 and T6/P8, *t*(35)=-2.32, *p*=.03 (Figure 28a). PSZ showed synchrony changes in only one of these electrode pairs (Figure 28b): a marginal increase between O1 and T6/P8, *t*(21)=1.82, *p*=.08. REL showed no synchrony changes to distractors for any of these electrode pairs (*p*s>.29). A marginal effect of group was observed only for Pz and F8, *F*(2,84)=2.77, *p*=.07; here, slight increases in PSZ differed from mild decreases in REL (*p*=.08). No group differences were observed for the other electrode pairs (*p*s>.32). Thus, CTRL showed synchrony changes only to distractors in the 64-81hz gamma window; PSZ showed marginal synchrony increases for only one pair where CTRL did, while REL showed none in the CTRL pairs, and minimal group differences were observed for these sites in the 64-81hz gamma window.

IPSC, 71-81hz, 100-400ms. One-sample *t*-tests on median IPSC (e.g., phase locking values) for the 71-81hz, 100-400ms post-stimulus gamma window also revealed synchrony changes as compared to baseline in CTRL in a variety of electrode pairs (Figure 29a): an increase between Pz and T4/T8, *t*(35)=2.63, *p*=.01; a decrease between C3 and P3, *t*(35)=-2.38, *p*=.02; an increase between Cz and P3, *t*(35)=2.20, *p*=.03; a decrease between F8 and Cz, *t*(35)=-1.90, *p*=.07; an increase between F8 and P4, *t*(35)=1.88, *p*=.07; a decrease between P4 and O1, *t*(35)=-1.88, *p*=.07; and an increase between Cz and T6/P8, *t*(35)=1.74, *p*=.09. Of these electrode pairs, PSZ showed synchrony increases between C3 and P3, *t*(21)=3.37, *p*=.003; and between P4 and O1, *t*(21)=1.83, *p*=.08 (Figure 29c). REL showed synchrony increases for only one of the

CTRL pairs: F8 and Cz, $t(29)=2.68$, $p=.01$ (Figure 29e). Main effects of group were observed for C3 and P3, $F(2,84)=6.29$, $p=.003$, where increases from baseline in PSZ differed from decreases in CTRL ($p=.002$); for F8 and Cz, $F(2,84)=6.48$, $p=.002$, where aforementioned REL increases differed from decreases in CTRL ($p=.002$); and for P4 and O1, $F(2,84)=3.91$, $p=.02$, where decreases in CTRL differed from slight increases in PSZ ($p=.03$). No group differences were observed for the other electrode pairs ($ps>.22$). Thus, PSZ and REL again showed synchrony changes for subsets of electrodes for which CTRL demonstrated synchrony changes to targets in the 71-81hz gamma window, and each of these observed changes differed meaningfully from those observed in CTRL.

CTRL additionally showed synchrony changes in the 71-81hz window in response to distractor stimuli (Figure 29b): an increase between F8 and T3/T7, $t(35)=2.42$, $p=.03$; a decrease between T4/T8 and T6/P8, $t(35)=-2.29$, $p=.03$; an increase between Pz and T4/T8, $t(35)=2.06$, $p=.05$; a decrease between F8 and T6/P8, $t(35)=-2.02$, $p=.06$; and a decrease between Cz and Pz, $t(35)=-1.81$, $p=.09$. Neither PSZ ($ps>.21$) nor REL ($ps>.10$) showed no synchrony changes in the 71-81hz window to distractors for these electrode pairs. However, group differences were observed for Pz and T4/T8, $F(2,84)=4.13$, $p=.02$, where increases in CTRL differed from minimal changes in REL ($p=.04$) and PSZ ($p=.06$). Additionally, a marginal effect of group was observed for T6/P8 and T4/T8, $F(2,84)=2.89$, $p=.06$, where decreases in CTRL were different from minimal changes in REL ($p=.048$). No group effects were observed for the other electrode pairs ($ps>.15$). Thus, PSZ and REL showed no synchrony changes in the 71-81hz window in response to distractors in the electrode pairs where CTRL showed

changes, though some observed changes in CTRL differed meaningfully from the other groups.

IPSC, 86-126hz, 100-400ms. One-sample *t*-tests on median IPSC (e.g., phase locking values) for the 86-126hz, 100-400ms post-stimulus gamma window similarly revealed synchrony changes as compared to baseline in CTRL in two electrode pairs (Figure 30a): a decrease between Fp1 and P4, $t(35)=-3.14$, $p=.004$; and an increase between T4/T8 and T6/P8, $t(35)=2.86$, $p=.007$. REL also showed an increase in synchrony between T4/T8 and T6/P8, $t(29)=2.32$, $p=.03$ (Figure 30e), while PSZ showed no synchrony changes for these electrode pairs ($ps>.23$). No group differences were observed for either of these electrode pairs ($ps>.53$). Thus, REL showed synchrony changes for one of the two electrode pairs that demonstrated synchrony changes to targets in the 86-126hz gamma window in CTRL, while PSZ did not show synchrony changes for these electrodes; however, observed changes did not differ meaningfully across groups.

CTRL additionally showed synchrony changes in the 86-126hz window in response to distractor stimuli (Figure 30b): a decrease between C3 and P3, $t(35)=-3.21$, $p=.005$; a decrease between Fp1 and C3, $t(35)=-2.91$, $p=.009$; a decrease between F8 and T4/T8, $t(35)=-2.73$, $p=.01$; an increase between Fp1 and T3/T7, $t(35)=2.35$, $p=.03$; an increase between T4/T8 and T5/P7, $t(35)=2.33$, $p=.03$; an increase between C3 and T3/T7, $t(35)=2.04$, $p=.06$; a decrease between Fp1 and O1, $t(35)=-1.99$, $p=.06$; an increase between Cz and O1, $t(35)=1.99$, $p=.06$; an increase between Fp1 and T5/P7, $t(35)=1.97$, $p=.06$; and a decrease between P4 and T4/T8, $t(35)=-1.90$, $p=.07$. PSZ

showed a marginal synchrony decrease for one of these pairs, namely Fp1 and T5/P7, $t(21)=-1.80$, $p=.09$ (Figure 30d), while REL showed no synchrony changes in the 86-126hz window for these electrode pairs (ps>.10). A main effect of group was observed for Cz and T6/P8, $F(2,84)=3.63$, $p=.03$, where decreases in CTRL differed from minimal changes in PSZ ($p=.02$). No group differences were observed for the other electrode pairs (ps>.22). Thus, in response to distractor stimuli in the 86-126hz gamma window, PSZ showed a decrease in synchrony for only one of several pairs where changes were observed in CTRL, while REL showed no synchrony changes in any of these pairs; however, observed changes were for the most part statistically equivalent.

Phase-Amplitude Coupling (PAC)

PCA of PAC values for various low- to high- frequency pairings, time points and electrode sites identified several relevant frequency pairings at particular electrode sites for examination in CTRL (see Figure 11); identified pairings for a given site were thereafter subjected to *t*-tests to determine whether observed coupling differed from baseline values. If so, PAC values were subjected to subsequent repeated measures ANOVA with factors of diagnostic grouping and time sample.

5hz (phase) to 34.5hz (power), O2. For coupling between 5hz (phase) and 34.5hz (amplitude) at O2, a one sample *t*-test revealed significant increases in PAC as compared to baseline, $t(35)=2.23$, $p=.03$. However, subsequent repeated measures ANOVA revealed no main or interaction effects related to diagnostic grouping or time sample (ps>.10). Thus, meaningful increases in PAC was observed for CTRL between

5hz and 34.5hz at O2, though these changes in PAC values did not differ across diagnostic groupings or time samples.

5hz (phase) to 42.5hz (power), O1. For coupling between 5hz (phase) and 42.5hz (amplitude) at O1, a one sample *t*-test showed slight increases in PAC as compared to baseline, $t(35)=1.72$, $p=.09$. However, subsequent repeated measures ANOVA revealed no main or interaction effects related to diagnostic grouping or time sample ($ps>.18$). Thus, meaningful increases in PAC was observed for CTRL between 5hz and 42.5hz at O1, but these changes in PAC values did not differ across diagnostic groupings or time samples.

7hz (phase) to 32.5hz (power), C4. For coupling between 7hz (phase) and 32.5hz (amplitude) at C4, a one sample *t*-test showed slight increases in PAC as compared to baseline, $t(35)=1.72$, $p=.09$. Subsequent repeated measures ANOVA revealed a marginal main effect of time sample, $F(1.58,132.70)=2.43$, $p=.10$. Here, PAC changes were slightly less at 100ms post-stimulus than at 550ms ($p=.06$) and less than at 600ms ($p=.01$). Values at 200ms post-stimulus were also slightly less than those at 600ms ($p=.096$). No effect of diagnostic grouping was observed, $F(2,84)=1.30$, $p=.28$. Thus, meaningful increases in PAC were observed for CTRL between 7hz and 32.5hz at C4, with changes in PAC values being slightly greater towards the end of the epoch.

7hz (phase) to 36.5hz (power), C4. For coupling between 7hz (phase) and 36.5hz (amplitude) at C4, a one sample *t*-test showed slight increases in PAC as compared to baseline, $t(35)=1.95$, $p=.06$. Subsequent repeated measures ANOVA

revealed a marginal main effect of time sample, $F(2.36,198.58)=2.80$, $p=.05$. Here, PAC changes were less at 100ms and 150ms post-stimulus than at 450ms (ps=.02) and less than at 600ms ($p=.01$). Values at 200ms post-stimulus were also slightly less than those at 450ms ($p=.06$). No effect of diagnostic grouping was observed, $F(2,84)=0.78$, $p=.46$. Thus, meaningful increases in PAC were observed for CTRL between 7hz and 36.5hz at C4, with PAC values being slightly higher towards later in the epoch versus earlier.

7hz (phase) to 40.5hz (power), P4. For coupling between 7hz (phase) and 40.5hz (amplitude) at P4, a one sample *t*-test showed slight increases in PAC as compared to baseline, $t(35)=1.96$, $p=.06$. Subsequent repeated measures ANOVA revealed a main effect of time sample, $F(2.99,251.17)=3.59$, $p=.01$. Here, PAC changes were less at 100ms post-stimulus than at 400ms ($p=.01$), 450ms ($p=.02$), 500ms ($p=.01$), 550ms ($p=.005$), and 600ms ($p=.02$). Values at 150ms post-stimulus were slightly less than those at 400ms ($p=.06$) and 500ms ($p=.08$), and less than those at 550ms ($p=.03$) 200ms post-stimulus were also slightly less than those at 450ms ($p=.06$). No effect of diagnostic grouping was observed, $F(2,84)=1.18$, $p=.31$. Thus, meaningful increases in PAC were observed for CTRL between 7hz and 40.5hz at P4, with PAC values again tending to be larger later in the epoch versus earlier.

7hz (phase) to 40.5hz (power), C3. For coupling between 7hz (phase) and 40.5hz (amplitude) at C3, a one sample *t*-test showed slight increases in PAC as compared to baseline, $t(35)=1.89$, $p=.07$. Repeated measures ANOVA again revealed a main effect of time sample, $F(3.44,288.98)=2.93$, $p=.03$. Here, PAC changes were slightly less at 100ms post-stimulus than at 550ms and 600ms (ps=.08). No effect of

diagnostic grouping was observed, $F(2,84)=0.20$, $p=.82$. Thus, slight increases in PAC were observed for CTRL between 7hz and 40.5hz at C3, with PAC values being slightly larger later in the epoch versus earlier.

7hz (phase) to 42.5hz (power), C4. For coupling between 7hz (phase) and 42.5hz (amplitude) at C4, a one sample *t*-test again showed slight increases in PAC as compared to baseline, $t(35)=2.02$, $p=.05$. Repeated measures ANOVA again revealed a main effect of time sample, $F(5.12,430.34)=4.53$, $p<.001$. Here, PAC changes were less at 100ms post-stimulus than at 500ms ($p=.002$), 550ms ($p=.006$) and 600ms ($p=.04$). Values at 150ms post-stimulus were also less than those at 500ms ($p=.008$) and 550ms ($p=.03$). PAC values at 200ms post-stimulus were also less than those at 500ms ($p=.002$), 550ms ($p=.008$), and 600ms ($p=.05$). Values at 250ms were also less than those at 500ms post-stimulus ($p=.047$). No effect of diagnostic grouping was observed, $F(2,84)=0.26$, $p=.77$. Thus, slight increases in PAC were observed for CTRL between 7hz and 42.5hz at C4, and PAC values again tended to be larger later in the epoch versus earlier.

7hz (phase) to 42.5hz (power), O1. For coupling between 7hz (phase) and 42.5hz (amplitude) at C4, a one sample *t*-test again showed slight increases in PAC as compared to baseline, $t(35)=2.02$, $p=.05$. Repeated measures ANOVA again revealed a main effect of time sample, $F(5.12,430.34)=4.53$, $p<.001$. Here, PAC changes were less at 100ms post-stimulus than at 500ms ($p=.002$), 550ms ($p=.006$) and 600ms ($p=.04$). Values at 150ms post-stimulus were also less than those at 500ms ($p=.008$) and 550ms ($p=.03$). PAC values at 200ms post-stimulus were also less than those at 500ms

(p=.002), 550ms (p=.008), and 600ms (p=.05). Values at 250ms were also less than those at 500ms post-stimulus (p=.047). Thus, slight increases in PAC were observed for CTRL between 7hz and 42.5hz at O1, and PAC values again tended to be larger later in the epoch versus earlier.

Furthermore, an interaction between diagnostic grouping and time sample was observed for change in coupling at O1 between 7hz and 42.5hz from baseline, F(10.25,430.34)=2.05, p=.03 (Figure 31). Here, a main effect of time sample were observed for CTRL, F(3.11,108.70)=4.43, p=.005, where changes in PAC values at 100ms were less than those at 350ms (p=.06), 400ms (p=.02), 500ms (p=.002), 550ms (p=.001), and 600ms (p=.09); values at 150ms were slightly less than those at 400ms (p=.06) and less than those at 500ms (p=.007) and 550ms (p=.004); and values at 200ms were less than those at 500ms post-stimulus (p=.04). PSZ showed a marginal effect of time, F(4.29,90.01)=2.09, p=.08, where changes in PAC values at 200ms post-stimulus were less than those at 600ms (p=.02). No effect of time sample was observed for REL, F(4.95,138.58)=1.56, p=.18. Thus, the observed main effect of time sample for coupling between 7hz and 42.5hz at O1 was driven primarily by an effect of time in CTRL; PSZ showed only a marginal effect of time, whereas REL showed no effect at all.

7hz (phase) to 50.5hz (power), C4. For coupling between 7hz (phase) and 50.5hz (amplitude) at C4, a one sample t-test showed an increase in PAC as compared to baseline, t(35)=2.13, p=.04. Repeated measures ANOVA revealed a marginal effect of time sample, F(4.41,370.04)=2.34, p=.05. Here, PAC changes were slightly less at 100ms post-stimulus than at 350ms (p=.08), and less than those at 550ms (p=.02). No

effect of diagnostic grouping was observed, $F(2,84)=0.36$, $p=.69$. Thus, increased PAC was observed for CTRL between 7hz and 50.5hz at C4, where PAC values again tended to increase as the epoch progressed.

7hz (phase) to 54.5hz (power), C3. For coupling between 7hz (phase) and 54.5hz (amplitude) at C3, a one sample *t*-test revealed an increase in PAC as compared to baseline, $t(35)=2.41$, $p=.02$. Repeated measures ANOVA again revealed an effect of time sample, $F(5.02,421.72)=3.09$, $p=.009$. Here, PAC changes were less at 100ms post-stimulus than at 300ms ($p=.001$), 350ms ($p=.004$), 450ms ($p=.06$), 500ms ($p=.005$), 550ms ($p=.006$) and 600ms ($p=.01$). No effect of diagnostic grouping was observed, $F(2,84)=0.71$, $p=.49$. Thus, increased PAC as compared to baseline was observed for CTRL between 7hz and 54.5hz at C3, where PAC values in the earliest time sample were less than those later.

Phase-Phase Coupling (PPC)

PCA of change in PPC values from baseline for various low- to high- frequency pairings, time points and electrode sites identified several relevant low and high-frequency pairings at particular electrode sites for examination in CTRL (see Figure 12). For each identified frequency pairing at a given electrode site, PPC values were averaged over time sample and submitted to a one sample *t*-test to determine whether PPC values changed from baseline. Thereafter, those pairings that showed change were subjected to repeated measures ANOVA utilizing factors of diagnostic grouping and time point.

4hz phase (low-frequency) to 44.5hz phase (high-frequency), O1. A one sample *t*-test for CTRL PPC change values between 4hz and 44.5hz averaged time sample revealed a marginal increase in phase-phase coupling from baseline, $t(35)=1.79$, $p=.08$. Subsequent repeated measures ANOVA revealed an interaction effect between diagnostic grouping and time sample, $F(7.67,322.33)=2.27$, $p=.02$ (Figure 32a). Here, REL alone showed a main effect of time sample, $F(3.37,94.42)=3.04$, $p=.03$, in which PPC change values at 350ms post-stimulus were marginally greater than those at 100ms ($p=.06$) and greater than those at 600ms ($p=.01$); values at 450ms were also greater than those at 600ms ($p=.03$). No effect of time was observed in CTRL or PSZ. Thus, a marginally increase in PPC was observed between 4hz and 44.5hz in CTRL at O1, and REL alone showed differential changes in PPC at different time samples.

4hz phase (low-frequency) to 48.5hz phase (high-frequency), C4. A one sample *t*-test for CTRL change in PPC values between 4hz and 48.5hz averaged across time sample revealed an increase in phase-phase coupling as compared to baseline at electrode C4, $t(35)=2.30$, $p=.03$. Subsequent repeated measures ANOVA revealed a marginal effect of time sample, $F(1.45,121.58)=3.06$, $p=.07$. Here, PPC values at 100ms post-stimulus were less than those at 300ms ($p=.04$), 350ms ($p=.007$), and 400ms ($p=.003$). PPC values at 150ms post-stimulus were also less than those at 350ms ($p=.06$) and 400ms ($p=.03$). No effect of diagnostic grouping was observed, $F(2,84)=0.70$, $p=.50$. Thus, an increase in PPC from baseline was observed for CTRL between 4hz and 48.5hz at electrode C4, and PPC for all subjects was greater mid-epoch as compared to earlier. However, no differences in PPC were observed across diagnostic groupings.

4hz phase (low-frequency) to 54.5hz phase (high-frequency), O2. A one sample *t*-test for CTRL change in PPC values between 4hz and 48.5hz at O2 averaged across time samples confirmed an increase in phase-phase coupling as compared to baseline, $t(35)=2.70$, $p=.01$. Subsequent repeated measures ANOVA showed a marginal effect of time sample, $F(1.96,165.02)=2.89$, $p=.06$. Here, PPC values at 100ms post-stimulus were slightly less than those at 400ms ($p=.06$), 500ms ($p=.01$), 550ms ($p=.02$) and 600ms ($p=.06$). No effect of diagnostic grouping was observed, $F(2,84)=1.00$, $p=.37$. Thus, phase-phase coupling between 4hz and 54.5hz increased from baseline in CTRL at O2, and PPC values tended to increase later in the epoch. However, no differences between diagnostic groupings were observed.

4hz phase (low-frequency) to 56.5hz phase (high-frequency), P4. A one sample *t*-test for CTRL PPC values between 4hz and 56.5hz averaged across time sample at P4 revealed a slight increase in phase-phase coupling as compared to baseline, $t(35)=1.69$, $p=.099$. Subsequent repeated measures ANOVA revealed a main effect of time sample, $F(3.60,302.80)=3.45$, $p=.01$. Here, PPC values at 100ms post-stimulus were less than those at 450ms ($p=.01$), and values at 150ms were less than those at 450ms ($p=.002$), 500ms ($p=.03$), and 550ms ($p=.05$). PPC values at 200ms post-stimulus were slightly less than those at 450ms ($p=.09$). No effect of diagnostic grouping was observed, $F(2,84)=1.26$, $p=.29$. Thus, an increase in PPC from baseline was observed for CTRL between 4hz and 56.5hz at P4, and PPC for all subjects was greater in later time samples as compared to earlier.

6hz phase (low-frequency) to 44.5hz phase (high-frequency), C4. A one sample *t*-test for CTRL PPC values between 4hz and 44.5hz averaged across time sample at C4 revealed an increase in phase-phase coupling as compared to baseline, $t(35)=2.55$, $p=.02$. Subsequent repeated measures ANOVA revealed a marginal interaction between diagnostic grouping and time sample, $F(8.57,359.99)=1.76$, $p=.08$ (Figure 32b). Here, CTRL showed a slight effect of time sample, $F(3.24,113.41)=2.58$, $p=.05$, where PPC values at 100ms post-stimulus were slightly less than those at 550ms ($p=.08$) and 600ms ($p=.06$). No effect of time sample was observed for PSZ, $F(1.96,41.23)=1.06$, $p=.36$, or REL, $F(3.63,101.53)=1.08$, $p=.37$. Thus, an increase in PPC from baseline was observed for CTRL between 6hz and 44.5hz at C4, and CTRL alone showed greater change in PPC values from baseline later as compared to earlier in the epoch.

6hz phase (low-frequency) to 52.5hz phase (high-frequency), O1. A one sample *t*-test for CTRL PPC values between 6hz and 52.5hz at O1 averaged across time sample revealed a mild increase in phase-phase coupling as compared to baseline, $t(35)=1.95$, $p=.06$. Repeated measures ANOVA again revealed a marginal effect of time sample, $F(1.85,154.99)=2.92$, $p=.06$. Here, PPC values at 100ms post-stimulus were less than those at 500ms ($p=.01$) and 550ms ($p=.02$); no other pairwise comparisons achieved significance. Thus, slight increases in PPC from baseline were observed for CTRL between 6hz and 52.5hz at O1, and PPC for all subjects was slightly greater later as compared to earlier in the epoch.

6hz phase (low-frequency) to 54.5hz phase (high-frequency), O1. A one sample *t*-test for CTRL change in PPC values between 6hz and 54.5hz at O1 averaged

across time sample revealed an increase in phase-phase coupling as compared to baseline, $t(35)=2.16$, $p=.04$. Subsequent repeated measures ANOVA revealed a main effect of time sample, $F(2.69,226.36)=5.61$, $p=.002$. Here, PPC values at 100ms post-stimulus were slightly less than those at 350ms ($p=.08$) and less than those at 400ms ($p=.002$), 450ms ($p=.001$), 500ms ($p<.001$), 550ms ($p=.002$), and 600ms ($p<.001$). PPC values at 150ms post-stimulus were similarly less than those at 400ms ($p=.02$), 450ms ($p=.02$), 500ms ($p=.006$), 550ms ($p=.02$), and 600ms ($p=.004$). PPC values at 200ms and 250ms were slightly less than those at 500ms ($ps<.09$) and 600ms ($ps<.07$) post stimulus. No effect of diagnostic grouping was observed, $F(2,84)=1.99$, $p=.14$. Thus, an increase in PPC from baseline was observed for CTRL between 6hz and 54.5hz at O1, and PPC for all subjects increased with later time samples. Increases in PPC from baseline for this frequency pair did not differ between diagnostic groupings.

6hz phase (low-frequency) to 58.5hz phase (high-frequency), O1. A one sample *t*-test for CTRL change in PPC values between 6hz and 58.5hz at O1 averaged across time sample revealed a slight increase in phase-phase coupling as compared to baseline, $t(35)=1.90$, $p=.07$. Subsequent repeated measures ANOVA revealed a main effect of time sample, $F(1.62,136.17)=4.08$, $p=.03$. Here, PPC values at 100ms post-stimulus were slightly less than those at 300ms ($p=.09$) and less than those at 350ms ($p=.04$), 400ms ($p=.03$), 450ms ($p=.002$), 500ms ($p<.001$), 550ms ($p<.001$), and 600ms ($p=.05$). PPC values at 150ms post-stimulus were slightly less than those at 500ms ($p=.06$). PPC values at 200ms were less than those at 500ms ($p=.04$) and 550ms ($p=.07$) post-stimulus. No effect of diagnostic grouping was observed, $F(2,84)=1.99$, $p=.14$.

Thus, a slight increase in PPC from baseline was observed for CTRL between 6hz and 58.5hz at O1, and PPC for all subjects was greater for later versus earlier time samples. Increases in PPC from baseline for this frequency pair did not differ between diagnostic groupings.

Predicting Behavioral Performance

Variables that showed main or interaction effects in previous analyses were submitted to repeated ridge regression analyses utilizing the nonparametric bootstrap quantile approach proposed by Abram and colleagues (2016). Separate ridge regression analyses were performed to predict overall performance on the WM task, performance on trials without distractors, and performance exclusively on trials that featured distractors. In each case, variables selected by the bootstrapping procedure were subsequently submitted to ordinary least squares regression including an additional factor of diagnostic grouping and allowing interactions between said factor and all other included predictors.

Predicting overall performance. The bootstrapped ridge regression for prediction of overall behavioral performance selected variables of evoked theta power in response to 2nd and 3rd stimuli, evoked theta power in response to targets, evoked delta power (2-3hz) in response to 3rd stimuli, evoked delta power (1-2hz) in response to second stimuli, induced delta power in response to 3rd stimuli, gamma power (64-81hz) in response to second stimuli, theta-band phase-synchrony between Oz and T6/P8, phase-amplitude coupling between 7hz and 50.5hz at electrode C4, and phase-phase coupling between 6hz and 44.5hz at electrode C4.

These variables were subsequently regressed on overall performance on the WM task, including and allowing for interaction with diagnostic grouping as a factor. Said model coefficients and associated statistics are presented in Table 3. Within this model, a diagnosis of PSZ predicted slightly poorer overall performance (β= -.50, t(86)=-1.92, p=.06) than CTRL, and increased induced delta power in response to third stimuli predicted slightly poorer performance than CTRL in PSZ alone (β= -.47, t= -1.87, p=.07). Increased evoked theta power to third stimuli (β=.42, t=2.04, p=.046), as well as increased evoked delta (1-2hz) power to second stimuli (β= .32, t=2.21, p=.03), predicted better overall WM performance in CTRL, with no significant differences in related coefficients for other diagnostic groupings. Additionally, increased gamma (64-81hz) power in response to second stimuli was similarly more predictive of poorer performance in PSZ than in CTRL (β= -.64, t= -2.61, p=.01); increased phase-amplitude coupling between 7hz and 50.5hz at C4 also predicted better performance more strongly for PSZ than for CTRL (β= .91, t=2.78, p=.008). No interactions involving a group status of REL were observed.

Within-group regressions for overall task performance utilizing only those predictors demonstrating main or interaction effects were subsequently run. For PSZ, induced gamma (64-81hz) power in response to 2nd stimuli (β= -.71, t(21)= -3.19, p=.006) and phase-amplitude coupling between 7hz and 50.5hz at C4 (β= .61, t(21)=2.31, p=.03; Figure 33) were supported as predictive of performance; no predictive power was found in PSZ for evoked theta power in response to third stimuli (β=.21, t(21)=.90, p=.38), evoked delta (1-2hz) power in response to 2nd stimuli (β=.29, t(21)=1.18, p=.25),

or induced delta power in response to 3rd stimuli (β= -.18, t(21)= -1.17, p=.26). In CTRL, increases in evoked theta power in response to third stimuli (β=.38, t(35)=3.75, p<.001) and evoked delta (1-2hz) power in response to 2nd stimuli (β=.32, t(35)=3.02, p=.005) predicted improved task performance overall. Increases in induced delta power in response to 3rd stimuli were also marginally predictive of increased performance for CTRL (β=.31, t(35)=1.86, p=.07). No predictive utility was observed in CTRL for induced gamma (64-81hz) power in response to 2nd stimuli (β= -.03, t(35)= -0.28, p=.79) or phase-amplitude coupling between 7hz and 50.5hz at C4 (β=.02, t(35)=0.17, p=.87). In REL, overall performance was predicted only by induced delta power in response to 3rd stimuli (β=.45, t(28)=2.30, p=.03); evoked theta power in response to 3rd stimuli (β=.00, t(28)=.02, p=.99), evoked delta (1-2hz) power in response to 2nd stimuli (β=.18, t(28)=1.01, p=.32), induced gamma (64-81hz) power in response to 2nd stimuli (β= -.04, t(28)= -0.28, p=.78) and phase-amplitude coupling between 7hz and 50.5hz at C4 (β=.22, t(28)=1.17, p=.25) were not predictive for REL. Thus, increasing evoked theta and delta power were predictive of better performance in CTRL and REL, whereas decreasing gamma power (64-81hz) as well as increasing phase-amplitude coupling between 7hz and 50.5hz were predictive of WM performance for PSZ alone.

Predicting performance on trials without distractors. The bootstrapped ridge regression for prediction of task performance on trials without distractors selected variables of evoked delta power (1-2z) in response to 2nd stimuli, induced theta power in response to 3rd stimuli, induced delta power in response to 3rd stimuli, induced gamma power (64-81hz) in response to second stimuli, induced gamma power (64-81hz) in

response to target stimuli, gamma-band (71-81hz) phase synchrony between Pz and T4/T8, and phase-amplitude coupling between 7hz and 50.5hz at electrode C4.

These variables were subsequently regressed on performance on trials without distractors on the WM task, including and allowing for interaction with diagnostic grouping as a factor. No effect of diagnostic grouping or interaction therewith was observed, so the model was rerun without the diagnostic factor to improve model fit and interpretability. Coefficients and associated statistics for this model are presented in Table __. Within this model, increasing evoked delta (1-2hz) power to second stimuli (β=.21, t(86)=2.19, p=.03) as well as increased phase synchrony in response to distractors between Pz and T4/T8 in the gamma band (71-81hz; β=.23, t(86)=2.26, p=.03) predicted better WM performance on target-only trials for all participants. Thus, increases in evoked delta power and gamma (71-81hz) phase-synchrony between parietal and temporal sites were predictive of better performance for all diagnostic groupings.

Predicting performance on trials with exclusively distractors. The bootstrapped ridge regression for prediction of task performance on trials with exclusively distractors selected variables of evoked theta power in response to 2nd stimuli, evoked theta power in response to 3rd stimuli, evoked theta power in response to target stimuli, evoked delta power (2-3hz) in response to 3nd stimuli, evoked delta power (1-2hz) in response to 2nd stimuli, induced delta power in response to 3rd stimuli, induced gamma power (64-81hz) in response to second stimuli, theta-band phase synchrony between Oz and T6/P8, gamma-band (36-56hz) phase synchrony between P3 and Fp1, phase-amplitude coupling between 7hz and 54.5hz at electrode C3, phase-phase coupling

between 6hz and 44.5hz at electrode C4, and phase-phase coupling between 6hz and 52.5hz at electrode O1.

These variables were subsequently regressed on performance on trials featuring distractors in the WM task, including and allowing for interaction with diagnostic grouping as a factor. Coefficients and associated statistics for this model are presented in Table __. Within this model, a diagnosis of PSZ predicted poorer overall performance (β= -.77, t(86)= -2.48, p=.02) than CTRL. Additionally, the coefficient for evoked theta power in response to 3rd stimuli was marginally different in PSZ than in CTRL (β= -.92, t(86)= -1.94, p=.06), as was that for induced gamma (64-81hz) power in response to second stimuli (β= -.54, t(86)= -1.97, p=.06). PSZ also showed a stronger predictive relationship between increases in gamma (36-56hz) phase-synchrony between P3 and Fp1 in response to distractors than CTRL (β= .73, t(86)=3.5, p=.003).

Within-group regressions for exclusively trials with distractors utilizing only those predictors demonstrating main or interaction effects were subsequently run. For PSZ, induced gamma (64-81hz) power in response to second stimuli (β= -.73, t(21)= -3.1, p=.006) and gamma (36-56hz) phase-synchrony between P3 and Fp1 in response to distractors (β= .52, t(21)=2.6, p=.02; Figure 34) were supported as predictive of performance; evoked theta power in response to third stimuli was not significantly predictive in said model (β=.18, t(21)=.77, p=.45). CTRL showed no predictive utility for induced gamma (64-81hz) power in response to second stimuli (β= -.13, t(35)= -1.23, p=.23) or gamma (36-56hz) phase-synchrony between P3 and Fp1 in response to distractors (β=.17, t(35)=1.5, p=.13), though evoked theta power in response to third

stimuli was predictive of performance in CTRL (β=.42, t(35)=4.3, p<.001). REL showed only marginal predictive value for evoked theta power in response to third stimuli (β=.42, t(28)=2.0, p=.05); gamma power (β=-.08, t(28)= -.50, p=.62) and gamma phase synchrony (β=.02, t(28)=.10, p=.92) were not predictive for REL. Thus, PSZ showed stronger predictive relationships than CTRL between performance on distractor trials and induced gamma (64-81hz) power as well as gamma (36-56hz) phase-synchrony between parietal and frontoparietal sites.

Discussion

Guided by the theorized importance of theta- / gamma- coupling to WM performance as outlined by Lisman and Idiart's (1995) model and its subsequent empirical support, theta- and gamma-band EEG indices were examined in PSZ and REL in comparison with CTRL. It was hypothesized that deficiencies in theta- / gamma-coupling may underlie the prominent WM dysfunction observed in PSZ, and that such deficiencies may also be evident in examinations of theta- and gamma-band activity independent of their interaction. EEG data collected during administration of a spatial working WM task in which memory stimuli were presented in sequence were examined to explore these theorized deficits. Power and phase-synchrony within the theta- and gamma-bands were first examined and analyzed independently. Phase-amplitude as well as phase-phase coupling between the two bands were next explored, followed finally by analysis of the relationships between electrophysiological measures and performance on the WM task in an effort to determine whether the any of the measures explored possess predictive utility.

It was posited that PSZ would demonstrate electrophysiological abnormalities as compared to CTRL in power and phase-synchrony analyses within the theta- and gamma-bands independent of their interaction. It was believed that such abnormalities may contribute to disturbances in theta-gamma coupling, which could explain WM deficits observed on a behavioral level. REL were also expected to show electrophysiological aberrances as compared to CTRL, but potentially to a lesser degree in light of known preserved behavioral performance on the WM task (Lynn, Kang & Sponheim, 2016).

Time-Frequency Power: Theta- and Delta-Band Activity

Theta- (and supplemental delta-) band analyses showed several effects of task manipulations on both evoked and induced low-frequency power. For both power measures across all low-frequency windows of interest examined, later stimuli (2nd and 3rd) elicited greater power increases than 1st stimuli (Figures 13, 15, 16, 17 and 19). These increases in power for later stimuli are consistent with past reports of modulations in theta amplitudes with changing WM load (e.g., Jensen & Tesche, 2002). These modulations have also been proposed to reflect an allocation of cognitive resources, especially as observed over frontal areas (Griesmayr et al., 2014), and a lack of diagnostic grouping effects in the evoked data suggests some preservation of WM and related higher-level cognitive processes in PSZ and REL.

The induced power low-frequency data, in addition to demonstrating stimulus order effects, showed mild group effects as well. Induced theta- (4-8hz, 100-250ms) power was greater in REL than in PSZ, with CTRL falling in between (Figure 18). Furthermore, induced delta-band (1-2hz, 100-300ms) energy showed a diagnostic grouping by presentation order interaction, where the strongest effect of order was observed for REL, a lesser effect observed for CTRL, and no effect observed for PSZ (Figure 20). The observation of maximal low-frequency power as well as the strongest order effects for REL mirrors findings related to ERP analyses of data from the same task, in which REL showed more pronounced effects of stimulus order on N1 responses in *retrieval* than CTRL, whereas PSZ showed no modulation at all (Lynn, Kang & Sponheim, 2016). As was posited for those findings, the sharper delineation of stimulus

order and greater overall delta-band responses may reflect WM processes that reflect compensatory responses that allow preserved WM performance in REL, a phenomenon that has been observed elsewhere in REL (see Zhang et al., 2016 for a review), whereas abnormalities in low-frequency power observed in PSZ suggest disturbed encoding memory stimuli in comparison to CTRL and REL.

In addition to modulation with stimulus order, low-frequency energy varied with stimulus type. Evoked theta-energy (4-8hz, 100-250ms) and induced delta-energy (1-3hz, 150-600ms) was modulated by stimulus type, with theta-responses being greater to targets than distractors (Figure 14) but delta-responses showing the opposite pattern (Figure 21). Modulation of theta- and delta- activity by task demands has been demonstrated many times previously, and is often discussed in the context of the relationship between activity in these bands and the P300 ERP potential (Güntekin & Başar, 2016). The inverse relationships observed here for theta- and delta-activity in relationship to stimulus type may relate to ongoing disagreement regarding whether delta-activity is more responsive to novelty or target detection, with results supporting both views having been published (see Güntekin & Başar, 2016). Here, we may explain increased theta-activity in response to targets a byproduct of its well-demonstrated positive correlation with WM load (e.g., Jensen & Tesche, 2002; Scharinger, Soutschek, Schubert & Gerjets, 2017), while delta's pronounced response to distractors may support its function as an index of novelty detection. As Güntekin and Başar (2016) point out, additional research is needed to parse and clarify the role of delta-activity in these processes.

Time-Frequency Power: Gamma-Band Activity

Induced power in the gamma-band showed moderate modulation related to diagnostic grouping in several examined windows of interest. Induced gamma-power in the 71-81hz, 100-400ms window showed a marginal interaction between group and stimulus presentation order, where CTRL and REL demonstrated mild effects of order on gamma-power but PSZ did not (Figure 23). Similarly, CTRL and REL showed effects of presentation order on gamma-power in the 64-81hz, 425-775ms window at primarily posterior electrode sites, whereas PSZ showed no such effect (Figure 22). Such findings are consistent with previously reported deficits in gamma-power observed in PSZ, particularly a failure to modulate gamma power with increased WM load, as is typically observed in healthy adults (Pina, Bodner & Ermentrout, 2018; Roux et al., 2012; Başar-Eroğlu et al., 2007; Haenschel et al., 2009; Barr et al., 2010; Williams & Boksa, 2010). Further notable is the inverse predictive relationship between increased gamma power in the 64-81hz window in response to 2nd stimuli and overall behavioral performance in PSZ alone. Of note, CTRL demonstrated a general trend of decreasing power with the presentation of each subsequent stimulus, and though PSZ showed no true effect, their data superficially suggest a similar pattern. As such, the inverse relationship between 64-81hz power and performance in PSZ may indicate gamma in this window as an index of successful stimulus encoding—with more successful encoding comes increased reductions in gamma and better task performance. In this context, it is also important to note that REL showed an opposite pattern for the 64-81hz gamma window: with each stimulus came slight increases in power. This reversed effect may reflect another

instance of a potential compensatory mechanism in REL for preserving WM performance (Zhang et al., 2016). Thus, findings related to time-frequency energy in the gamma-band support the notion that the relationship between gamma-activity and WM is disturbed in PSZ, and may reflect neural compensatory mechanisms in REL.

Interactions between diagnostic grouping and stimulus type were also observed for gamma-band activity. CTRL alone showed increased gamma power to targets versus distractors in the 64-81hz, 425-775ms and 71-81hz, 100-400ms windows of interest established by PCA; neither PSZ nor REL showed such modulation to stimulus type. Gamma-activity has been implicated in processes of selective attention, with increases in synchronization, phase-resetting and elicited power having been reported in response to relevant stimuli (reviewed in Fell et al., 2003). As such, differences in modulation of gamma by stimulus type observed between diagnostic groupings may reflect differential allocations of attention, be it voluntary or a byproduct of deficits in attentional control. However, ERP results derived from the same sample showed pronounced differences in REL retrieval N1s on the basis of relevant stimulus type (Lynn, Kang & Sponheim, 2016), suggesting some segmentation of stimulus relevance in at least REL that does not fully support an attentional explanation. Furthermore, gamma-activity related to attention function has been demonstrated to occur in lower gamma sub-bands (Gamma-activity has also been regularly implicated in visual processes and the binding of perceptual information, with increased synchrony and amplitude having been shown to accompany successful maintenance of stimulus features (Honkanen et al., 2015), particularly in relatively higher gamma sub-bands (Castelhano et al., 2014). Failure to modulate

gamma-amplitude to stimulus type in PSZ and REL may be more likely explained as deficits related to visual processing, for which REL compensate through attentional or other means; the notion of increased attention as compensation in REL better fits with the aforementioned increased delineation of N1 responses related to stimulus type during retrieval, given N1's well-demonstrated function as an index of attention (Lynn, Kang & Sponheim, 2016). Regardless, the shared failure to modulate gamma-power in these windows of interest in relation to stimulus type in PSZ and REL may reflect a common liability for the disorder.

Time-Frequency Phase-Synchrony: Theta-Band

CTRL showed meaningful changes in phase synchrony in the theta-band window of interest (4-8hz, 100-250ms) for a number of the electrode pairs selected in conjunction with principal components analyses. Namely, CTRL showed increases in synchrony as compared to baseline between frontal / central sites and more posterior sites in both target-only trials and those that featured distractors. Theta synchrony between frontal and parietal regions has also been implicated in tasks of cognitive control and choice paradigms (Cooper et al., 2015; Womelsdorf, Vinck, Leung & Everling, 2010), and increases in such synchrony here is consistent with demands of the performed WM task. Alternatively, increased theta-synchrony between prefrontal cortex and hippocampus has been implicated in task-learning via experimentation in non-human primates (Crivelli-Decker, Hsieh, Clarke & Ranganath, 2018), and though scalp-measured EEG lacks the spatial resolution of fMRI or intracranial EEG, observed frontal to posterior synchrony at the scalp may similarly reflect CTRL participants' developing understanding of implicit

task rules during task performance. Regardless, inter-areal theta-synchronization seems to play a crucial role in general information processing and transfer (Solomon et al., 2017; Womelsdorf et al, 2010), potentially through the coordinated timing of synaptic inputs across regions of the brain (Fell & Axmacher, 2011), and increased intra-areal synchronization in the theta-band seems to suggest normative cognitive processing in a variety of contexts.

PSZ and REL failed to demonstrate changes in phase synchrony similar to those observed in CTRL; in fact, only PSZ showed any change in the pairs identified in CTRL, and it was a significant change in the opposite direction: CTRL showed decreases in theta synchrony between T6/P8 and Oz, where PSZ showed increases within this pair. Desynchronization in theta and other regions is often implicated in the suppression of erroneous allocation of attention and other cognitive resources (Kawamata et al., 2007), and such suppression may explain differences in synchrony changes observed in CTRL in response to targets vs. distractors. Additionally, differences between groups in this case may reflect faulty suppression in PSZ. Notably, though theta phase-synchrony in this particular pair was selected by penalized regression analyses for modeling behavioral performance, it was found to have predictive utility within or across diagnostic groupings. Thus, though abnormalities in theta-band phase synchrony were observed in PSZ as compared to CTRL, they did not appear to have a direct effect on PSZs' task performance.

Time-Frequency Phase-Synchrony: Gamma-Band

CTRL demonstrated a variety of synchrony changes in the various gamma-band windows examined as well. These changes included both increases and decreases from baseline and were dependent on the frequency and time window observed: early in the epoch (100-400ms post-stimulus) between roughly 70hz and 120hz, CTRL showed increases in synchrony between electrodes over midline parietal and right temporal areas, right frontal and right parietal areas, and midline central and right temporal areas, along with simultaneous decreases between electrodes over right frontal and midline central areas, right parietal and left occipital areas, and left prefrontal and right parietal areas. Both increased and decreased synchrony between varying electrode pairs were also observed between left / midline central and left parietal electrodes in CTRL. As sensory processing, WM and other higher-level cognitive processes are typically associated with increased gamma-band synchrony and power (Miller, Lundqvist & Bastos, 2018; Palva, Monto, Kulashekhar & Palva, 2010), relatively high levels of decreases in synchrony observed in CTRL are difficult to reconcile, and may reflect spurious changes related to an arbitrarily-selected high alpha level along with the choice to forgo multiple comparison correction in the phase analyses for exploratory purposes. Alternatively, most WM research focuses on a longer maintenance period, and demonstrated synchrony processes may not be well-solidified so soon after stimulus presentation. However, group differences in synchrony were notably observed for synchrony between left central and left parietal sites, right frontal and midline central sites, and right parietal and left occipital sites. In all cases, CTRL showed decreases in synchrony that differed from increases in PSZ or REL. Again, however, phase synchrony in none of these pairs

factored into derived models for predicting WM task performance. As such, these focused differences in synchrony between groups may reflect veritable differences in WM processes, but they do not serve a strong predictive function regarding WM performance.

CTRL likewise demonstrated high-frequency synchrony changes later in the epoch. Synchrony changes to target stimuli between 425-775ms were limited to the 36-56hz window identified by PCA, and consisted primarily of increases: increases between electrodes over right temporal and right parietal areas, left central and right parietal areas, and right temporal and left parietal areas. However, mild decreases between electrodes over left temporal and left parietal were also observed in this window of interest. In contrast, synchrony was largely decreased in CTRL as compared to baseline in response to distractor stimuli in the 36-56hz window: decreases were observed between electrodes over left prefrontal and left parietal areas, left prefrontal and right parietal areas, left prefrontal and left temporal areas, left central and right parietal areas, and left parietal and right parietal areas. However, increases were also observed between left parietal and right temporal areas, midline parietal and left parietal areas, and midline parietal and right temporal areas. Thus, synchrony changes were again relatively mixed, though increases were slightly more prominent in response to targets and decreases more common in response to distractor stimuli for CTRL.

PSZ and REL showed minimal change in synchrony for these electrode pairs, and several group differences observed for synchrony in response to distractors, many involving synchrony between the prefrontal Fp1 and electrodes over parietal, central and

temporal areas; for these pairings involving Fp1, CTRL showed decreased synchrony as compared to PSZ or REL in all cases (Figure 27). This may in fact reflect differential processing of distractor stimuli in CTRL as compared to PSZ and REL, with CTRL allocating fewer cognitive resources to the distractors than the other groups. Such an interpretation is further supported by the predictive utility found for 36-56hz synchrony between Fp1 and P3 in predicting performance on distractor trials in PSZ alone; as synchrony increased, so did PSZ performance on distractor trials. If PSZ and REL are indeed paying more attention to distractors than CTRL, increased performance with increased prefrontal to parietal synchrony may reflect better processing of these stimuli in for PSZ. Thus, phase synchrony differences between groups in response to distractors between prefrontal and parietal areas were especially significant in light of their utility in predicting task performance in PSZ and may support different processing of distractors between groups.

Phase-Amplitude Coupling

The primary focus of this project was to explore cross-frequency coupling between theta- and gamma-band activity and its relationship to WM dysfunction in PSZ on the basis of Lisman and Idiart's (1995) well supported model for how coupling in these frequencies maintain stimuli in WM. Both phase-amplitude and phase-phase coupling were examined.

In an effort to utilize data-driven methods to guide coupling analyses, PCA was employed to attempt to isolate frequency pairings that demonstrated notable changes in

coupling measures in response to the task. PCA on PAC values identified several focused frequency pairings at particular electrode sites, which were subsequently tested to determine whether PAC for each electrode / frequency pairing differed from baseline. Increases in PAC were found between 5hz and 34.5hz as well as 42.5hz at occipital sites, with no observed increase over the time course of the epoch. Increases in PAC were also observed between 7hz and 32.5hz, 36.5hz, 40.5hz, 42.5hz, 50.5hz and 54.5hz at central electrode sites, as well as between 7hz and 40.5hz over right parietal areas and 7hz and 42.5hz over left occipital areas. For the PAC values featuring a low-/phase-frequency of 7hz, a main effect of time sample was observed in all pairs, with PAC values increasing to a maximum near 550ms or 600ms post-stimulus. Additionally, an interaction between diagnostic grouping and time sample was observed for PAC between 7hz and 42.5hz at left-occipital O1, in which CTRL showed the standard increase in PAC over the time course of the epoch, PSZ showed a very limited increase, and REL showed no increase at all (Figure 31). The overall increase in PAC with time may represent a mechanism in which additional neuronal or cognitive resources are recruited to perpetuate the representation of a stimulus or set of stimuli, and such deviance in PAC for the PSZ and REL from CTRL (albeit focused) may suggest a difficulty in these groups in stimulus maintenance. Still, PAC between 7hz and 24.5hz at this (or any) site was not found to relate to WM task performance. This difference in the modulation of PAC by time was the only indication in those frequency pairings and electrode sites examined that there may exist differences between diagnostic groups in the process of PAC itself; no other effects of diagnostic grouping were observed for PAC.

Though measures of PAC appeared to be for the most part equivalent across diagnostic groupings, additional differences were observed in the relationships between PAC and task performance. An interaction was observed between diagnostic grouping and the predictive ability of PAC between 7hz and 50.5hz at right central C4 in regards to prediction of overall task performance, in which PAC was predictive of task performance for PSZ but not CTRL or REL. Thus, though a relatively focused finding, it nonetheless suggests a special relevance for PAC in WM function in PSZ. This dependence may be circumscribed to particular frequency pairings, locations, or sub-tasks of WM for PSZ as compared to CTRL or REL; alternatively, CTRL and REL may be less sensitive to the effects of such focused PAC, so that narrowly focused samplings of PAC are less linked to WM function overall. Apparently intact PAC in PSZ seems to contradict the decreased PAC in PSZ during WM reported by Barr and colleagues (2017). However, Rajji and colleagues (2017) reported a selective increase in PAC during WM tasks that required ordering in healthy adults, whereas no PAC increase was observed for tasks that contained no ordering component. Such a finding may explain the discrepancy here, as the WM task herein does not focus on the ordering of stimuli but rather their spatial position. Regardless, preserved PAC in PSZ as well as predictive utility being observed exclusively in PSZ supports the notion that PAC is important to WM performance in PSZ—perhaps uniquely so.

Phase-Phase Coupling

Considerable increases in phase-phase coupling from baseline were also observed in the frequency pairs and electrode sites identified by a separate PCA. PPC as verified

by *t*-tests was found to increase between 4hz and 44.5hz at left-occipital O1, between 4hz and 48.5hz at right central C4, between 4hz and 54.5hz at right-occipital O2, and between 4hz and 56.5hz at right parietal P4. Additionally, PPC increases from baseline were observed between 6hz and 44.5hz at right central C4, and between 6hz and 52.5hz, 54.5hz, and 58.5hz at occipital sites. As with the PAC findings, PPC increased in most cases as the epoch progressed; again, this may suggest the recruitment of more neural resources in order to maintain stimuli over longer periods.

Though no main effects of diagnostic grouping were observed in the PPC data, interactions between diagnostic grouping and time sample were again observed, as with the PAC analyses. Diagnostic grouping interacted with time between 4hz and 44.5hz at O1, where REL alone demonstrated slight increases in PPC with time (Figure 32a), as well as between 6hz and 44.5hz at C4, where only CTRL showed marginal increases as the epoch progressed (Figure 32b). Of note, no examined phase-phase coupling measures were predictive of WM performance, so these observed differences do not appear to have had a direct effect on WM ability as measured in this task. However, though these findings are relatively focused in terms of particular frequency bands and electrode sites, and though little has been written about effects of time in cross-frequency coupling, such differences could suggest wider-scale aberrances in REL or PSZ that may relate to WM performance.

Predicting WM Task Performance

Bootstrap enhanced ridge regression was used to identify and select relevant predictors for further analysis via ordinary least squares regression, as described by Abram and colleagues (2016). Separate models were constructed for prediction of overall task performance, performance on trials without distractor stimuli, and trials that featured distractors. Within these models, several electrophysiological measures were predictive of task performance. Within-diagnostic-grouping regressions found increases in low frequency power in response to 2nd and 3rd stimuli to be predictive of overall performance in CTRL and REL but not PSZ. As discussed, theta and delta power has been shown to increase with WM load (Jensen & Tesche, 2002), and a positive relationship between such increases and WM performance can reasonably be attributed to successful encoding and maintenance of WM stimuli. It would be further defensible to expect a similar relationship in PSZ; however, it is possible that no such relationship was derived from these data given a failure of PSZ to modulate low-frequency power in response to the order in which stimuli were presented. Thus, variance for PSZ in these measures may not have been sufficient to demonstrate such a relationship, and larger, more varied samples may well reveal it. Furthermore, as discussed above, PSZ alone did demonstrate a relationship between behavioral performance and power in the 64-81hz gamma band, which may be a more reliable neural index for behavior in PSZ, potentially as a byproduct of disturbed electrophysiological processes as relating to WM. Additionally notable is the predictive relationship observed between evoked delta (1-2hz) in response to second stimuli and performance on target-only trials for all groups; thus,

low frequency power's to track with overall behavioral performance in PSZ alone may be related to faulty utilization of distractor stimuli in PSZ.

Measures of phase-synchrony between sites were also shown to have limited predictive power, particularly in PSZ. As noted, phase-synchrony in the 36-56hz gamma window between prefrontal Fp1 and parietal P3 was uniquely predictive of performance on distractor trials in PSZ (Figure 34), and synchrony changes in said window in response to distractors was one of few examined phase-synchrony measures that differed between groups (Figure 27). Again, though scalp-level EEG is difficult to accurately map onto activity within the brain, communication between these general areas is consistent with well-demonstrated networks involved in visual WM featuring communication between prefrontal and parietal areas (Palva et al., 2010). Thus, increased gamma-band synchrony between these two electrode sites may reflect more effective processing of distractor stimuli in PSZ, allowing for better behavioral performance. Similar explanations may be offered for the predictive relationship between increases in gamma-band (71-81hz) synchrony between Pz and T4/T8 in response to distractors and performance on *target only* trials for all participants; as gamma synchrony in this window increased in response to distractor stimuli, so did task performance. Further notable is the moderate group effect that was observed for this same measure, with CTRL showing slightly higher gamma synchrony between these electrodes than REL (Figure 27). Again, increased neural synchronization between these sites may reflect more effective processing of distractors, here in all participants, that predicts better WM performance. Thus, synchrony measures were additionally

predictive of WM ability, again most likely understood in the context of their reflecting effective processing of WM stimuli.

Measures of cross-frequency coupling demonstrated limited predictive utility in regards to WM performance. As stated, measures of phase-phase coupling were not found to be predictive of task performance in any of the constructed models. Furthermore, only one measure of phase-amplitude coupling (between 7hz and 50.5hz at C4) was found to have predictive utility, and this was for PSZ alone (Figure 33). Though it is difficult at present to parse the significance of activity between these precise frequency bands, its relationship to behavior in PSZ alone does preliminarily suggest a unique influence of PAC in WM ability for people with the disorder. Additional investigation in this area may flesh out this influence as well as uncover other areas where cross-frequency coupling relates to behavior.

Thus, various time-frequency indices of neural activity were predictive of WM task performance. Measures of low-frequency power had predictive utility for all groups depending on the behavioral index examined, though they were not predictive for PSZ in overall performance. Instead, task performance in PSZ showed a special sensitivity to indices of gamma activity, and gamma synchrony in response to distractors is particularly notable for its predictive relationship with performance on target-only trials for all participants, suggesting increased ability to effectively process distractors may reflect better WM performance on other indices. PSZ alone showed a predictive relationship between measures of cross-frequency coupling and behavioral performance; though a focused finding, this may speak to a special dependence of WM ability on theta-gamma

coupling in PSZ, as well as the prospect of coupling with higher gamma frequencies predicting WM performance in all groups.

Limitations

Several limitations of the present investigation should be noted and considered. Perhaps most notably, type I error, or the erroneous rejection of the null hypothesis—e.g., asserting an effect when in fact none actually exists—is a potential concern in any scientific investigation, traditionally addressed by keeping the significance threshold α comfortably low (typically .05, without correction). Type I error may be of increased concern in this study, as in many cases "marginal" effects with statistical significance levels between $p = .05$ and .10 were highlighted and discussed. Furthermore, analyses of phase-synchrony and cross-frequency coupling forwent multiple comparisons testing in determining whether changes in those indices differed from those at baseline. This decision was made due to the largely exploratory nature of these analyses, which cast a wide net across a variety of frequencies and electrode sites in hopes to hone in on those of relevance. As such, some of the reported effects, particularly those with less statistical significance, may represent type I error. However, multiple comparisons corrections were employed in all ANOVAs, including those examining task and group effects in the phase synchrony and cross-frequency coupling data. Furthermore, measures identified as differing from baseline were regressed on indices of behavioral performance, and those that showed predictive utility can reasonably be more confidently considered as veritable.

Also notable is the significant gender imbalance in the analyzed sample. With such varied gender breakdowns across groups, it is possible that reported group effects are strongly influenced by, or owed entirely to, gender effects. To examine this possibility, significant effects reported above were re-run examining only males, and the results are reported in Appendix B.

Of further potential concern are limitations related to the task design, particularly in the context of time-frequency analysis. In time-frequency decomposition, distortions occur at the beginning and ends of analyzed epochs due to the convolution of a wavelet or other windowing function with data that does not span the entire length of the temporal window (frequently termed "edge effects"; Roach & Mathalon, 2008). Edge effects are most easily addressed by ensuring the data subjected to time-frequency decomposition extend temporally well beyond those regions intended for analysis. In the case of the data from the WM task analyzed herein, the desire was to apply time-frequency methods to individual stimuli as presented in sequence. However, the inter-stimulus interval for these stimuli was only 1 second, meaning that extension of the analyzed epoch much further than this would run the risk of contamination from activity related to other stimuli or participant responses. As such, time-frequency decomposition methods were applied to a narrower time window than typically or ideally used in most cases, leading to notable edge effects at the ends of the analyzed epoch. Longer time-series are also preferred for analyzing very low-frequency data to allow the wider windowing functions more data with which to convolve. To address edge effects in the current investigation, time-frequency surfaces were examined, and an alternative baseline period (0-50ms, as

described above) determined to be visually free from contamination related to edge-effects was selected for baseline correction and comparisons. Regarding concerns related to low-frequency analyses on a relatively short window, few options for correction were available with the present data. However, this limitation is most likely to affect the lowest frequencies, e.g. the delta-band activity that was added to analysis upon inspection of time-frequency surfaces. Windows of interest used in analyzing these data were relatively wide, and no claims regarding the precise timing of activity in the delta-band were made in light of acknowledged compromised temporal resolution.

Potential confounding from medication effects should also be acknowledged and considered. PSZ in the current investigation had no restrictions regarding medication, and the vast majority were prescribed regular antipsychotic or related medications. The potential for the side effects of such medication affecting neural or behavioral outcomes is regularly acknowledged, though often unexamined beyond such acknowledgement. One notable exception comes from Lui and colleagues (2010), who found increased activity in regional BOLD signals and decreased functional connectivity across more widely distributed networks. As such, it is likely that presented results may be affected in some capacity by the effects of medication, and this fact should be considered in interpretation of results. However, as medication is common and encouraged in PSZ in the population at large, analysis of a similarly medicated sample may have greater real-world applicability than a similar study of unmedicated PSZ.

Future Directions

The current investigation presents initial findings on differences in cross-frequency coupling during WM in PSZ and their REL as compared to REL, as well as the relationship between coupling measures and WM performance. Replication of findings reported herein in independent samples are needed, particularly for the electrode pairings and frequencies that demonstrated synchrony effects as well as the frequency pairings and sites that showed effects of cross-frequency coupling. Furthermore, data-driven techniques such as those herein may uncover additional areas of potential relevance for uncovering the relationship between WM function and theta-gamma coupling. Theta- and gamma- activity should also be examined further in other experimental settings to clarify the specificity of reported abnormalities in PSZ and REL to WM, or whether similar anomalies are observed in other cognitive contexts or at rest. Clarifying the confounding effects of medication would similarly help to better understand the source of observed deficits. Examination of the association between neural abnormalities and polygenic risk scores would likewise help to inform how these electrophysiological aberrations are influenced by genetic liability. Contribution to emerging study of how neuromodulation affects theta-gamma coupling and related behavioral performance may afford the opportunity to make assertions regarding causality. Finally, presented results continue to suggest a special relevance of distracting stimuli for PSZ and REL. Continued understanding of this relevance and its neural underpinnings may further help to understand and potentially remedy observed abnormalities of WM related to the disorder.

Conclusions

Time-frequency analysis methods for EEG were used to explore the potential role of cross-frequency coupling between theta- and gamma-activity in WM deficits related to schizophrenia. EEG data collected from PSZ, REL and CTRL during performance of a WM task were first subjected to power and phase-synchrony analyses with the theta- and gamma-bands independently before examined the systematic interaction between activity in the two bands. Relationships between these various indices and performance on the WM task were further assessed. It was theorized that PSZ would demonstrate abnormalities as compared to CTRL in within-band time-frequency indices that would translate into aberrant cross-frequency coupling, which would further correlate with task performance. In light of previous results (Lynn, Kang & Sponheim, 2016), it was further expected that REL would show (potentially unique) abnormalities that would also correlate with their WM performance, which was previously found to be equivalent to CTRL on this task.

PSZ showed reductions in induced theta-power as compared to REL, with CTRL measures of theta power falling in between. Additionally, PSZ failed to modulate induced delta-power (added to the analyses after data inspection) in response to stimulus presentation order, in contrast to CTRL and REL. In light of the documented role of theta- and delta-power as indices of WM load, these abnormalities in PSZ support deficits in the relative ability of PSZ to effectively encode presented WM stimuli, both in sequence and overall, as compared to the other groups. Similar failures in PSZ to modulate gamma-power in response to presentation order as compared to CTRL and REL further support encoding difficulties in PSZ, and the predictive utility of gamma (64-

81hz) power as an index of WM performance in PSZ alone suggests that deficits in gamma activity may reflect memory deficits unique to the disorder. PSZ and REL also failed to modulate gamma-power (64-81hz) in response to stimulus type, potentially reflecting a common liability for visual processing deficits for which REL compensate to preserve behavioral performance.

Additionally, PSZ and REL showed increased gamma (36-56hz) phase-synchrony between prefrontal and several other areas in response to distractors as compared to CTRL. Such increases suggest differences in PSZ and REL versus CTRL regarding the treatment of distractor stimuli in the task, potentially related to attentional allocation. Furthermore, increased prefrontal-parietal synchrony in response to distractors in this frequency range predicted WM performance for PSZ alone, suggesting those PSZ who could more effectively process and utilize distractors performed better on the task.

Measures of cross-frequency coupling revealed various instances across examined sites and frequency pairings of increases as compared to baseline in response to WM stimuli; however, only slight differences in the time course of coupling changes were observed between groups. Notably, one focused index of change in phase-amplitude coupling was uniquely predictive of overall performance in PSZ, preliminarily supporting the notion that changes in theta-gamma coupling may in fact play a unique role in WM function for PSZ.

Though additional clarifying work is necessary, this study further demonstrates electrophysiological abnormalities in PSZ related to WM. The unique relationships

between particular measures and behavioral performance in PSZ may offer avenues for further investigation in an effort to better understand neural deficiencies exhibited by PSZ in regards to WM and potentially at large. Additionally, the examination of measures where REL showed differences from PSZ in conjunction with those where REL and PSZ showed similar abnormalities may help to better flesh out genetic liabilities for the disorder as well as potential compensatory or insulatory mechanisms that afford REL increased function as compared to PSZ, both in WM and day-to-day life.

Much investigation regarding cross-frequency coupling and its role in WM deficits in schizophrenia remains to be done. However, these preliminary investigations support increased coupling with WM load for all groups, and slight differences in the time course of such increases in PSZ and REL as compared to CTRL. Furthermore, cross-frequency coupling's limited predictive ability for PSZ in this study warrants further exploration, both within these data and in similar studies. As manipulations of theta-gamma coupling in healthy adults has been shown to improve WM performance (e.g., Reinhart & Nguyen, 2019; Alekseichuk et al., 2016; D. J. Lee et al., 2013), additional understanding of how and where coupling is aberrant in people with schizophrenia may help to inform treatment that serves to improve WM ability, day-to-day function and overall quality of life in people with the disorder.

References

Abram, S. V., Helwig, N. E., Moodie, C. A., DeYoung, C. G., MacDonald III, A. W., & Waller, N. G. (2016). Bootstrap enhanced penalized regression for variable selection with neuroimaging data. *Frontiers in Neuroscience*, 10, 344. doi:10.3389/fnins.2016.00344

Alekseichuk, I., Turi, Z., de Lara, G. A., Antal, A., & Paulus, W. (2016). Spatial working memory in humans depends on theta and high gamma synchronization in the prefrontal cortex. *Current Biology*, 26, 1513-1521.

Allen, A. J., Griss, M. E., Folley, B. S., Hawkins, K. A. & Pearlson, G. D. (2009). Endophenotypes in schizophrenia: A selective review. *Schizophrenia Research*, *109*, 24–37.

Allen, E. A., Liu, J., Kiehl, K. A., Gelernter, J., Pearlson, G. D., Perrone-Bizzozero, N. I. & Calhoun, V. D. (2011). Components of cross-frequency modulation in health and disease. *Frontiers in Systems Neuroscience*, *5*.

Andrade, R. (1991). Cell excitation enhances muscarinic cholinergic responses in rat association cortex. *Brain Research*, *548*, 81–93.

Anguera, J. A., Reuter-Lorenz, P. A., Willingham, D. T. & Seidler, R. D. (2010). Contributions of spatial working memory to visuomotor learning. *Journal of Cognitive Neuroscience*, *22*, 1917–1930.

Atkinson, R., & Shiffrin, R. (1968). Human memory: A proposed system and its control processes. In Spence, K., & Spence, J., (Eds.), *The psychology of learning and motivation*. (Vol. 2; pp. 89-105). New York: Academic Press.

Axmacher, N., Henseler, M. M., Jensen, O., Weinreich, I., Elger, C. E. & Fell, J. (2010). Cross-frequency coupling supports multi-item working memory in the human hippocampus. *Proceedings of the National Academy of Sciences*, *107*, 3228–3233.

Bachman, P., Kim, J., Yee, C. M., Therman, S., Manninen, M., Lönnqvist, J., … Cannon, T. D. (2009). Efficiency of working memory encoding in twins discordant for schizophrenia. *Psychiatry Research: Neuroimaging*, *174*, 97–104.

Bahramisharif, A., Jensen, O., Jacobs, J., & Lisman, J. (2018). Serial representation of items during working memory maintenance at letter-selective cortical sites. *PLOS: Biology*, 16, e2003805.

Barr, M., Farzan, F., Tran, L. C., Chen, R., Fitzgerald, P. & Daskalakis, Z. (2010). Evidence for excessive frontal evoked gamma oscillatory activity in schizophrenia during working memory. *Schizophrenia Research*, *121*, 146–152.

Barr, M. S., Rajji, T. K., Zomorrodi, R., Radhu, N., George, T. P., Blumberger, D. M., & Daskalakis, Z. J. (2017). Impaired theta-gamma coupling during working memory performance in schizophrenia. *Schizophrenia Research*, 189, 104-110.

Başar-Eroğlu, C., Başar, E., Demiralp, T. & Schürmann, M. (1992). P300-response: possible psychophysiological correlates in delta and theta frequency channels. A review. *International Journal of Psychophysiology*, *13*, 161–179.

Başar-Eroğlu, C., Brand, A., Hildebrandt, H., Kedzior, K. K., Mathes, B. & Schmiedt, C. (2007). Working memory related gamma oscillations in schizophrenia patients. *International Journal of Psychophysiology*, *64*, 39–45.

Başar-Eroğlu, C., Mathes, B., Brand, A. & Schmiedt-Fehr, C. (2011). Occipital gamma response to auditory stimulation in patients with schizophrenia. *International Journal of Psychophysiology*, *79*(1), 3–8.

Başar-Eroğlu, C., Schmiedt-Fehr, C., Marbach, S., Brand, A. & Mathes, B. (2008). Altered oscillatory alpha and theta networks in schizophrenia. *Brain Research*, *1235*, 143–152.

Begić, D., Hotujac, L. & Jokić-Begić, N. (2000). Quantitative EEG in "positive"and "negative"schizophrenia. *Acta Psychiatrica Scandinavica*, *101*, 307–311.

Belluscio, M. A., Mizuseki, K., Schmidt, R., Kempter, R. & Buzsáki, G. (2012). Cross-frequency phase-phase coupling between theta and gamma oscillations in the hippocampus. *Journal of Neuroscience*, *32*, 423–435.

Benchenane, K., Tiesinga, P. H. & Battaglia, F. P. (2011). Oscillations in the prefrontal cortex: A gateway to memory and attention. *Current Opinion in Neurobiology*, *21*, 475–485.

Berger, B., Minarik, T., Griesmayr, B., Stelzig-Schoeler, R., Aichhorn, W., & Sauseng, P. (2016). Brain oscillatory correlates of altered executive functioning in positive and negative symptomatic schizophrenia patients and healthy controls. *Frontiers in Psychology*, 7, 705. doi: 10.3389/fpsyg.2016.00705

Bernat, E.M., Williams, W.J., & Gehring, W.J. (2005). Decomposing ERP time-frequency energy using PCA.

Clinical Neurophysiology, 116, 1314-1334.Bieri, K. W., Bobbitt, K. N. & Colgin, L. L. (2014). Slow and fast gamma rhythms coordinate different spatial coding modes in hippocampal place cells. *Neuron*, *82*, 670–681.

Bland, B. H. (1986). The physiology and pharmacology of hippocampal formation theta rhythms. *Progress in Neurobiology*, *26*, 1–54.

Boutros, N. N., Zouridakis, G., & Overall, J. (1991). Replication and extension of P50 findings in schizophrenia. *Clinical Electroencephalography, 22*, 40–45.

Bragin, A., Jandó, G., Nádasdy, Z., Hetke, J., Wise, K. & Buzsáki, G. (1995). Gamma (40-100 Hz) oscillation in the hippocampus of the behaving rat. *Journal of Neuroscience*, *15*, 47–60.

Buzsáki, G., Buhl, D., Harris, K., Csicsvari, J., Czeh, B. & Morozov, A. (2003). Hippocampal network patterns of activity in the mouse. *Neuroscience*, *116*(1), 201–211.

Buzsáki, G., Leung, L.-W. S. & Vanderwolf, C. H. (1983). Cellular bases of hippocampal EEG in the behaving rat. *Brain Research Reviews*, *6*, 139–171.

Cabral, H. O., Vinck, M., Fouquet, C., Pennartz, C. M., Rondi-Reig, L. & Battaglia, F. P. (2014). Oscillatory dynamics and place field maps reflect hippocampal ensemble processing of sequence and place memory under NMDA receptor control. *Neuron*, *81*, 402–415.

Caeser, M., Brown, D. A., Gähwiler, B. H., & Knöpfel, T. (1993). Characterization of a calcium-dependent current generating a slow afterdepolarization of CA3

pyramidal cells in rat hippocampal slice cultures. *European Journal of Neuroscience, 5,* 560-569.

Canolty, R. T., Edwards, E., Dalal, S. S., Soltani, M., Nagarajan, S. S., Kirsch, H. E., … Knight, R. T. (2006). High gamma power is phase-locked to theta oscillations in human neocortex. *Science*, *313*, 1626–1628.

Castelhano, J., Duarte, I. C., Wibral, M., Rodriguez, E., & Castelo-Branco, M. (2014). The dual facet of gamma oscillations: Separate visual and decision making circuits as revealed by simultaneous EEG/MRI. *Human Brain Mapping*, 35, 5219-5235.

Chaieb, L., Leszczynski, M., Axmacher, N., Höhne, M., Elger, C. E. & Fell, J. (2015). Theta-gamma phase-phase coupling during working memory maintenance in the human hippocampus. *Cognitive Neuroscience*, *6*, 149–157.

Chang, H.-T. (1950). The repetitive discharges of corticothalamic reverberating circuit. *Journal of Neurophysiology*, *13*, 235–257.

Chen, C.-M. A., Stanford, A. D., Mao, X., Abi-Dargham, A., Shungu, D. C., Lisanby, S. H., … Kegeles, L. S. (2014). GABA level, gamma oscillation, and working memory performance in schizophrenia. *NeuroImage: Clinical*, *4*, 531–539.

Cho, R., Konecky, R. & Carter, C. (2006). Impairments in frontal cortical gamma synchrony and cognitive control in schizophrenia. *Proceedings of the National Academy of Sciences*, *103*, 19878–19883.

Chrobak, J. J. & Buzsáki, G. (1998). Gamma oscillations in the entorhinal cortex of the freely behaving rat. *Journal of Neuroscience*, *18*, 388–398.

Chrobak, J. J., Lörincz, A. & Buzsáki, G. (2000). Physiological patterns in the hippocampo-entorhinal cortex system. *Hippocampus*, *10*(4), 457–465.

Clementz, B. A. & Blumenfeld, L. D. (2001). Multichannel electroencephalographic assessment of auditory evoked response suppression in schizophrenia. *Experimental Brain Research*, *139*, 377–390.

Clementz, B. A., Blumenfeld, L. D. & Cobb, S. (1997). The gamma band response may account for poor P50 suppression in schizophrenia. *Neuroreport*, *8*, 3889–3893.

Conklin, H. M., Curtis, C. E., Calkins, M. E. & Iacono, W. G. (2005). Working memory functioning in schizophrenia patients and their first-degree relatives: Cognitive functioning shedding light on etiology. *Neuropsychologia*, *43*, 930–942.

Cooper, P. S., Wong, A. S., Fulham, W. R., Thienel, R., Mansfield, E., Michie, P. T., & Karayandis, F. (2015). Theta frontoparietal connectivity associated with proactive and reactive cognitive control processes. *NeuroImage*, 108, 354-363.

Crivelli-Decker, J., Hsieh, L., Clarke, A., & Ranganath, C. (2018). Theta oscillations promote temporal sequence learning. *Neurobiology of Learning and Memory*, 153, 92-103.

Csicsvari, J., Jamieson, B., Wise, K. D. & Buzsáki, G. (2003). Mechanisms of gamma oscillations in the hippocampus of the behaving rat. *Neuron*, *37*, 311–322.

Cunningham, M. O., Davies, C. H., Buhl, E. H., Kopell, N. & Whittington, M. A. (2003). Gamma oscillations induced by kainate receptor activation in the entorhinal cortex in vitro. *Journal of Neuroscience*, *23*, 9761–9769.

Davenport, N. D., Sponheim, S. R. & Stanwyck, J. J. (2006). Neural anomalies during visual search in schizophrenia patients and unaffected siblings of schizophrenia patients. *Schizophrenia Research*, *82*, 15–26.

De Almeida, L., Idiart, M., Villavicencio, A. & Lisman, J. (2012). Alternating predictive and short-term memory modes of entorhinal grid cells. *Hippocampus*, *22*, 1647–1651.

De Beni, R., Pazzaglia, F., Gyselinck, V. & Meneghetti, C. (2005). Visuospatial working memory and mental representation of spatial descriptions. *European Journal of Cognitive Psychology*, *17*, 77–95.

Demiralp, T., Bayraktaroglu, Z., Lenz, D., Junge, S., Busch, N. A., Maess, B., … Herrmann, C. S. (2007). Gamma amplitudes are coupled to theta phase in human EEG during visual perception. *International Journal of Psychophysiology*, *64*, 24–30.

Dias, E. C., Butler, P. D., Hoptman, M. J. & Javitt, D. C. (2011). Early sensory contributions to contextual encoding deficits in schizophrenia. *Archives of General Psychiatry*, *68*, 654–664.

Doege, K., Bates, A., White, T., Das, D., Boks, M. & Liddle, P. (2009). Reduced event-related low frequency EEG activity in schizophrenia during an auditory oddball task. *Psychophysiology*, *46*, 566–577.

Donkers, F. C., Schwikert, S. R., Evans, A. M., Cleary, K. M., Perkins, D. O. & Belger, A. (2011). Impaired neural synchrony in the theta frequency range in adolescents at familial risk for schizophrenia. *Frontiers in Psychiatry*, *2*.

Ergen, M., Marbach, S., Brand, A., Başar-Eroğlu, C. & Demiralp, T. (2008). P3 and delta band responses in visual oddball paradigm in schizophrenia. *Neuroscience Letters*, *440*, 304–308.

Fell, J. & Axmacher, N. (2011). The role of phase synchronization in memory processes. *Nature Reviews: Neuroscience*, *12*, 105–118.

Fell, J., Fernández, G., Klaver, P., Elger, C. E., & Fries, P. (2003). Is synchronized neuronal gamma activity relevant for selective attention? *Brain Research Reviews*, 42, 265-272.

Fell, J., Klaver, P., Elfadil, H., Schaller, C., Elger, C. E. & Fernández, G. (2003). Rhinal-hippocampal theta coherence during declarative memory formation: Interaction with gamma synchronization? *European Journal of Neuroscience*, *17*, 1082–1088.

Fox, S., Wolfson, S. & Ranck Jr, J. (1986). Hippocampal theta rhythm and the firing of neurons in walking and urethane anesthetized rats. *Experimental Brain Research*, *62*, 495–508.

Freedman, R., Adler, L. E., Waldo, M. C., Pachtman, E., & Franks, R. D. (1983). Neurophysiological evidence for a defect in inhibitory pathways in schizophrenia: Comparison of medicated and drug-free patients. *Biological Psychiatry, 18,* 537–551.

Fujimoto, T., Okumura, E., Takeuchi, K., Kodabashi, A., Otsubo, T., Nakamura, K., … others. (2013). Dysfunctional cortical connectivity during the auditory oddball task in patients with schizophrenia. *Open Neuroimaging Journal*, *7*, 15–26.

Glahn, D. C., Therman, S., Manninen, M., Huttunen, M., Kaprio, J., Lönnqvist, J. & Cannon, T. D. (2003). Spatial working memory as an endophenotype for schizophrenia. *Biological Psychiatry*, *53*, 624–626.

Goghari, V. M., Brett, C., Tabraham, P., Johns, L., Valmaggia, L., Broome, M., … McGuire, P. (2014). Spatial working memory ability in individuals at ultra high risk for psychosis. *Journal of Psychiatric Research*, *50*, 100–105.

Gottesman, I. I. & Gould, T. D. (2003). The endophenotype concept in psychiatry: Etymology and strategic intentions. *American Journal of Psychiatry*, *160*, 636–645.

Goutagny, R., Gu, N., Cavanagh, C., Jackson, J., Chabot, J.-G., Quirion, R., … Williams, S. (2013). Alterations in hippocampal network oscillations and theta-gamma coupling arise before A-beta overproduction in a mouse model of Alzheimer's disease. *European Journal of Neuroscience*, *37*, 1896–1902.

Griesmayr, B., Berger, B., Stelzig-Schoeler, R., Aichhorn, W., Bergmann, J. & Sauseng, P. (2014). EEG theta phase coupling during executive control of visual working memory investigated in individuals with schizophrenia and in healthy controls. *Cognitive, Affective, & Behavioral Neuroscience*, *14*, 1340–1355.

Güntekin, B., & Başar, E. (2016). Review of evoked and event-related delta responses in the human brain. *International Journal of Psychophysiology,* 103, 43-52.

Haenschel, C., Bittner, R. A., Haertling, F., Rotarska-Jagiela, A., Maurer, K., Singer, W. & Linden, D. E. (2007). Contribution of impaired early-stage visual processing to working memory dysfunction in adolescents with schizophrenia: A study with

event-related potentials and functional magnetic resonance imaging. *Archives of General Psychiatry*, *64*, 1229–1240.

Haenschel, C., Bittner, R. A., Waltz, J., Haertling, F., Wibral, M., Singer, W., … Rodriguez, E. (2009). Cortical oscillatory activity is critical for working memory as revealed by deficits in early-onset schizophrenia. *Journal of Neuroscience*, *29*(30), 9481–9489.

Haig, A. R., Gordon, E., De Pascalis, V., Meares, R. A., Bahramali, H. & Harris, A. (2000). Gamma activity in schizophrenia: Evidence of impaired network binding? *Clinical Neurophysiology*, *111*, 1461–1468.

He, B. J., Zempel, J. M., Snyder, A. Z. & Raichle, M. E. (2010). The temporal structures and functional significance of scale-free brain activity. *Neuron*, *66*, 353–369.

Hentschke, H., Perkins, M. G., Pearce, R. A. & Banks, M. I. (2007). Muscarinic blockade weakens interaction of gamma with theta rhythms in mouse hippocampus. *European Journal of Neuroscience*, *26*, 1642–1656.

Hirano, S., Nakhnikian, A., Hirano, Y., Oribe, N., Kanba, S., Onitsuka, T., … Spencer, K. M. (2018). Phase-amplitude coupling of the electroencephalogram in the auditory cortex in schizophrenia. *Biological Psychiatry*, 3, 69-76.

Holz, E. M., Glennon, M., Prendergast, K. & Sauseng, P. (2010). Theta-gamma phase synchronization during memory matching in visual working memory. *Neuroimage*, *52*, 326–335.

Honaken, R., Rouhinen, S., Wang, S. H., Palva, J. M., & Palva, S. (2015). Gamma oscillations underlie the maintenance of feature-specific information and the contents of visual working memory. *Cerebral Cortex*, 24, 3788-3801.

Hong, L. E., Summerfelt, A., Mitchell, B. D., McMahon, R. P., Wonodi, I., Buchanan, R. W. & Thaker, G. K. (2008). Sensory gating endophenotype based on its neural oscillatory pattern and heritability estimate. *Archives of General Psychiatry*, *65*, 1008–1016.

Ishii, R., Shinosaki, K., Ikejiri, Y., Ukai, S., Yamashita, K., Iwase, M., … Takeda, M. (2000). Theta rhythm increases in left superior temporal cortex during auditory hallucinations in schizophrenia: A case report. *Neuroreport*, *11*, 3283–3287.

Jensen, O. & Lisman, J. E. (1998). An oscillatory short-term memory buffer model can account for data on the Sternberg task. *Journal of Neuroscience*, *18*, 10688–10699.

Jensen, O. & Tesche, C. D. (2002). Frontal theta activity in humans increases with memory load in a working memory task. *European Journal of Neuroscience*, *15*, 1395–1399.

Joliot, M., Ribary, U. & Llinas, R. (1994). Human oscillatory brain activity near 40 Hz coexists with cognitive temporal binding. *Proceedings of the National Academy of Sciences*, *91*, 11748–11751.

Kalweit, A. N., Amanpour-Gharaei, B., Colitti-Klausnitzer, J., & Manahan-Vaughan, D. (2017). Changes in neuronal oscillations accompany the loss of hippocampal LTP

that occurs in an animal model of psychosis. *Frontiers in Behavioral Neuroscience*, 11, 36.

Kang, S. S., MacDonald III, A. W., Chafee, M. V., Im, C., Bernat, E. M., Davenport, N. D., & Sponheim, S. R. (2018). Abnormal cortical neural synchrony during working memory in schizophrenia. *Clinical Neurophysiology*, 129, 210-221.

Kang, S. S., Sponheim, S. R., Chafee, M. V. & MacDonald, A. W. (2011). Disrupted functional connectivity for controlled visual processing as a basis for impaired spatial working memory in schizophrenia. *Neuropsychologia*, *49*, 2836–2847.

Kirihara, K., Rissling, A. J., Swerdlow, N. R., Braff, D. L. & Light, G. A. (2012). Hierarchical organization of gamma and theta oscillatory dynamics in schizophrenia. *Biological Psychiatry*, *71*, 873–880.

Kissler, J., Müller, M. M., Fehr, T., Rockstroh, B. & Elbert, T. (2000). MEG gamma band activity in schizophrenia patients and healthy subjects in a mental arithmetic task and at rest. *Clinical Neurophysiology*, *111*, 2079–2087.

Koch, C., & Crick, F. (1994). Some further ideas regarding the neuronal basis of awareness. In Koch, C., & Davis, J. L. (Eds.), *Large scale neuronal theories of the brain* (pp. 93-109). Cambridge, MA: MIT Press.

Koene, R. A. & Hasselmo, M. E. (2007). First-in-first-out item replacement in a model of short-term memory based on persistent spiking. *Cerebral Cortex*, *17*, 1766–1781.

Kwon, J. S., O'Donnell, B. F., Wallenstein, G. V., Greene, R. W., Hirayasu, Y., Nestor, P. G., … McCarley, R. W. (1999). Gamma frequency-range abnormalities to

auditory stimulation in schizophrenia. *Archives of General Psychiatry*, *56*, 1001–1005.

König, T., Lehmann, D., Saito, N., Kuginuki, T., Kinoshita, T. & Koukkou, M. (2001). Decreased functional connectivity of EEG theta-frequency activity in first-episode, neuroleptic-naïve patients with schizophrenia: preliminary results. *Schizophrenia Research*, *50*, 55–60.

Kustermann, T., Popov, T., Miller, G. A., & Rockstroh, B. (2018). Verbal working memory-related neural network communication in schizophrenia. *Psychophysiology*, 55, e13088.

Lakatos, P., Shah, A. S., Knuth, K. H., Ulbert, I., Karmos, G. & Schroeder, C. E. (2005). An oscillatory hierarchy controlling neuronal excitability and stimulus processing in the auditory cortex. *Journal of Neurophysiology*, *94*, 1904–1911.

Lee, D. J., Gurkoff, G. G., Izadi, A., Berman, R. F., Ekstrom, A. D., Muizelaar, J. P., … Shahlaie, K. (2013). Medial septal nucleus theta frequency deep brain stimulation improves spatial working memory after traumatic brain injury. *Journal of Neurotrauma*, *30*, 131–139.

Lee, J. & Park, S. (2005). Working memory impairments in schizophrenia: A meta-analysis. *Journal of Abnormal Psychology*, *114*, 599–611.

Lee, S. Y., Namkoong, K., Cho, H. H., Song, D.-H. & An, S. K. (2010). Reduced visual P300 amplitudes in individuals at ultra-high risk for psychosis and first-episode schizophrenia. *Neuroscience Letters*, *486*, 156–160.

Lee, Y.-Y. & Yang, C.-Y. (2014). Utilizing the extent of theta-gamma synchronization to estimate visuospatial memory ability. *Australasian Physical & Engineering Sciences in Medicine*, *37*, 665–672.

Leicht, G., Karch, S., Karamatskos, E., Giegling, I., Möller, H.-J., Hegerl, U., … Mulert, C. (2011). Alterations of the early auditory evoked gamma-band response in first-degree relatives of patients with schizophrenia: Hints to a new intermediate phenotype. *Journal of Psychiatric Research*, *45*, 699–705.

Leicht, G., Kirsch, V., Giegling, I., Karch, S., Hantschk, I., Möller, H.-J., … Mulert, C. (2010). Reduced early auditory evoked gamma-band response in patients with schizophrenia. *Biological Psychiatry*, *67*, 224–231.

Lisman, J. E. & Buzsáki, G. (2008). A neural coding scheme formed by the combined function of gamma and theta oscillations. *Schizophrenia Bulletin*, *34*, 974–980.

Lisman, J. E. & Idiart, M. A. (1995). Storage of 7+/-2 short-term memories in oscillatory subcycles. *Science*, *267*, 1512–1515.

Lisman, J. E. & Jensen, O. (2013). The theta-gamma neural code. *Neuron*, *77*, 1002–1016.

Lisman, J. E. & Redish, A. D. (2009). Prediction, sequences and the hippocampus. *Philosophical Transactions of the Royal Society B: Biological Sciences*, *364*, 1193–1201.

Llinas, R. & Ribary, U. (1993). Coherent 40-Hz oscillation characterizes dream state in humans. *Proceedings of the National Academy of Sciences*, *90*, 2078–2081.

Lui, S., Tao, L., Deng, W., Jiang, L., Wu, Q., Tang, H., … Gong, Q. (2010). Short-term effects of antipsychotic treatment on cerebral function in drug-naïve first-episode schizophrenia revealed by "resting state" functional magnetic resonance imaging. *Archives of General Psychiatry*, 67, 783-792.

Lynn, P., Kang, S. S., & Sponheim, S. (2016). Impaired retrieval processes evident during visual working memory in schizophrenia. *Schizophrenia Research: Cognition*, 5, 47-55.

MacDonald, A. W. & Schulz, S. C. (2009). What we know: Findings that every theory of schizophrenia should explain. *Schizophrenia Bulletin*, *35*, 493–508.

Maris, E., van Vugt, M. & Kahana, M. (2011). Spatially distributed patterns of oscillatory coupling between high-frequency amplitudes and low-frequency phases in human iEEG. *Neuroimage*, *54*, 836–850.

Martínez, A., Gaspar, P. A., Hillyard, S. A., Bickel, S., Lakatos, P., Dias, E. C. & Javitt, D. C. (2015). Neural oscillatory deficits in schizophrenia predict behavioral and neurocognitive impairments. *Frontiers in Human Neuroscience*, *9*.

Meilinger, T., Knauff, M. & Bülthoff, H. H. (2008). Working memory in wayfinding—A dual task experiment in a virtual city. *Cognitive Science*, *32*, 755–770.

Miller, E. K., Lundqvist, M., & Bastos, A. M. (2018). Working memory 2.0. *Neuron*, 100, 463-475.

Michaels, T. I., Long, L. L., Stevenson, I. H., Chrobak, J. J., & Chen, C. A. (2018). Effects of chronic ketamine on hippocampal cross-frequency coupling:

implications for schizophrenia pathophysiology. *European Journal of Neuroscience*, 48, 2903-2914.

Miller, K. J., Hermes, D., Honey, C. J., Sharma, M., Rao, R. P., Den Nijs, M., … Leuthardt, E. C. (2010). Dynamic modulation of local population activity by rhythm phase in human occipital cortex during a visual search task. *Frontiers in Human Neuroscience*, *4*.

Minzenberg, M. J., Firl, A. J., Yoon, J. H., Gomes, G. C., Reinking, C. & Carter, C. S. (2010). Gamma oscillatory power is impaired during cognitive control independent of medication status in first-episode schizophrenia. *Neuropsychopharmacology*, *35*, 2590–2599.

Missonnier, P., Herrmann, F. R., Zanello, A., Bâ, M. B., Curtis, L., Canovas, D., … Merlo, M. C. (2012). Event-related potentials and changes of brain rhythm oscillations during working memory activation in patients with first-episode psychosis. *Journal of Psychiatry & Neuroscience*, *37*, 95.

Moran, L. V. & Hong, L. E. (2011). High vs low frequency neural oscillations in schizophrenia. *Schizophrenia Bulletin*, 659–663.

Mormann, F., Fell, J., Axmacher, N., Weber, B., Lehnertz, K., Elger, C. E. & Fernández, G. (2005). Phase/amplitude reset and theta-gamma interaction in the human medial temporal lobe during a continuous word recognition memory task. *Hippocampus*, *15*, 890–900.

Nakamura, K., Mikami, A. & Kubota, K. (1992). Oscillatory neuronal activity related to visual short-term memory in monkey temporal pole. *Neuroreport*, *3*(1), 117–120.

Nishida, H., Takahashi, M. & Lauwereyns, J. (2014). Within-session dynamics of theta-gamma coupling and high-frequency oscillations during spatial alternation in rat hippocampal area CA1. *Cognitive Neurodynamics*, *8*, 363–372.

Nyhus, E. & Curran, T. (2010). Functional role of gamma and theta oscillations in episodic memory. *Neuroscience & Biobehavioral Reviews*, *34*, 1023–1035.

O'Keefe, J. & Recce, M. L. (1993). Phase relationship between hippocampal place units and the EEG theta rhythm. *Hippocampus*, *3*, 317–330.

Oribe, N., Hirano, Y., Kanba, S., del Re, E. C., Seidman, L. J., Mesholam-Gately, R., … Niznikiewicz, M. A. (2013). Early and late stages of visual processing in individuals in prodromal state and first episode schizophrenia: An ERP study. *Schizophrenia Research*, *146*, 95–102.

Otto, T., Eichenbaum, H., Wible, C. G. & Wiener, S. I. (1991). Learning-related patterns of CA1 spike trains parallel stimulation parameters optimal for inducing hippocampal long-term potentiation. *Hippocampus*, *1*, 181–192.

Park, J. Y., Jhung, K., Lee, J. & An, S. K. (2013). Theta-gamma coupling during a working memory task as compared to a simple vigilance task. *Neuroscience Letters*, *532*, 39–43.

Park, J. Y., Lee, Y.-R. & Lee, J. (2011). The relationship between theta-gamma coupling and spatial memory ability in older adults. *Neuroscience Letters*, *498*, 37–41.

Park, S., Holzman, P. S. & Goldman-Rakic, P. S. (1995). Spatial working memory deficits in the relatives of schizophrenic patients. *Archives of General Psychiatry*, *52*, 821–828.

Pastoll, H., Solanka, L., van Rossum, M. C. & Nolan, M. F. (2013). Feedback inhibition enables theta-nested gamma oscillations and grid firing fields. *Neuron*, *77*, 141–154.

Perez, V. B., Vogel, E. K., Luck, S. & Kappenman, E. (2012). What ERPs can tell us about working memory. *The Oxford Handbook of Event-Related Potential Components*, 361–372.

Philips, J. L., Shiffrin, R. M., & Atkinson, R. C. (1967). Effects of list length on short term memory. *Journal of Verbal Learning and Verbal Behavior, 6,* 156-163.

Pina, J. E., Bodner, M., & Ermentrout, B. (2018). Oscillations in working memory and neural binding: A mechanism for multiple memories and their interactions. *PLOS: Computational Biology*, 14, e1006517. doi: 10.1371/journal.pcbi.1006517

Palva, J. M., Monto, S., Kulashekhar, S. & Palva, S. (2010). Neuronal synchrony reveals working memory networks and predicts individual memory capacity. *Proceedings of the National Academy of Sciences*, 107, 7580-7585.

Pavlov, Y. G., & Kotchoubey, B. (2017). EEG correlates of working memory performance in females. *BMC Neuroscience,* 18, 26.

Pirkola, T., Tuulio-Henriksson, A., Glahn, D., Kieseppä, T., Haukka, J., Kaprio, J., … Cannon, T. D. (2005). Spatial working memory function in twins with schizophrenia and bipolar disorder. *Biological Psychiatry*, *58*, 930–936.

Poppe, A. B., Carter, C. S., Minzenberg, M. J. & MacDonald, A. W. (2015). Task-based functional connectivity as an indicator of genetic liability to schizophrenia. *Schizophrenia Research*, *162*, 118–123.

Potkin, S., Turner, J., Brown, G., McCarthy, G., Greve, D., Glover, G., … FBIRN. (2009). Working memory and DLPFC inefficiency in schizophrenia: The FBIRN study. *Schizophrenia Bulletin*, *35*, 19–31.

Quilichini, P., Sirota, A. & Buzsáki, G. (2010). Intrinsic circuit organization and theta-gamma oscillation dynamics in the entorhinal cortex of the rat. *Journal of Neuroscience*, *30*, 11128–11142.

Rajji, T. K., Zomorrodi, R., Barr, M. S., Blumberger, D. M., Mulsant, B. H., & Daskalakis, Z. J. (2017). Ordering information in working memory and modulation of gamma by theta oscillations in humans. *Cerebral Cortex*, 27, 1482-1490.

Reinhart, R. M., Mathalon, D. H., Roach, B. J. & Ford, J. M. (2011). Relationships between pre-stimulus gamma power and subsequent P300 and reaction time breakdown in schizophrenia. *International Journal of Psychophysiology*, *79*, 16–24.

Reinhart, R. M. G., & Nguyen, J. A. (2019). Working memory revived in older adults by synchronizing rhythmic brain circuits. *Nature Neuroscience*. doi: 10.1038/s41593-019-0371-x

Roach, B. J., & Mathalon, D. H. (2008). Event-related EEG time-frequency analysis: An overview of measures and an analysis of early gamma band phase locking in schizophrenia. *Schizophrenia Bulletin*, 34, 907-926.

Roemer, R. A. & Shagass, C. (1990). Replication of an evoked potential study of lateralized hemispheric dysfunction in schizophrenics. *Biological Psychiatry*, *28*, 275–291.

Roux, F., Wibral, M., Mohr, H. M., Singer, W., & Uhlhaas, P. J. (2012). Gamma-band activity in human prefrontal cortex codes for the number of relevant items maintained in working memory. *Journal of Neuroscience,* 32, 12411-12420.

Ryman, S. G., Cavanagh, J. F., Wertz, C. J., Shaff, N. A., Dodd, A. B., Stevens, B., … Mayer, A. R. (2018). Impaired midline theta power and connectivity during proactive cognitive control in schizophrenia. *Biological Psychiatry*, 84, 675-683.

Sauseng, P., Griesmayr, B., Freunberger, R. & Klimesch, W. (2010). Control mechanisms in working memory: A possible function of EEG theta oscillations. *Neuroscience & Biobehavioral Reviews*, *34*, 1015–1022.

Sauseng, P., Klimesch, W., Gruber, W. R. & Birbaumer, N. (2008). Cross-frequency phase synchronization: a brain mechanism of memory matching and attention. *Neuroimage*, *40*, 308–317.

Sauseng, P., Klimesch, W., Heise, K. F., Gruber, W. R., Holz, E., Karim, A. A., … Hummel, F. C. (2009). Brain oscillatory substrates of visual short-term memory capacity. *Current Biology*, *19*, 1846–1852.

Saylik, R., Raman, E., & Szameitat, A. J. (2018). Sex differences in emotion recognition and working memory tasks. *Frontiers in Psychology*, 9, 1072.

Schack, B., Vath, N., Petsche, H., Geissler, H.-G. & Möller, E. (2002). Phase-coupling of theta-gamma EEG rhythms during short-term memory processing. *International Journal of Psychophysiology*, *44*, 143–163.

Sharinger, C., Soutschek, A., Schubert, T, & Gerjets, P. (2017). Comparison of the working memory load in *N*-back and working memory. *Frontiers in Human Neuroscience, 11*, 6. doi: 10.3389/fnhum.2017.00006

Schmiedt, C., Brand, A., Hildebrandt, H. & Başar-Eroğlu, C. (2005). Event-related theta oscillations during working memory tasks in patients with schizophrenia and healthy controls. *Cognitive Brain Research*, *25*, 936–947.

Schomburg, E. W., Fernández-Ruiz, A., Mizuseki, K., Berényi, A., Anastassiou, C. A., Koch, C. & Buzsáki, G. (2014). Theta phase segregation of input-specific gamma patterns in entorhinal-hippocampal networks. *Neuron*, *84*, 470–485.

Sederberg, P. B., Kahana, M. J., Howard, M. W., Donner, E. J. & Madsen, J. R. (2003). Theta and gamma oscillations during encoding predict subsequent recall. *Journal of Neuroscience*, *23*, 10809–10814.

Shenton, M. E., Faux, S. F., McCarley, R. W., Ballinger, R., Coleman, M., Torello, M. & Duffy, F. H. (1989). Correlations between abnormal auditory P300 topography and positive symptoms in schizophrenia: A preliminary report. *Biological Psychiatry*, *25*, 710–716.

Siegel, M., Warden, M. R. & Miller, E. K. (2009). Phase-dependent neuronal coding of objects in short-term memory. *Proceedings of the National Academy of Sciences*, *106*, 21341–21346.

Siegle, J. H. & Wilson, M. A. (2014). Enhancement of encoding and retrieval functions through theta phase-specific manipulation of hippocampus. *eLife*, *3*.

Simmonite, M., Bates, A. T., Groom, M., Hollis, C. & Liddle, P. F. (2015). Reduced event-related low frequency EEG activity in patients with early onset schizophrenia and their unaffected siblings. *Psychiatry Research: Neuroimaging*, *232*, 51–57.

Sinclair, B. R., Seto, M. G. & Bland, B. H. (1982). Theta-cells in CA1 and dentate layers of hippocampal formation: Relations to slow-wave activity and motor behavior in the freely moving rabbit. *Journal of Neurophysiology*, *48*, 1214–1225.

Singer, W. (1993). Synchronization of cortical activity and its putative role in information processing and learning. *Annual Review of Physiology*, *55*, 349–374.

Sirota, A., Montgomery, S., Fujisawa, S., Isomura, Y., Zugaro, M. & Buzsáki, G. (2008). Entrainment of neocortical neurons and gamma oscillations by the hippocampal theta rhythm. *Neuron*, *60*, 683–697.

Skaggs, W. E., McNaughton, B. L., Wilson, M. A. & Barnes, C. A. (1996). Theta phase precession in hippocampal neuronal populations and the compression of temporal sequences. *Hippocampus*, *6*, 149–172.

Slewa-Younan, S., Gordon, E., Harris, A. W., Haig, A. R., Brown, K. J., Flor-Henry, P. & Williams, L. M. (2004). Sex differences in functional connectivity in first-

episode and chronic schizophrenia patients. *American Journal of Psychiatry*, *161*, 1595–1602.

Snitz, B. E., MacDonald, A. W. & Carter, C. S. (2006). Cognitive deficits in unaffected first-degree relatives of schizophrenia patients: A meta-analytic review of putative endophenotypes. *Schizophrenia Bulletin*, *32*, 179–194.

Solomon, E. A., Kragel, J. E., Sperling, M. R., Sharan, A., Worrell, G., Kucewicz, M., … Kahana, M. J. (2017). Widespread theta synchrony and high-frequency desynchronization underlies enhanced cognition. *Nature Communications*, 8, 1704.

Soltesz, I. & Deschenes, M. (1993). Low-and high-frequency membrane potential oscillations during theta activity in CA1 and CA3 pyramidal neurons of the rat hippocampus under ketamine-xylazine anesthesia. *Journal of Neurophysiology*, *70*, 97–116.

Spellman, T. J. & Gordon, J. A. (2015). Synchrony in schizophrenia: A window into circuit-level pathophysiology. *Current Opinion in Neurobiology*, *30*, 17–23.

Spencer, K. M., Nestor, P. G., Niznikiewicz, M. A., Salisbury, D. F., Shenton, M. E. & McCarley, R. W. (2003). Abnormal neural synchrony in schizophrenia. *Journal of Neuroscience*, *23*, 7407–7411.

Spencer, K. M., Nestor, P. G., Perlmutter, R., Niznikiewicz, M. A., Klump, M. C., Frumin, M., … McCarley, R. W. (2004). Neural synchrony indexes disordered perception and cognition in schizophrenia. *Proceedings of the National Academy of Sciences of the United States of America*, *101*(49), 17288–17293.

Spencer, K. M., Niznikiewicz, M. A., Shenton, M. E. & McCarley, R. W. (2008). Sensory-evoked gamma oscillations in chronic schizophrenia. *Biological Psychiatry*, *63*, 744–747.

Sponheim, S. R., McGuire, K. A. & Stanwyck, J. J. (2006). Neural anomalies during sustained attention in first-degree biological relatives of schizophrenia patients. *Biological Psychiatry*, *60*, 242–252.

Steriade, M., Dossi, R. C., Pare, D. & Oakson, G. (1991). Fast oscillations (20-40 Hz) in thalamocortical systems and their potentiation by mesopontine cholinergic nuclei in the cat. *Proceedings of the National Academy of Sciences*, *88*, 4396–4400.

Sternberg, S. (October, 1964). Estimating the distribution of additive reaction-time components. Paper presented at the annual meeting of the Psychometric Society.

Sternberg, S. (1966). High-speed scanning in human memory. *Science*, *153*, 652–654.

Storm, J. F. (1989). An after-hyperpolarization of medium duration in rat hippocampal pyramidal cells. *Journal of Physiology*, *409*, 171–190.

Symond, M. B., Harris, A. W., Gordon, E. & Williams, L. M. (2005). "Gamma synchrony" in first-episode schizophrenia: A disorder of temporal connectivity? *American Journal of Psychiatry*, *162*, 459–465.

Takahashi, H., Iwase, M., Nakahachi, T., Sekiyama, R., Tabushi, K., Kajimoto, O., … Takeda, M. (2005). Spatial working memory deficit correlates with disorganization symptoms and social functioning in schizophrenia. *Psychiatry and Clinical Neurosciences*, *59*, 453–460.

Takahashi, M., Nishida, H., Redish, A. D. & Lauwereyns, J. (2014). Theta phase shift in spike timing and modulation of gamma oscillation: A dynamic code for spatial alternation during fixation in rat hippocampal area CA1. *Journal of Neurophysiology*, *111*, 1601–1614.

Tamura, M., Spellman, T. J., Rosen, A. M., Gogos, J. A., & Gordon, J. A. (2017). Hippocampal-prefrontal theta-gamma coupling during performance of a spatial working memory task. *Nature Communications*, 8, 2182.

Tort, A. B., Komorowski, R. W., Manns, J. R., Kopell, N. J. & Eichenbaum, H. (2009). Theta-gamma coupling increases during the learning of item-context associations. *Proceedings of the National Academy of Sciences*, *106*, 20942–20947.

Tort, A. B., Kramer, M. A., Thorn, C., Gibson, D. J., Kubota, Y., Graybiel, A. M. & Kopell, N. J. (2008). Dynamic cross-frequency couplings of local field potential oscillations in rat striatum and hippocampus during performance of a T-maze task. *Proceedings of the National Academy of Sciences*, *105*, 20517–20522.

Trimper, J. B., Stefanescu, R. A. & Manns, J. R. (2014). Recognition memory and theta-gamma interactions in the hippocampus. *Hippocampus*, *24*, 341–353.

Uhlhaas, P. J. & Singer, W. (2010). Abnormal neural oscillations and synchrony in schizophrenia. *Nature Reviews: Neuroscience*, *11*, 100–113.

Uresti-Cabrera, L. A., Diaz, R., Vaca-Palomares, I. & Fernandez-Ruiz, J. (2015). The effect of spatial working memory deterioration on strategic visuomotor learning across aging. *Behavioural Neurology*, *2015*.

Van der Meij, R., Kahana, M. & Maris, E. (2012). Phase-amplitude coupling in human electrocorticography is spatially distributed and phase diverse. *The Journal of Neuroscience*, *32*, 111–123.

Voloh, B., Valiante, T. A., Everling, S. & Womelsdorf, T. (2015). Theta-gamma coordination between anterior cingulate and prefrontal cortex indexes correct attention shifts. *Proceedings of the National Academy of Sciences*, *112*, 8457–8462.

Von der Malsburg, C. & Schneider, W. (1986). A neural cocktail-party processor. *Biological Cybernetics*, *54*, 29–40.

Voytek, B., Canolty, R. T., Shestyuk, A., Crone, N. E., Parvizi, J. & Knight, R. T. (2010). Shifts in gamma phase-amplitude coupling frequency from theta to alpha over posterior cortex during visual tasks. *Frontiers in Human Neuroscience*, *4*.

White, T., Cullen, K., Rohrer, L. M., Karatekin, C., Luciana, M., Schmidt, M., … Lim, K. O. (2008). Limbic structures and networks in children and adolescents with schizophrenia. *Schizophrenia Bulletin*, *34*, 18–29.

Williams, L. M., Whitford, T. J., Gordon, E., Gomes, L., Brown, K. J., & Harris, A. W. F. (2009). Neural synchrony in patients with a first episode of schizophrenia: tracking relations with grey matter and symptom profile. *Journal of Psychiatry and Neuroscience*, 34, 21-29.

Williams, S., & Boksa, P. (2010). Gamma oscillations and schizophrenia. *Journal of Psychiatry and Neuroscience,* 35, 75-77.

Wilson, T. W., Hernandez, O. O., Asherin, R. M., Teale, P. D., Reite, M. L., & Rojas, D. C. (2008). Cortical gamma generators suggest abnormal circuitry in early-onset psychosis. *Cerebral Cortex*, 18, 371-378.

Womelsdorg, T., Vinck, M., Leung, L. S., & Everling, S. (2010). Selective theta-synchronization of choice-relevant information subserves goal-directed behavior. *Frontiers in Human Neuroscience*, 4, 210.

Won, G. H., Kim, J. W., Choi, T. Y., Lee, Y. S., Min, K. J., & Seol, K. H. (2018). Theta-phase gamma-amplitude coupling as a neurophysiological marker in neuroleptic-naïve schizophrenia. *Psychiatry Research*, 260, 406-411.

Wulff, P., Ponomarenko, A. A., Bartos, M., Korotkova, T. M., Fuchs, E. C., Bähner, F., … Monyer, H. (2009). Hippocampal theta rhythm and its coupling with gamma oscillations require fast inhibition onto parvalbumin-positive interneurons. *Proceedings of the National Academy of Sciences*, *106*, 3561–3566.

Wynn, J. K., Light, G. A., Breitmeyer, B., Nuechterlein, K. H., & Green, M. F. (2005). Event-related gamma activity in schizophrenia patients during a visual backward-masking task. *American Journal of Psychiatry*, *162*, 2330-2336.

Yamamoto, J., Suh, J., Takeuchi, D. & Tonegawa, S. (2014). Successful execution of working memory linked to synchronized high-frequency gamma oscillations. *Cell*, *157*, 845–857.

Yeap, S., Kelly, S. P., Sehatpour, P., Magno, E., Garavan, H., Thakore, J. H. & Foxe, J. J. (2008). Visual sensory processing deficits in Schizophrenia and their relationship

to disease state. *European Archives of Psychiatry and Clinical Neuroscience*, *258*, 305–316.

Yeap, S., Kelly, S. P., Sehatpour, P., Magno, E., Javitt, D. C., Garavan, H., … Foxe, J. J. (2006). Early visual sensory deficits as endophenotypes for schizophrenia. *Archives of General Psychiatry*, *63*, 1180–1188.

Yeragani, V. K., Cashmere, D., Miewald, J., Tancer, M. & Keshavan, M. S. (2006). Decreased coherence in higher frequency ranges (beta and gamma) between central and frontal EEG in patients with schizophrenia: A preliminary report. *Psychiatry Research*, *141*, 53–60.

Zhang, R., Picchioni, M., Allen, P., & Toulopoulou, T. (2016). Working memory in unaffected relatives of patients with schizophrenia: a meta-analysis of functional magnetic resonance imaging studies. *Schizophrenia Bulletin*, 42, 1068–1077.

Zhang, Y., Zhang, Y., Yu, H., Yang, Y., Li, W. & Qian, Z. (2017). Theta-gamma-coupling in hippocampus during working memory deficits induced by low frequency electromagnetic field exposure. *Physiology & Behavior*, 179, 135-142.

Zhao, Y. L., Tan, S. P., De Yang, F., Wang, L. L., Feng, W. F., Chan, R. C., … others. (2011). Dysfunction in different phases of working memory in schizophrenia: Evidence from ERP recordings. *Schizophrenia Research*, *133*, 112–119.

Appendix A

Supplemental Results

Evoked power.

Theta-band (4-8hz).

Time-frequency energy – order of stimulus presentation. In addition to the above-reported effect of stimulus presentation order, ANOVA also revealed an interaction effect between presentation order and electrode site, $F(10,810)=2.45$, $p=.02$. Here, effects of order were observed at Pz, $F(2,162)=9.96$, $p<.001$ (2^{nd}, > 1^{st}, 3^{rd}, ps<.05); P4, $F(2,162)=10.09$, $p<.001$ ($2^{nd} > 1^{st}$, 3^{rd}, ps<.03); T6/P8, $F(2,162)=14.69$, $p<.001$ ($2^{nd} > 3^{rd} > 1^{st}$, ps<.04); and C3, $F(2,162)=6.12$, $p=.004$ ($2^{nd} > 1^{st}$, $p=.002$). Thus, the effect of order was strongest over parietal and central cortex.

Time-frequency energy – stimulus type. In addition to the above reported effect of stimulus type, ANOVA revealed a main effect of electrode site, $F(5,405)=5.22$, $p<.001$; here, evoked power was greater overall at T6/P8 than at C4 ($p=.001$) and F3 ($p=.006$); greater at P4 than at C4 ($p=.006$) and F3 ($p=.03$); and marginally greater at Pz than at C4 ($p=.096$). Thus, overall evoked energy varied from electrode to electrode.

Delta-band (2-4hz).

Time-frequency energy – order of stimulus presentation. In addition to the above reported effect of stimulus presentation order, ANOVA revealed a marginal interaction between electrode site and stimulus order for the 2-4hz delta window, $F(10,810)=2.25$,

p=.08. Here, effects of order were observed at Pz, $F(2,162)=8.05$, $p<.001$ (2^{nd}, $3^{rd} > 1^{st}$, $ps<.009$); $F(2,162)=6.00$, $p=.003$ (2^{nd}, $3^{rd} > 1^{st}$, $ps<.02$); C3, $F(2,162)=6.06$, $p=.003$ (2^{nd}, $3^{rd} > 1^{st}$, $ps<.01$); and C4, $F(2,162)=6.36$, $p=.002$ (2^{nd}, $3^{rd} > 1^{st}$, $ps<.04$). Additionally, a marginal effect of order was observed at T6/P8, $F(2,162)=2.39$, $p=.099$ ($2^{nd} > 1^{st}$, $p=.08$). Thus, the strength of the effect of presentation order on evoked 2-4hz delta varied from site to site.

Delta Band (1-2hz).

Time-frequency energy – order of stimulus presentation. In addition to the above-reported effect of presentation order, ANOVA also revealed an interaction between electrode site and stimulus order, $F(10,810)=2.41$, $p=.02$. Here, an effect of stimulus order was observed at P4, $F(2,162)=9.41$, $p<.001$ (2^{nd}, $3^{rd} > 1^{st}$), and a marginal effect was observed at C3, $F(2,162)=2.46$, $p=.096$ ($2^{nd} > 1^{st}$, $p=.08$). Thus, the overall effect of order in evoked delta (1-2hz) power was driven primarily by differences at subset of electrode sites.

A marginal effect of diagnostic grouping was also observed, $F(2,81)=2.65$, $p=.08$. Here, though energy values varied superficially across diagnostic groupings, post-hoc testing revealed no meaningful differences between groups.

Induced Power.

Theta-band (4-8hz).

Time-frequency energy – order of stimulus presentation. In addition to the above reported effects of presentation order and diagnostic grouping, ANOVA revealed an

interaction effect between stimulus order and electrode site, $F(12,972)=3.32$, $p<.001$. Here, an effect of order was observed at T6/P8, $F(2,162)=3.44$, $p=.03$, where theta power increased more to 3rd stimuli than to 2nd ($p=.03$); and C4, $F(2,162)=9.63$, $p<.001$, where power increases to 2nd and 3rd stimuli differed from decreases to 1st ($ps<.004$). Marginal effects of order were observed at Oz, $F(2,162)=2.36$, $p=.098$ (2nd > 1st, $p=.08$); and Fp1, $F(2,162)=3.15$, $p=.05$ (2nd > 1st, $p=.03$). Thus, the effect of order was limited to certain electrode sites, with the strongest observed effect occurring over right-central cortex.

Time-frequency energy – stimulus type. In addition to the effect of diagnostic group reported above, ANOVA revealed an interaction effect between stimulus type and electrode site, $F(6,486)=3.61$, $p=.002$. Here, main effects of stimulus type were observed at T6/P8, $F(1,81)=5.28$, $p=.02$, where power increases to targets exceeded those to distractors ($p=.02$); and Fp1, $F(1,81)=7.49$, $p=.008$, where increases to distractors exceeded those to targets ($p=.008$). Marginal effects of stimulus type were observed at O2, $F(1,81)=3.89$, $p=.05$ (D>T, $p=.05$); and C4, $F(1,81)=2.90$, $p=.09$ (T>D, $p=.09$). Thus, the effect of stimulus type varied from site to site, with frontoparietal and occipital sites showing greater responses to distractors, and central and temporoparietal sites showing greater responses to targets.

Delta-band (1-3hz).

Time-frequency energy – order of stimulus presentation. In addition to the above reported effects of presentation order and presentation order by diagnostic grouping, ANOVA further revealed a main effect of electrode site for the 1-2hz delta window,

$F(6,486)=3.41$, $p=.006$. Here, energy values at Fp1 exceeded those at Oz, $p=.04$, and O2, $p=.047$. Energy at T6/P8 was also greater than at Oz, $p=.045$, and marginally greater than that at O2, $p=.05$. Thus, induced delta energy at frontoparietal and temporoparietal sites exceeded that at occipital sites.

An interaction effect between electrode site and stimulus order was also observed, $F(12,972)=2.22$, $p=.009$. Here, effects of stimulus order on delta energy were observed at Oz, $F(2,162)=7.83$, $p=.002$ (2^{nd} and $3^{rd} > 1^{st}$, ps<.004); and O2, $F(2,162)=7.15$, $p=.002$ (2^{nd} and $3^{rd} > 1^{st}$, ps<.03). Thus, the effect of order on delta (1-2hz) induced power was driven by differences at occipital sites.

Gamma-band (64-81hz).

Time-frequency energy – stimulus type - 64-81hz, 425-775ms. In addition to the interaction effect between diagnostic grouping and stimulus type, ANOVA also revealed a marginal interaction effect between stimulus type and electrode site, $F(6,486)=2.12$, $p=.06$. Here, an effect of stimulus type was observed only for T5/P7, $F(1,85)=8.12$, $p=.005$, where increases to targets differed from decreases to distractors ($p=.006$). Thus, stimulus type affected energy values in the 64-81hz window only at an electrode site over temporoparietal cortex.

Phase-amplitude coupling (PAC).

One sample *t*-tests showed no meaningful change in PAC from baseline for coupling between 4hz (phase) and 52.5hz (amplitude) at O2, $t(35)=1.52$, $p=.14$; between 7hz (phase) and 44.5hz (amplitude) at C3, $t(35)=1.26$, $p=.21$; between 7hz (phase) and

46.5hz (amplitude) at O2, $t(35)=1.61$, $p=.12$; and between 7hz (phase) and 48.5hz (amplitude) at O2, $t(35)=1.64$, $p=.11$. Thus, no meaningful change in phase-amplitude coupling was observed for CTRL for these frequency pairs and electrode sites, and no further analyses were conducted for them.

Phase-phase coupling (PPC).

4hz phase (low-frequency) to 40.5hz phase (high-frequency), C4.

One sample *t*-tests showed no meaningful change in PPC values from baseline for coupling between 4hz and 40.5hz at C4, $t(35)=1.27$, $p=.10$; between 4hz and 52.5hz at O1, $t(35)=0.59$, $p=.56$; between 6hz and 34.5hz at O1, $t(35)=1.63$, $p=.11$; between 6hz and 36.5hz at C4, $t(35)=0.88$, $p=.38$; between 6hz and 40.5hz at O1, $t(35)=0.88$, $p=.38$; between 6hz and 42.5hz at P4, $t(35)=1.10$, $p=.28$; between 6hz and 44.5hz at P3, $t(35)=1.32$, $p=.20$; between 6hz and 48.5hz at O1, $t(35)=1.19$, $p=.24$; between 6hz and 48.5hz at O2, $t(35)=0.30$, $p=.77$; between 6hz and 56.5hz at O2, $t(35)=1.49$, $p=.15$; between 7hz and 46.5hz at C4, $t(35)=1.40$, $p=.17$; between 8hz and 34.5hz at C3, $t(35)=0.62$, $p=.54$; and between 8hz and 38.5hz at P4, $t(35)=1.40$, $p=.17$. Thus, no meaningful change in PPC from baseline was observed for these frequency pairings and electrode sites, and no further analyses on them were conducted.

Appendix B

The participant sample for these analyses was significantly unbalanced in terms of gender distribution. In light of PSZ having only 2 female participants, it stands to reason that any potential gender effects would be observed in CTRL and REL. In order to explore this potential confound of gender on reported effects, Type II repeated measures ANOVAs were re-run on only CTRL and REL for all effects involving group or a task manipulation other than electrode site or time sample in cross-frequency coupling analyses. Here, the intent was to examine for each dependent variable whether a main or interaction effect involving gender was observed for the CTRL and REL alone; if so, the influence of gender may play a role in the related effects reported in the main text.

Evoked Power

Theta-band.

Time-frequency energy – order of stimulus presentation. ANOVA for CTRL and REL only demonstrated neither a main effect of gender, $F(1,61)=0.00$, $p=.95$, nor an interaction between gender and presentation order, $F(2,122)=0.77$, $p=.45$. Thus, the reported effect of presentation order on evoked theta power values is unlikely to have been strongly influenced by gender.

Time-frequency energy – stimulus type. As above, ANOVA for CTRL and REL only demonstrated neither a main effect of gender, $F(1,61)=0.09$, $p=.76$, nor an interaction between gender and type of stimulus, $F(1,61)=1.37$, $p=.25$. Thus, the reported

effect of stimulus type on evoked power theta values is again unlikely to have been significantly influenced by gender.

Delta-band (2-4hz).

Time-frequency energy – order of stimulus presentation. Repeated measures ANOVA on CTRL and REL only showed neither a main effect of gender, $F(1,61)=0.13$, $p=.72$, nor an interaction between gender and presentation order, $F(2,122)=0.66$, $p=.52$. Thus, gender effects are unlikely to have strongly influenced the effect of presentation order on induced delta (2-4hz) power values reported in the main text.

Time-frequency energy – stimulus type. As above, ANOVA on CTRL and REL only showed neither a main effect of gender, $F(1,61)=0.35$, $p=.56$, nor an interaction between gender and presentation order, $F(1,61)=0.44$, $p=.51$. Thus, gender effects are unlikely to have strongly influenced the effect of stimulus type on induced delta (2-4hz) power values reported in the main text.

Delta-band (1-2hz).

Time-frequency energy – order of stimulus presentation. Repeated measures ANOVA on CTRL and REL only showed a marginal interaction effect for gender and presentation order, $F(2,122)=2.58$, $p=.09$. Here, females showed a marginal effect of order, $F(2,52)=3.04$, $p=.08$, in which values for 2nd stimuli were greater than those for 3rd; males showed no effect of presentation order, $F(2,70)=1.19$, $p=.30$. Thus, gender effects may have slightly influenced the effect of presentation order on evoked delta (1-2hz) power values reported in the main text.

Induced Power

Theta-band.

Time-frequency energy – order of stimulus presentation. ANOVA on CTRL and REL only demonstrated a marginal interaction between gender and presentation order, $F(2,122)=2.80$, $p=.07$. Here, females showed a strong effect of presentation order, $F(2,52)=10.79$, $p<.001$, in which responses to 3rd stimuli were greater than those to 1st ($p<.001$), and 2nd stimuli were marginally greater than those to 1st ($p=.096$). No effect of order was observed in the males, $F(2,70)=0.64$, $p=.53$. Thus, the effect of presentation order on induced theta power reported in the main text was likely influenced by gender imbalances in the CTRL and REL.

No interaction between diagnostic grouping and gender was observed, $F(1,61)=1.27$, $p=.26$. Thus, the marginal effect of diagnostic grouping reported in text is unlikely to have been strongly affected by gender influences.

Time-frequency energy – stimulus type. Repeated measures ANOVA for CTRL and REL only demonstrated an interaction effect between gender and stimulus type, $F(1,61)=6.15$, $p=.02$. Here, females showed a strong effect of stimulus type, $F(1,26)=15.08$, $p=.001$, where responses to distractors were greater than those to targets. No effect of stimulus type was observed in the males, $F(1,35)=0.15$, $p=.70$. However, the effect reported in text was that of diagnostic grouping, and no interaction between gender and diagnostic grouping was observed, $F(1,61)=0.97$, $p=.33$. Thus, the reported effect of

diagnostic grouping on induced theta values was unlikely to have been strongly influenced by gender effects.

Delta-band.

Time-frequency energy – order of stimulus presentation. Repeated measures ANOVA on CTRL and REL only showed neither a main effect of gender, $F(1,61)=1.78$, $p=.19$, nor interaction effects with diagnosis or presentation order *(p*s>.63). Thus, the reported effect of presentation order on induced delta values, as well as the interaction effect between diagnostic grouping and presentation order, are unlikely to have been strongly influenced by gender effects in the CTRL and REL.

Time-frequency energy – stimulus type. ANOVA on CTRL and REL only demonstrated neither a main effect of gender, $F(1,61)=1.30$, $p=.26$, nor an interaction effect between gender and stimulus type, $F(1,61)=0.93$, $p=.34$. Thus, the effect of stimulus type on induced delta values reported in the main text is unlikely to have been significantly influenced by gender effects.

Gamma-band.

Time-frequency energy – order of stimulus presentation.

64-81hz, 425-775ms. ANOVA on CTRL and REL only showed neither a main effect of gender, $F(1,61)=0.43$, $p=.51$, nor interaction effects between gender and presentation order or gender and diagnostic grouping (*p*s>.20). Thus, the reported interaction between diagnostic grouping, electrode site and presentation order for induced

gamma (64-81hz) values is unlikely to have been strongly influenced by gender effects in CTRL and REL.

71-81hz, 100-400ms. Repeated measures ANOVA on CTRL and REL only revealed a marginal three-way-interaction effect between gender, diagnostic grouping and presentation order, $F(2,122)=2.86$, $p=.08$. However, neither REL nor CTRL showed a main effect of gender or an interaction between gender and presentation order (*p*s>.15). Thus, the interaction reported in the main text between diagnostic grouping and presentation order for 71-81hz gamma values is unlikely to have been strongly influenced by gender effects.

Time-frequency energy – stimulus type.

64-81hz, 425-775ms. ANOVA on CTRL and REL only showed neither a main effect of gender, $F(1,61)=0.14$, $p=.71$, nor an interaction effect between gender and stimulus type, $F(1,61)=0.33$, $p=.57$. Thus, the interaction between diagnostic grouping and stimulus type reported in text for induced gamma (64-81hz) values is unlikely to have been strongly influenced by gender effects in CTRL and REL.

71-81hz, 100-400ms. ANOVA on CTRL and REL only showed neither a main effect of gender, $F(1,61)=0.46$, $p=.51$, nor an interaction effects between gender and stimulus type or gender and diagnostic grouping (*p*s>.37). Thus, the interaction between diagnostic grouping and stimulus type reported in text for induced gamma (71-81hz) values is again unlikely to have been strongly influenced by gender effects in CTRL and REL.

Intersite Phase Clustering (Phase Locking Value)

Theta-band.

IPSC, 4-8hz, 100-250ms, targets. Gender effects in CTRL and REL were assessed in those electrode pairs where group differences were observed. No main or interaction effects involving gender were observed for C3 and T6/P8 (*p*s>.34), T6/P8 and Oz (*p*s>.40), or F3 and O2 (*p*s>.31). Thus, no electrode pairs that showed group differences for phase synchrony in response to targets for the theta time window were significantly influenced by gender effects in CTRL and REL.

Gamma-band.

IPSC, 36-56hz, 425-775ms, distractors. Again, gender effects in CTRL and REL were assessed in those electrode pairs where group differences were observed. ANOVA for changes in IPSC values in response to distractors showed a significant main effect of gender for T4/T8 and T5/P7, $F(1,61)=5.91$, $p=.02$, where males showed increased values that differed from decreases in females ($p=.02$). No main or interaction effects involving gender were observed for Fp1 and T5/P7 (*p*s>.10), Fp1 and Cz (*p*s>.53), Fp1 and T3/T7 (*p*s>.21), Fp1 and P3 (*p*s>.31), and Pz and T4/T8 (*p*s>.10). Thus, reported group differences in phase synchrony changes for the 36-56hz gamma window in response to distractors between T4/T8 and T5/P7 were likely influenced by gender effects, whereas other reported group effects were likely not.

IPSC, 64-81hz, 425-775ms, distractors. Gender effects were assessed in the one electrode pair showing group differences for this window of interest. No main or

interaction effects involving gender were observed for Pz and F8 (*p*s>.96); thus, gender effects did not influence observed group differences for this window of interest.

IPSC, 71-81hz, 100-400ms, targets. Gender effects in CTRL and REL were assessed in those electrode pairs where group differences were observed. No main or interaction effects involving gender were observed for C3 and P3 (*p*s>.17), for F8 and Cz (*p*s>.21), and for P3 and O1 (*p*s>.63). Thus, no reported group effects in synchrony changes in response to targets for the 71-81hz window of interest were significantly affected by gender effects.

IPSC, 71-81hz, 100-400ms, distractors. Again, gender effects in CTRL and REL were assessed in those electrode pairs where group differences were observed. No main or interaction effects involving gender were observed for Pz and T4/T8 (*p*s>.56) or for T6/P8 and T4/T8 (*p*s>.39). Thus, no reported group effects in synchrony changes in response to distractors for the 71-81hz window of interest were significantly affected by gender effects.

IPSC, 86-126hz, 100-400ms, distractors. Gender effects in CTRL and REL were assessed in the single electrode pair where group differences were observed for this window of interest. No main or interaction effect involving gender were observed for Cz and T6/P8 (*p*s>.16). Thus, the reported group effect in synchrony changes in response to distractors for the 86-126hz window of interest was again not significantly affected by gender effects.

Discussion

The potential confound of gender effects was investigated in CTRL and REL for all analyses that showed group or task differences that were not differences across electrodes sites or the effect of time sample in cross-frequency coupling analyses. For most of the analyses, no effects containing gender were observed, suggesting these reported effects were not significantly affected by gender imbalances. However, gender effects were observed in a few cases. A gender by presentation order interaction was observed for changes in evoked delta (1-2hz) values in which females showed a slight effect of presentation order and males did not, which clearly influences the reported effect. A similar interaction between gender and presentation order was observed for the induced theta values; here, females showed a strong effect of presentation order, while males did not, and this again clearly influenced the reported effect. Finally, gender effects were reported for synchrony changes between T4/T8 and T5/P7 in the 36-56hz gamma window, where males showed increased synchrony and females showed decreases.

Thus, females showed stronger effects of presentation order for selective low-frequency power measures. Females have been shown to perform better on spatial WM tasks (Saylik, Raman & Szameitat, 2018), as well as to demonstrate unique EEG correlates of performance as compared to males (Pavlov & Kotchoubey, 2017), and the modulation of low frequency activity by presentation order in females may reflect underlying advantages in females' processing of stimulus order despite no observed differences in task performance between genders. Notably, low frequency activity was found to be predictive of performance in CTRL and REL but not PSZ, and the predictive

value of those measures may in fact reflect the predictive value of gender; these qualifications of the above effects should be considered in interpretation. The phase-synchrony measure found to be affected was not found to be predictive of behavior. Gender-balanced samples should continue to be striven for in future examinations of WM in schizophrenia in hopes that such potential confounds could be minimized.

Table 1. Participant characteristics.

	CTRL (n = 36)	PSZ (n = 22)	REL (n = 29)	Test Statistic (Degrees of Freedom)	p-value
% Female	30.6%	9.1%	58.6%	$\chi^2(2) = 14.0$	$p < .001$
Age (years)	47.1 (11.4)	43.8 (10.0)	43.8 (10.7)	$F(2, 84) = 1.0$	$p = .38$
Years of education	15.0 (1.9)	13.9 (1.9)	14.5 (2.2)	$F(2, 84) = 2.2$	$p = .12$
IQ	107.2[a] (14.3)	91.3[a,b] (19.9)	104.6[b] (15.0)	$F(2, 84) = 6.8$	$p = .002$
BPRS	28.6[a] (5.1)	45.0[a,b] (10.0)	32.2[b] (7.6)	$F(2, 84) = 34.6$	$p < .001$
- Positive	4.4[a] (0.8)	11.6[a,b] (5.4)	5.0[b] (1.7)	$F(2, 84) = 47.3$	$p < .001$
- Negative	4.3[a] (0.5)	7.3[a,b] (2.9)	4.6[b] (1.1)	$F(2, 84) = 28.6$	$p < .001$
- Disorganized	4.4 (1.0)	5.0 (1.2)	4.6 (1.5)	$F(2, 84) = 1.4$	$p = .25$

Parentheses indicate standard deviations unless noted otherwise. p-values indicate differences in measures across diagnostic categories: schizophrenia probands (PSZ), controls (CTRL) and relatives of PSZ (REL). Paired superscripts indicate differences between groups for a given measure, $p < .05$.

Table 2. Proportion of trials correct on spatial working memory task.

	CTRL (n = 36)	PSZ (n = 22)	REL (n = 29)	F-value	p-value
Overall	.79[a] (.08)	.71[a,b] (.11)	.80[b] (.08)	$F(2, 84) = 6.8$	$p = .002$
Two-Stimulus Trials	.81 (.09)	.76[b] (.13)	.83[b] (.09)	$F(2, 84) = 3.6$	$p = .03$
Three-Stimulus Trials	.78[a] (.08)	.70[a,b] (.11)	.79[b] (.08)	$F(2, 84) = 7.5$	$p = .001$
No Distractor Trials	.73 (.09)	.68[b] (.09)	.74[b] (.09)	$F(2, 84) = 3.0$	$p = .05$
Distractor Trials	.84[a] (.09)	.74[a,b] (.14)	.86[b] (.10)	$F(2, 84) = 7.9$	$p < .001$
Probe at Previous Target	.84 (.13)	.77[b] (.17)	.86[b] (.13)	$F(2, 84) = 3.3$	$p = .04$
Probe at Previous Distractor	.88[a] (.10)	.73[a,b] (.17)	.88[b] (.14)	$F(2, 84) = 10.4$	$p < .001$
Probe Elsewhere	.64 (.17)	.62 (.15)	.66 (.16)	$F(2, 84) = 0.3$	$p = .75$
Probe at 1st Position	.79 (.17)	.74 (.18)	.83 (.10)	$F(2, 84) = 2.2$	$p = .12$
Probe at 2nd Position	.87[a] (.11)	.76[a,b] (.15)	.87[b] (.12)	$F(2, 84) = 6.0$	$p = .004$
Probe at 3rd Position	.89[a] (.09)	.76[a,b] (.16)	.89[b] (.13)	$F(2, 84) = 9.1$	$p < .001$

Parentheses indicate standard deviations unless noted otherwise. p-values indicate differences across diagnostic categories: schizophrenia probands (PSZ), controls (CTRL) and relatives of PSZ (REL). Paired superscripts indicate differences between groups for a given index, $p < .05$.

Table 3. Regression results for predicting overall WM task performance.

Predictor	β	β 95% CI [LL, UL]	sr^2	sr^2 95% CI [LL, UL]	t	p
(Intercept)	-0.02	[-0.32, 0.28]			-0.29	.77
PSZ	-0.50	[-1.03, 0.02]	.02	[-.01, .06]	-0.60	.55
REL	0.24	[-0.23, 0.71]	.01	[-.01, .03]	1.18	.24
Evoked Theta, 2nd	0.07	[-0.41, 0.56]	.00	[-.01, .01]	0.17	.86
Evoked Theta, 3rd	0.42*	[0.01, 0.84]	.03	[-.01, .07]	2.20	.03
Evoked Theta, Target	0.05	[-0.69, 0.79]	.00	[-.00, .00]	0.14	.89
Evoked Delta (2-3hz), 3rd	-0.16	[-0.51, 0.19]	.01	[-.01, .02]	-0.87	.39
Evoked Delta (1-2hz), 2nd	0.32*	[0.03, 0.60]	.03	[-.01, .08]	2.27	.03
Induced Delta, 3rd	0.32	[-0.08, 0.72]	.02	[-.02, .05]	1.62	.11
Induced Gamma (64-81hz), 2nd	0.00	[-0.28, 0.28]	.00	[-.00, .00]	-0.13	.90
Theta Sync., OZ-T6/P8	-0.31	[-0.75, 0.14]	.01	[-.02, .04]	-1.38	.17
PAC, 7-50.5hz-C4	-0.02	[-0.24, 0.20]	.00	[-.00, .00]	-0.83	.41
PPC, 6-44.5hz-C4	0.00	[-0.33, 0.33]	.00	[-.00, .00]	0.04	.97
PSZ: Evoked Theta, 2nd	-0.92	[-2.19, 0.34]	.01	[-.02, .04]	-1.70	.09
REL: Evoked Theta, 2nd	0.16	[-0.77, 1.10]	.00	[-.01, .01]	0.32	.75
PSZ: Evoked Theta, 3rd	-0.01	[-1.00, 0.97]	.00	[-.00, .00]	0.21	.84
REL: Evoked Theta, 3rd	-0.94*	[-1.79, -0.09]	.03	[-.01, .08]	-2.27	.03
PSZ: Evoked Theta, Target	0.18	[-0.93, 1.30]	.00	[-.01, .01]	0.46	.65
REL: Evoked Theta, Target	0.35	[-0.78, 1.49]	.00	[-.01, .02]	0.68	.50
PSZ: Evoked Delta (2-3hz), 3rd	0.48	[-0.19, 1.14]	.01	[-.02, .04]	1.31	.20
REL: Evoked Delta (2-3hz), 3rd	0.10	[-0.71, 0.92]	.00	[-.00, .01]	0.29	.77
PSZ: Evoked Delta (1-2hz), 2nd	-0.10	[-0.71, 0.51]	.00	[-.01, .01]	-0.26	.79
REL: Evoked Delta (1-2hz), 2nd	-0.28	[-0.83, 0.26]	.01	[-.01, .03]	-0.99	.33
PSZ: Induced Delta, 3rd	-0.47	[-0.97, 0.03]	.02	[-.02, .06]	-1.41	.16
REL: Induced Delta, 3rd	0.29	[-0.35, 0.93]	.01	[-.01, .02]	0.73	.47
PSZ: Induced Gamma (64-81hz), 2nd	-0.64*	[-1.12, -0.15]	.04	[-.01, .10]	-2.06	.04
REL: Induced Gamma (64-81hz), 2nd	-0.14	[-0.56, 0.27]	.00	[-.01, .02]	-0.57	.57
PSZ: Theta Sync., Targets, OZ-T6/P8	-0.04	[-0.63, 0.54]	.00	[-.00, .00]	-0.16	.88
REL: Theta Sync., Targets, OZ-T6/P8	0.16	[-0.39, 0.70]	.00	[-.01, .01]	0.55	.59
PSZ:PAC, 7-50.5hz-C4	0.91**	[0.25, 1.57]	.05	[-.01, .11]	3.02	.004
REL:PAC, 7-50.5hz-C4	0.32	[-0.12, 0.77]	.01	[-.02, .04]	1.44	.16
PSZ:PPC, 6-44.5hz-C4	-0.10	[-0.82, 0.63]	.00	[-.00, .01]	0.61	.54
REL:PPC, 6-44.5hz-C4	0.13	[-0.31, 0.57]	.00	[-.01, .01]	0.44	.66
Fit:	R^2 = .648** 95% CI[.22,.59]					

Note. A significant β-weight indicates the semi-partial correlation is also significant. β represents standardized regression weights. sr^2 represents the semi-partial correlation squared. *LL* and *UL* indicate the lower and upper limits of a confidence interval, respectively.
* indicates $p < .05$. ** indicates $p < .01$.

Table 4. Regression results for predicting WM performance on target-only trials.

Predictor	β	β 95% CI [LL, UL]	sr^2	sr^2 95% CI [LL, UL]	t	p	Fit
(Intercept)	-0.03	[-0.34, 0.29]			-0.17	.86	
PSZ	-0.24	[-0.77, 0.29]	.01	[-.02, .04]	-0.91	.37	
REL	0.26	[-0.21, 0.74]	.01	[-.03, .05]	1.10	.27	
Evoked Delta (1-2hz), 2nd	0.23*	[0.03, 0.43]	.05	[-.03, .12]	2.26	.03	
Induced Theta, 3rd	0.10	[-0.11, 0.32]	.01	[-.02, .04]	0.95	.34	
Induced Delta, 3rd	0.14	[-0.08, 0.36]	.02	[-.03, .06]	1.29	.20	
Induced Gamma (64-81hz), 2nd	-0.00	[-0.31, 0.31]	.00	[-.00, .00]	-0.01	.99	
Induced Gamma (64-81hz), Targets	-0.24	[-0.55, 0.07]	.02	[-.03, .07]	-1.54	.13	
Gamma (71-81hz) Sync., Distractors, Pz-T4/T8	0.24*	[0.03, 0.44]	.05	[-.03, .12]	2.28	.03	
PAC, 7hz-50.5hz/C4	0.14	[-0.06, 0.34]	.02	[-.03, .07]	1.40	.17	
							R^2 = .292** 95% CI[.06,.37]

Note. A significant β-weight indicates the semi-partial correlation is also significant. β represents standardized regression weights. sr^2 represents the semi-partial correlation squared. *LL* and *UL* indicate the lower and upper limits of a confidence interval, respectively. * indicates p < .05. ** indicates p < .01.

Table 5. Regression results for predicting WM performance on trials featuring distractor stimuli.

Predictor	β	β 95% CI [LL, UL]	sr^2	sr^2 95% CI [LL, UL]	t	p
(Intercept)	0.10	[-0.20, 0.40]			0.67	.51
PSZ	-0.77*	[-1.39, -0.15]	.04	[-.01, .08]	-2.48	.02
REL	0.03	[-0.43, 0.50]	.00	[-.00, .00]	0.15	.88
Evoked Theta, 2nd	0.25	[-0.26, 0.76]	.01	[-.01, .02]	1.00	.32
Evoked Theta, 3rd	0.32	[-0.10, 0.74]	.01	[-.01, .04]	1.52	.13
Evoked Theta, Targets	-0.08	[-0.83, 0.68]	.00	[-.00, .00]	-0.21	.84
Evoked Delta (2-3hz), 3rd	0.04	[-0.34, 0.42]	.00	[-.00, .00]	0.21	.84
Evoked Delta (1-2hz), 2nd	0.20	[-0.09, 0.49]	.01	[-.01, .04]	1.38	.17
Induced Delta, 3rd	0.08	[-0.36, 0.51]	.00	[-.01, .01]	0.36	.72
Induced Gamma (64-81hz), 2nd	-0.12	[-0.42, 0.18]	.00	[-.01, .02]	-0.81	.42
Theta Sync., OZ to T6/P8	-0.17	[-0.62, 0.29]	.00	[-.01, .02]	-0.74	.46
Gamma (36-56hz) Sync., Ds, P3 to Fp1	0.02	[-0.28, 0.32]	.00	[-.00, .00]	0.12	.90
PAC, 7hz-54.5hz, C3	0.20	[-0.06, 0.46]	.01	[-.01, .04]	1.51	.14
PPC, 6hz-44.5hz, C4	0.08	[-0.27, 0.42]	.00	[-.01, .01]	0.45	.66
PPC, 6hz-52.5hz, O1	0.14	[-0.13, 0.40]	.01	[-.01, .02]	1.03	.31
PSZ: Evoked Theta, 2nd	-0.71	[-2.18, 0.76]	.01	[-.01, .02]	-0.97	.34
REL: Evoked Theta, 2nd	-0.12	[-1.15, 0.91]	.00	[-.00, .00]	-0.23	.82
PSZ: Evoked Theta, 3rd	-0.92	[-1.88, 0.03]	.02	[-.01, .06]	-1.94	.06
REL: Evoked Theta, 3rd	-0.69	[-1.58, 0.20]	.01	[-.01, .04]	-1.57	.12
PSZ: Evoked Theta, Targets	1.01	[-0.20, 2.23]	.02	[-.01, .05]	1.67	.10
REL: Evoked Theta, Targets	0.60	[-0.54, 1.75]	.01	[-.01, .03]	1.06	.29
PSZ: Evoked Delta (2-3hz), 3rd	0.16	[-0.56, 0.87]	.00	[-.01, .01]	0.44	.67
REL: Evoked Delta (2-3hz), 3rd	0.06	[-0.78, 0.90]	.00	[-.00, .00]	0.14	.89
PSZ: Evoked Delta (1-2hz), 2nd	0.37	[-0.32, 1.06]	.01	[-.01, .03]	1.09	.28
REL: Evoked Delta (1-2hz), 2nd	-0.31	[-0.86, 0.24]	.01	[-.01, .03]	-1.12	.27
PSZ: Induced Delta, 3rd	-0.03	[-0.56, 0.50]	.00	[-.00, .00]	-0.13	.90
REL: Induced Delta, 3rd	0.33	[-0.33, 0.99]	.01	[-.01, .02]	1.01	.32
PSZ: Induced Gamma (64-81hz), 2nd	-0.55	[-1.10, 0.01]	.02	[-.01, .06]	-1.97	.06
REL: Induced Gamma (64-81hz), 2nd	0.15	[-0.30, 0.59]	.00	[-.01, .01]	0.67	.51
PSZ: Theta Sync., OZ to T6/P8	0.02	[-0.55, 0.59]	.00	[-.00, .00]	0.08	.94
REL: Theta Sync., OZ to T6/P8	0.23	[-0.34, 0.81]	.00	[-.01, .02]	0.81	.42
PSZ: Gamma (36-56hz) Sync., Ds, P3 to Fp1	0.71**	[0.25, 1.18]	.06	[.00, .11]	3.08	.003
REL:Gamma (36-56hz) Sync., Ds, P3 to Fp1	0.04	[-0.47, 0.54]	.00	[-.00, .00]	0.14	.89
PSZ:PAC, 7hz-54.5hz, C3	-0.47	[-1.46, 0.53]	.01	[-.01, .02]	-0.95	.35
REL:PAC, 7hz-54.5hz, C3	0.07	[-0.33, 0.47]	.00	[-.01, .01]	0.36	.72
PSZ:PPC, 6hz-44.5hz, C4	-0.02	[-0.68, 0.64]	.00	[-.00, .00]	-0.06	.95
REL:PPC, 6hz-44.5hz, C4	0.11	[-0.33, 0.55]	.00	[-.01, .01]	0.49	.63
PSZ:PPC, 6hz-52.5hz, O1	-0.11	[-0.79, 0.58]	.00	[-.00, .01]	-0.32	.75
REL:PPC, 6hz-52.5hz, O1	0.14	[-0.33, 0.61]	.00	[-.01, .01]	0.61	.54
Fit:	R^2 = .710** 95% CI[.24,.63]					

Note. A significant β-weight indicates the semi-partial correlation is also significant. β represents standardized regression weights. sr^2 represents the semi-partial correlation squared. *LL* and *UL* indicate the lower and upper limits of a confidence interval, respectively. * indicates p < .05. ** indicates p < .01.

Table 6. Summary of notable results.

	Power findings	**Synchrony findings**	**Theta-gamma coupling findings**
Delta Band	- Induced power greater for increased WM load in REL and CTRL but not PSZ - Evoked power greater for increased WM load in all groups - Power greater for distractors vs. targets - **Greater delta to later stimuli predicted better WM performance for CTRL and REL alone** - **Greater delta to 2nd stimuli predicted WM performance on trials with distraction for all groups**	*Not assessed*	*Not assessed*
Theta Band	- Power greater for REL vs. PSZ - Power greater for increased WM load - Power greater for targets vs. distractors - **Greater theta to 3rd stimuli predicted WM performance for CTRL alone**	- CTRL generally showed increases in synchrony between frontal / central sites and posterior sites - PSZ showed uniquely increased synchrony between temporal site and occipital site	- PAC increased between 7hz and various frequencies between 32.5hz and 54.5hz at central sites, 7hz and 40.5hz at parietal site, and 7hz and 42.5hz at occipital sites - PPC increased between 4hz and various frequencies between 44.5hz and 56.5hz at central and posterior sites; PPC increased between 6hz and various frequencies between 52.5hz to 58.5hz at occipital sites - Coupling generally greater later in epoch vs. earlier - **PAC between 7hz and 50.5hz at C4 predicted WM performance for PSZ alone**
Gamma Band	- Generally increased power (*64-81hz*) with increased WM load at certain sites in CTRL and REL but not PSZ - Increased power (*64-81hz*) to targets vs. distractors in CTRL but not REL or PSZ	- Highly varied changes in synchrony depending on window of interest - Increases in CTRL vs. decreases in PSZ and REL between prefrontal site and various posterior sites - **Greater synchrony (*36-56hz*) between prefrontal and posterior site to distractors predicted WM performance on target-only trials in PSZ alone**	
Relevance to Lisman and Idiart (1995) Model	- Aberrations in measures of power and phase synchrony within theta and / or gamma may suggest deficiencies in coordinated activities of neural ensembles within these frequency bands - It was hypothesized that such deficiencies in coordination within frequencies would be visible in measures of cross-frequency coupling, and conceivably explain these deficiencies		- PAC represents the most direct measure of the theta-/gamma- neural code as described by Lisman and Idiart (1995) - Because consistent phase-shift across trials also represents coordinated activity in neural ensembles, PPC and PAC have been suggested to be different expressions of the same phenomenon (Belluscio et al., 2012; Canolty et al., 2006). As such, PPC was examined in addition to PAC

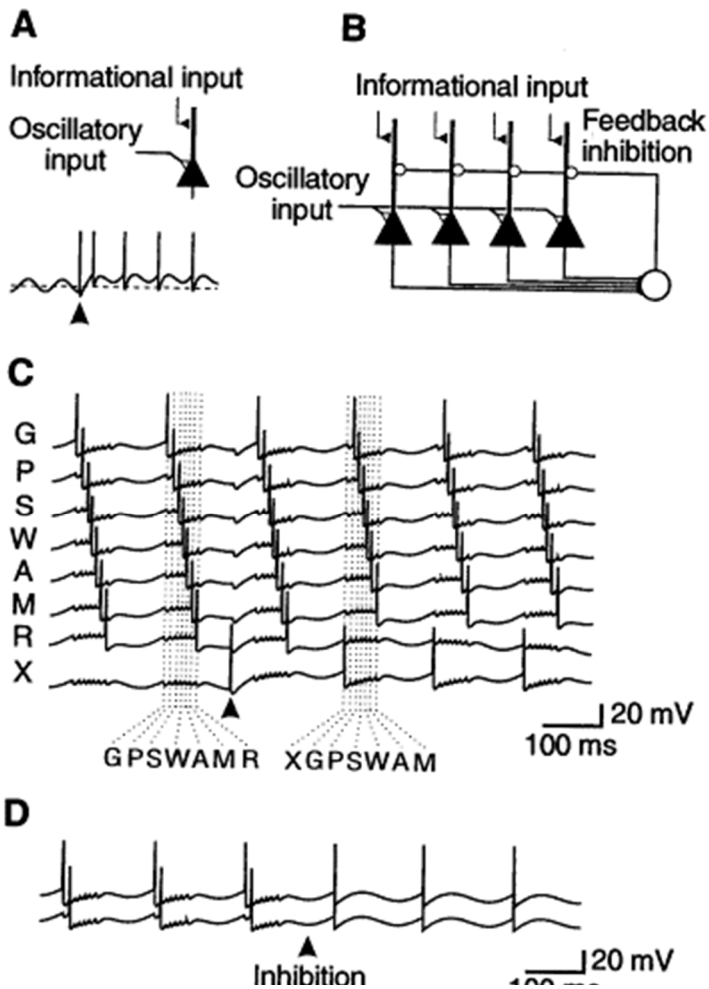

Figure 1. *Single cell information storage*. A) The afterdepolarization (ADP) allows information storage in a single cell. The neuron receives a suprathreshold informational input and a second, subthreshold input that induces the membrane potential to oscillate at theta frequency (negative phase due to inhibition). Simulations show membrane potential before and after informational input (arrowhead). B) Network in which pyramidal cells make converging excitatory synapses onto an inhibitory interneuron that produces feedback inhibition of pyramidal cells. C) The network can maintain the firing and correct phase of seven groups of cells that are active during different subcycles of the low-frequency oscillation. Each trace illustrates the synchronous firing of a group of cells whose spatial pattern encodes the memory of a letter. The dashed lines during the second and fourth theta cycles show the different subcycles. The limited memory capacity of the network is demonstrated by its failure to store eight memories. Input of the memory X is successful (arrowhead), but R is lost. D) If feedback inhibition is removed (arrowhead), the "40-hz" oscillation and phase information is rapidly lost. The two traces represent two of the seven memories stored in the network. A small phase difference (too small to be shown) persists for one cycle after removal of inhibition. Reproduced from Lisman and Idiart (1995).

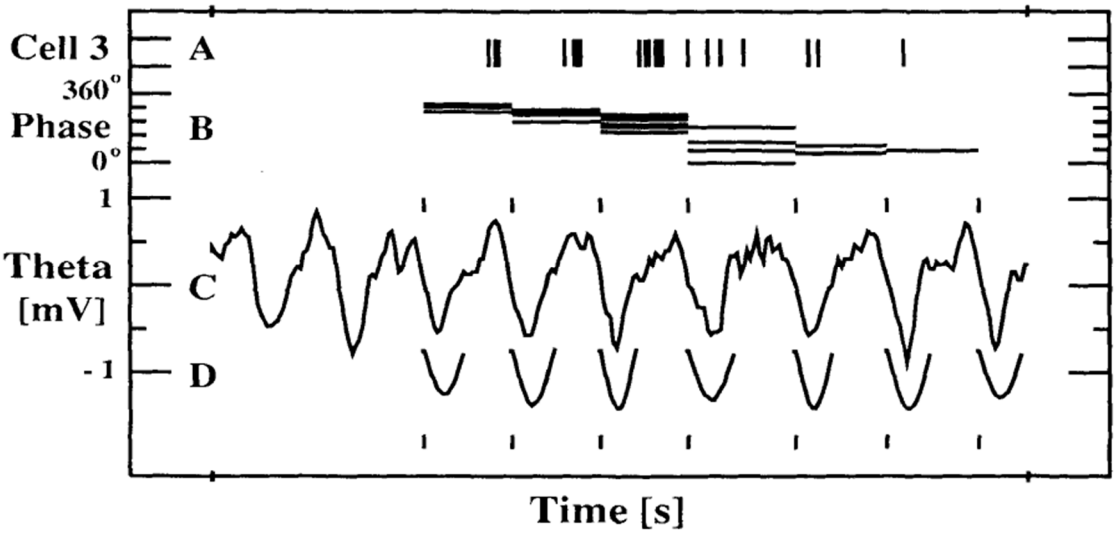

Figure 2. Phase precession. Extraction of the firing phase shift for each spike during a single run through the field of a CA3 place cell on the linear track. (A) Each firing of cell 3 as a single vertical line during the 1 second of data. (B) Phase of each spike relative to the theta cycle within which it falls as a horizontal line. (C) Hippocampal theta activity recorded at the same time as the single unit. (D) Result of the theta template matching algorithm. Note that the amplitude and the time between onsets of each template match varies to fit the variations in the theta. The small vertical ticks above the electroencephalogram (EEG) and below the template fits mark the beginning of each theta cycle. The cell clearly fires six bursts of spikes during this run through the place field. Comparison of each burst with the concomitant theta wave shows that each successive burst fires on an earlier part of the theta. This is shown clearly by the descending staircase of the phase correlates in B. EEG voltage in C is + 1 to - 1 mV. Total time between marks on the x axis is 1 second. Reproduced from O'Keefe and Recce (1993).

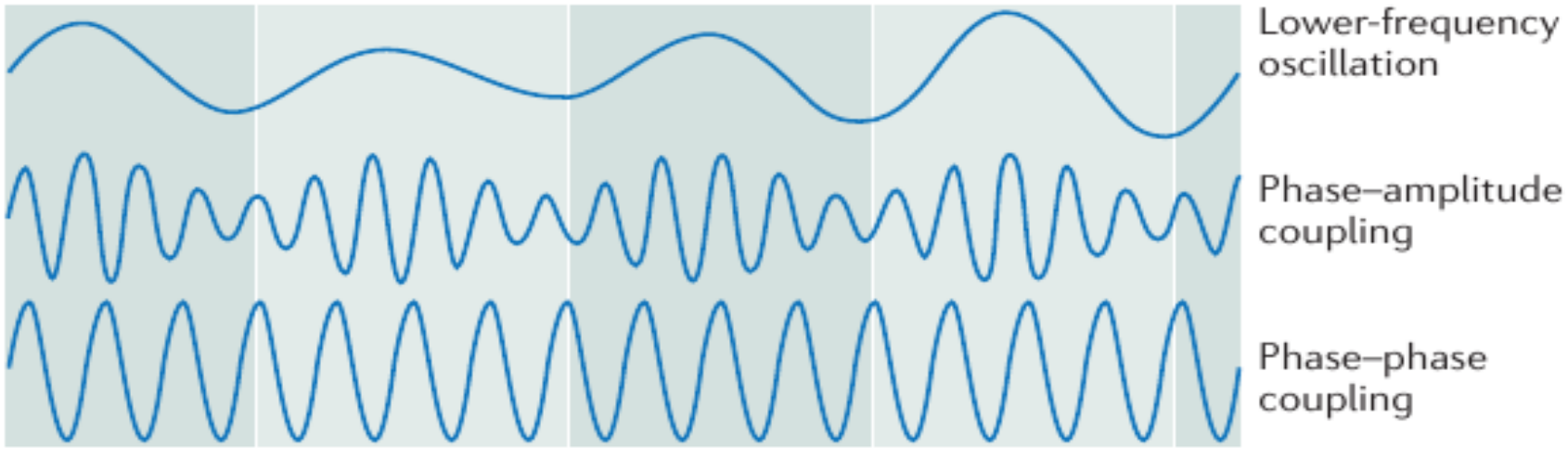

Figure 3. Cross-frequency coupling. Schematic overview of two cases in which oscillatory activity of a higher-frequency oscillation may be related to the phase of a lower-frequency oscillation. Dark and light boxes separate consecutive cycles of the lower-frequency oscillation. The lower-frequency oscillation of fluctuating amplitude (top) shows phase-amplitude coupling with a higher-frequency oscillation of fluctuating amplitude (middle). In this example, amplitudes of the higher-frequency oscillation are maximal during the up-phase of the lower-frequency oscillation. A higher-frequency oscillation of stable amplitude (bottom), shows phase-phase coupling with the low-frequency oscillation. Here, peaks of the higher-frequency oscillation always coincide with the same phase values of the lower-frequency oscillations. Reproduced from Fell and Axmacher (2011).

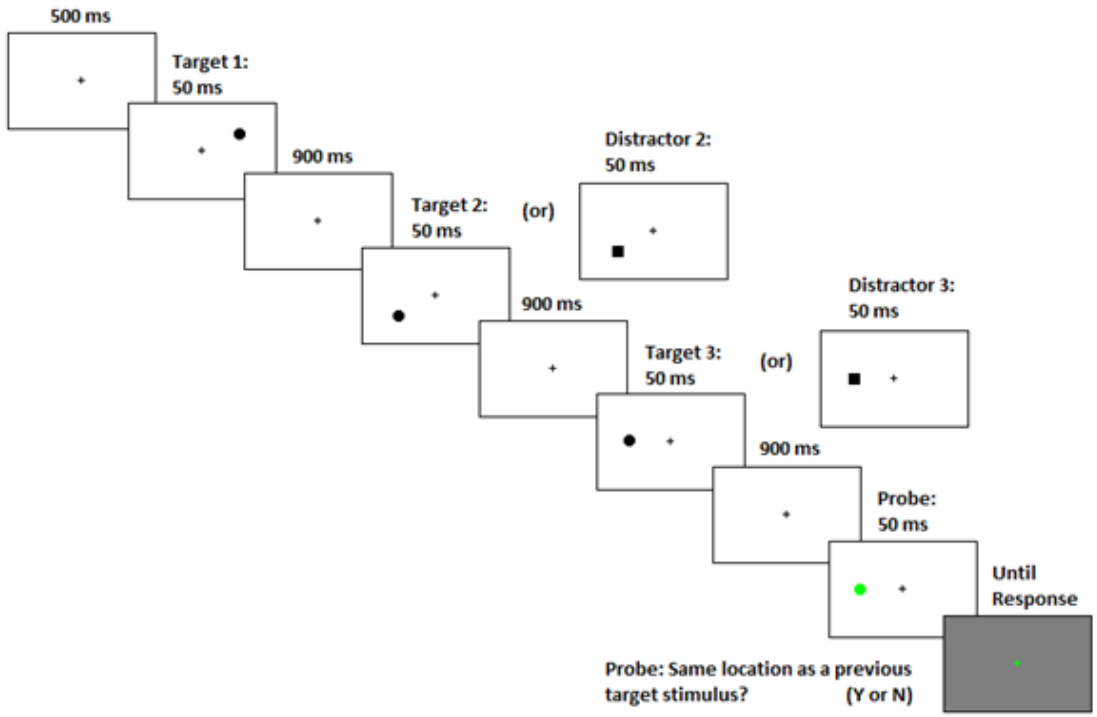

Figure 4. SPAM Task. Participants were administered a spatial working memory task in which either two or three memory stimuli were sequentially presented on the screen. Each stimulus was presented at one of sixteen possible locations configured circularly around a central fixation. These stimuli were either "targets" (black circles) or "distractors" (black squares); a maximum of one distractor could appear per trial. After the memory stimuli were presented, a probe stimulus (a green circle) was subsequently presented, and participants were asked to indicate whether or not the probe stimulus appeared in the position of a previous *target* stimulus; if the probe appeared in the position of a previous distractor, the participants were instructed to respond "no." The task included 2 two-stimulus blocks and 6 three-stimulus blocks of 36 trials each, presented in a pseudo-randomized order. Participants who performed at less than 60% accuracy on two-stimulus trials were excluded from behavioral and ERP analyses. Stimuli were presented in one of 16 locations on an invisible circle with a radius subtending a visual angle of 9.3 degrees. Stimuli subtended a visual angle of 1.6 degrees, and potential locations were separated by 22.5 degrees of arc around the circumference of the circle.

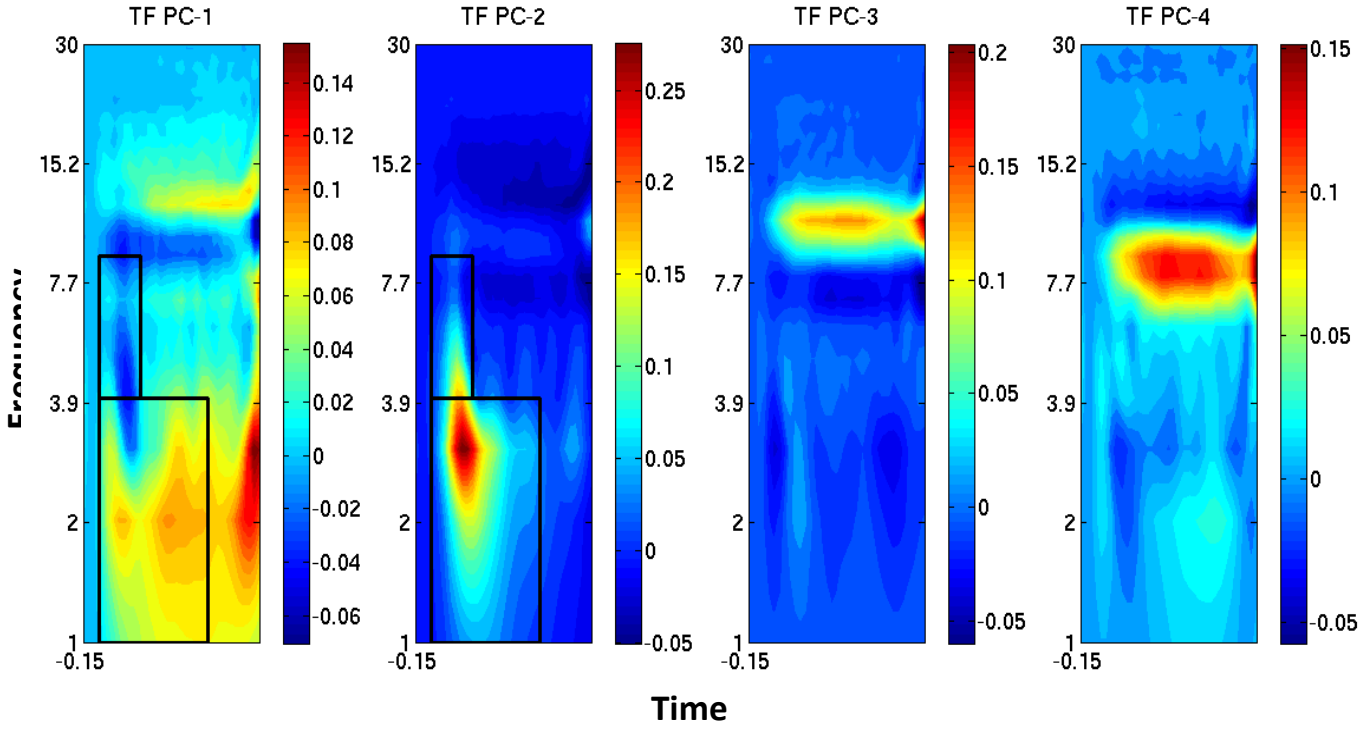

Figure 5. PCA for induced theta power. Chosen PCA solution for determining theta window of interest for induced power. On the basis of PCs 1 and 2, a window of 4-8hz between 150ms and 300ms post-stimulus was initially selected for theta given the a priori focus of these analyses on theta activity. However, given the apparent prominence of activity in slightly lower frequencies within these same PCs, a delta window of 1-3hz between 150ms and 600ms was also selected for analysis.

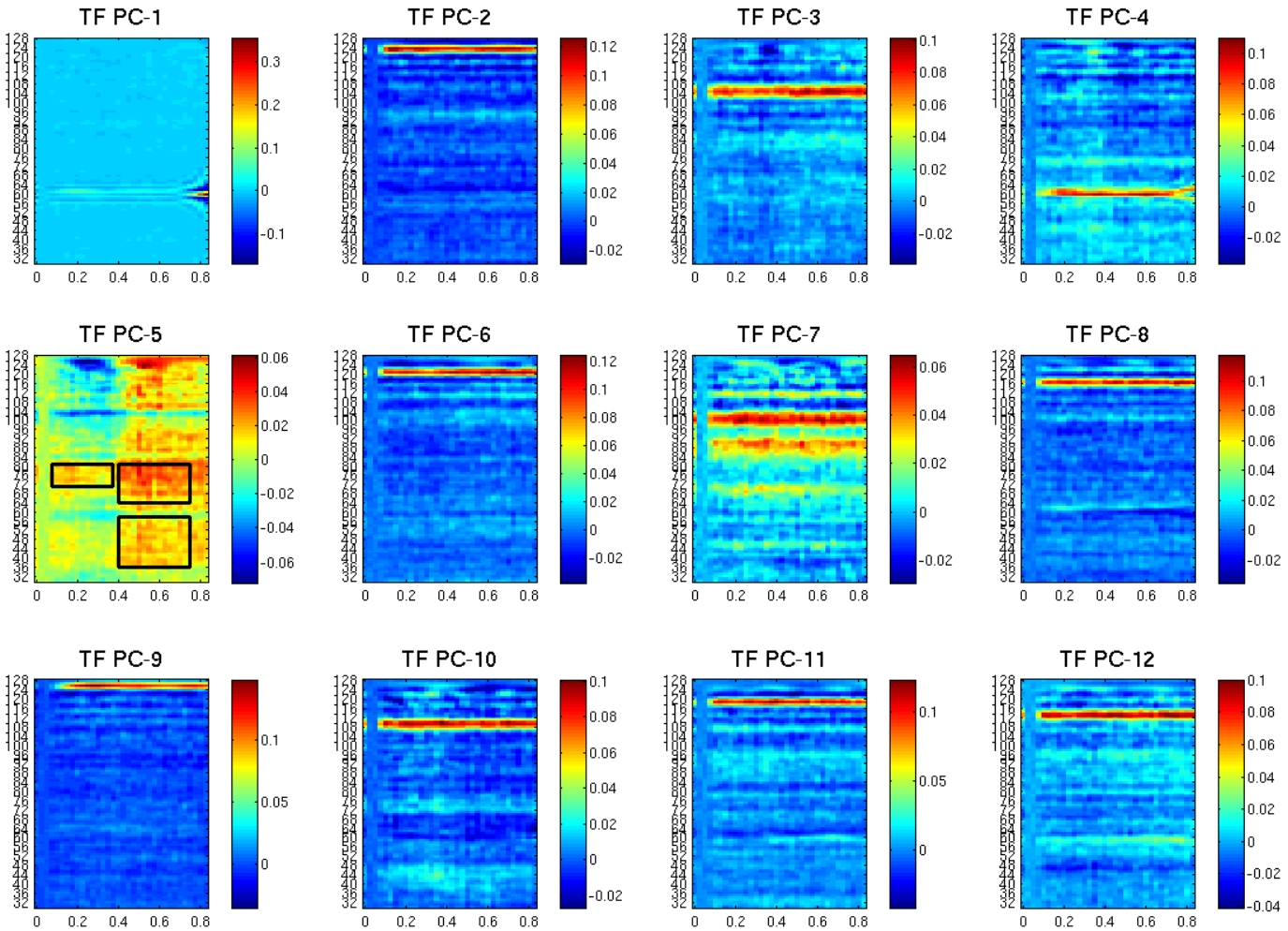

Figure 6. PCA for induced gamma power (1 of 2). One of two chosen PCA solutions for determining gamma windows of interest for induced power. On the basis of PC5, windows of 36-56hz from 425-775ms post-stimulus, 64-81hz from 425-775ms post-stimulus, and 71-81hz from 100-400ms post-stimulus were selected for induced gamma analyses.

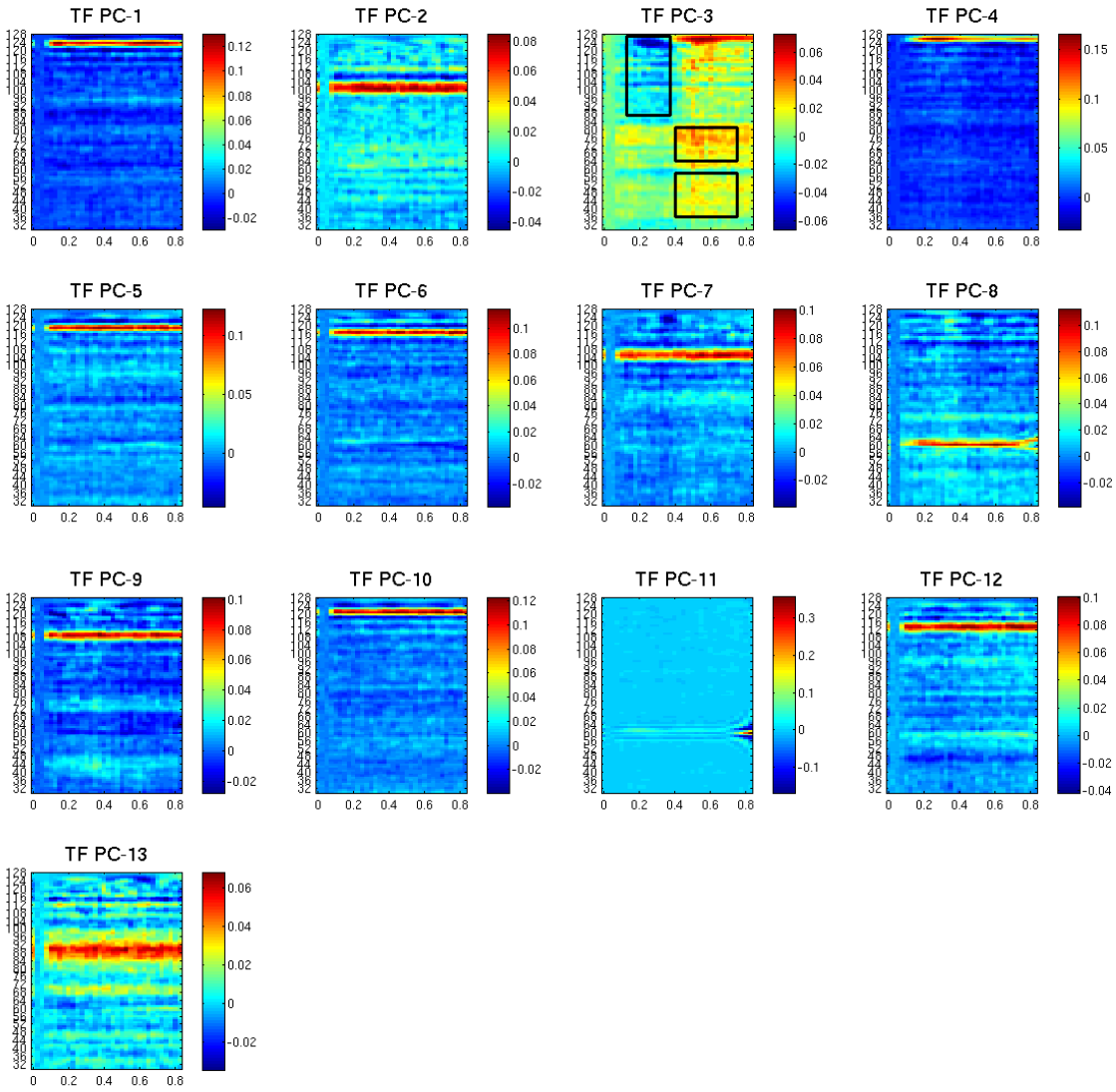

Figure 7. PCA for induced gamma power (2 of 2). One of two chosen PCA solutions for determining gamma windows of interest for induced power. On the basis of PC3, an additional window of 86-126hz from 100-400ms post-stimulus was added for induced gamma analyses, while windows of 36-56hz and 64-81hz from 425-775ms post-stimulus already established (see Figure 6) were supported.

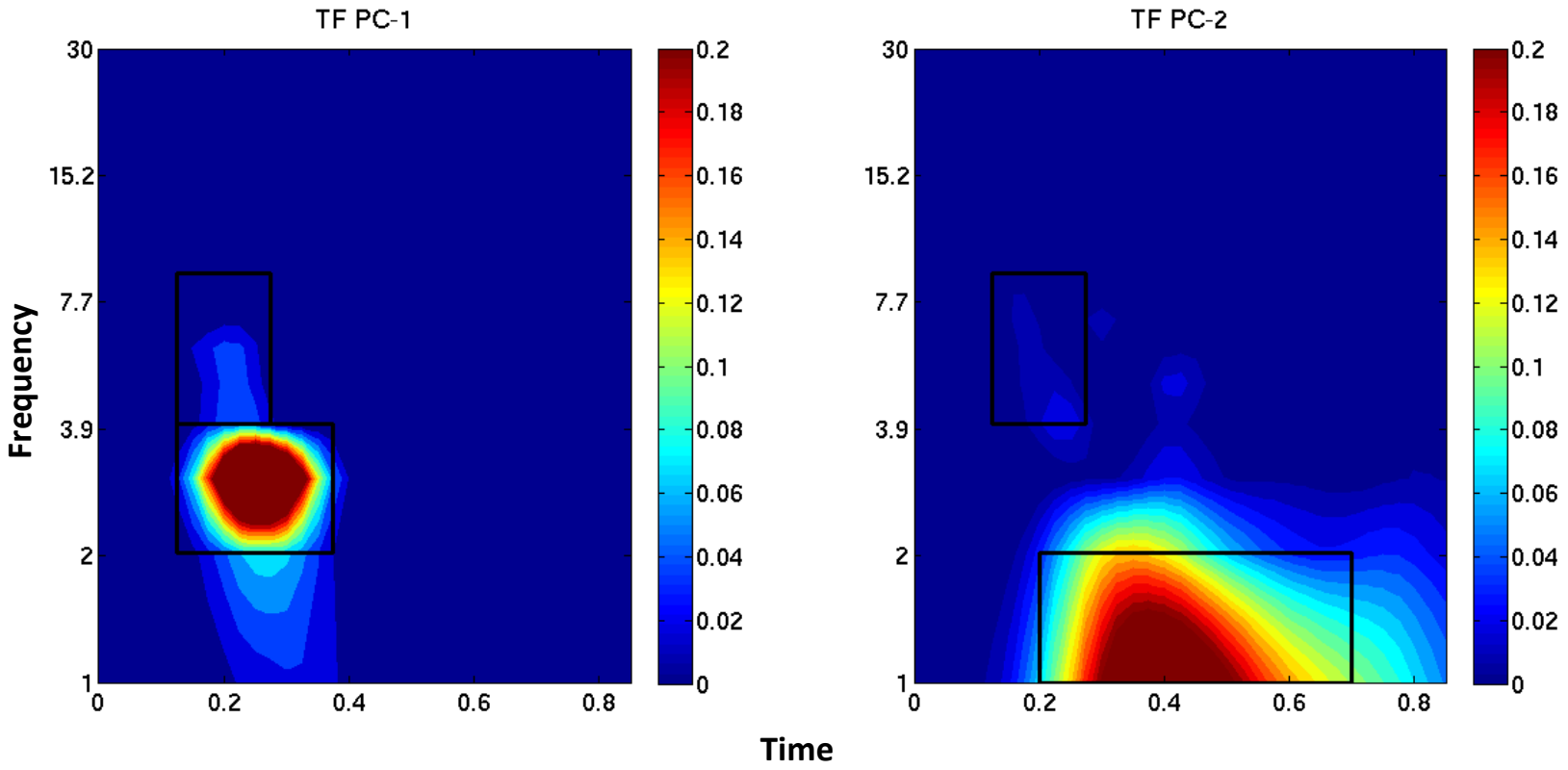

Figure 8. *PCA for evoked theta power.* Chosen PCA solution for determining theta window of interest for evoked power. On the basis these PCs, the same window of 4-8hz between 150ms and 300ms post-stimulus was selected for theta. Two separate windows were selected for lower frequencies: 2-4hz between 150ms and 400ms, and 1-2hz between 200ms and 700ms. Note the color bar scale has been adjusted to emphasis the less prominent but still present theta-band response.

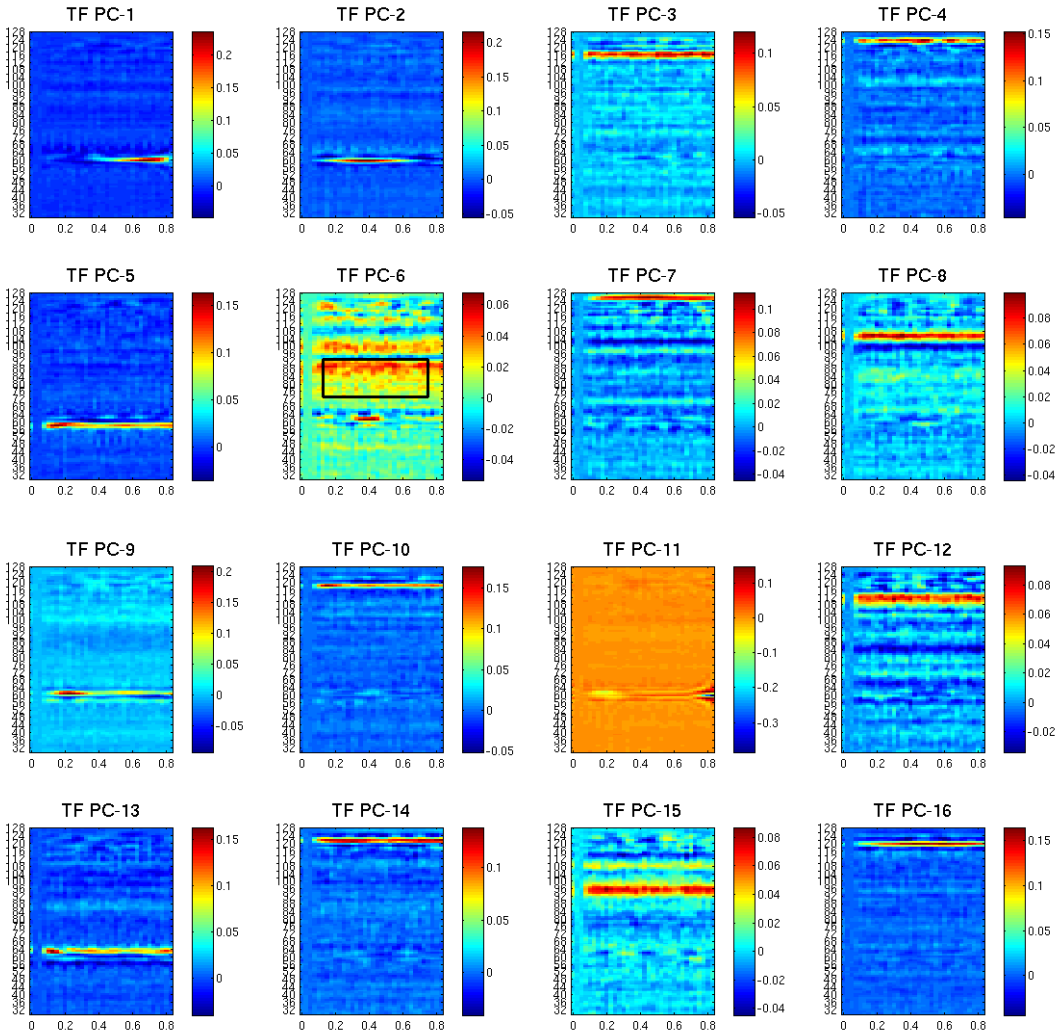

Figure 9. PCA for evoked gamma power. Chosen PCA solution for determining gamma window of interest for evoked power. On the basis of PC6, a window of 73-93hz from 150-775ms post-stimulus was selected for analyses of evoked gamma activity.

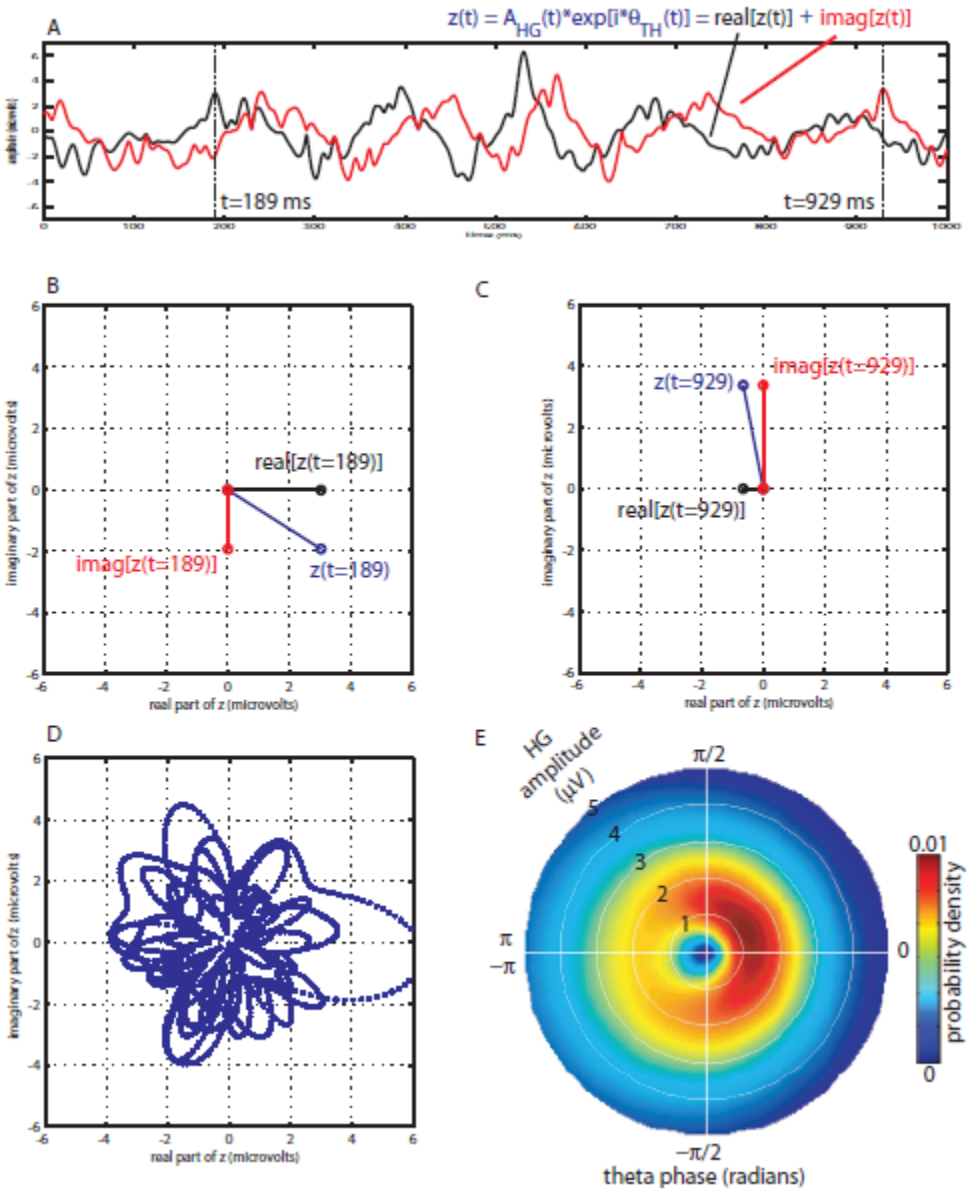

Figure 10. Modulation index example. A) The real (black) and imaginary (red) parts of $z(t)$ with two time points marked at t = 189 ms and t = 929 ms. B) The value of the composite signal $z(t)$ at t = 189 ms in the complex plane (blue), together with the values of the real (black) and imaginary (red) parts. C) As in B, for t = 929 ms. D) The values of $z(t)$ for all sample points over the one second interval examined. E) The estimated joint probability density function (PDF) for $z(t)$, which can be thought of as a normalized histogram of values assumed by z in the complex plane. Note that if the distribution of theta phase is uniform and the high gamma band (HG) amplitude time series and the theta phase time series are statistically independent, then this PDF will be radially symmetric. Since the phase distribution is uniform (data not shown), then any the observed asymmetry must be due to statistical dependence between the two time series. From Canolty et al. (2006).

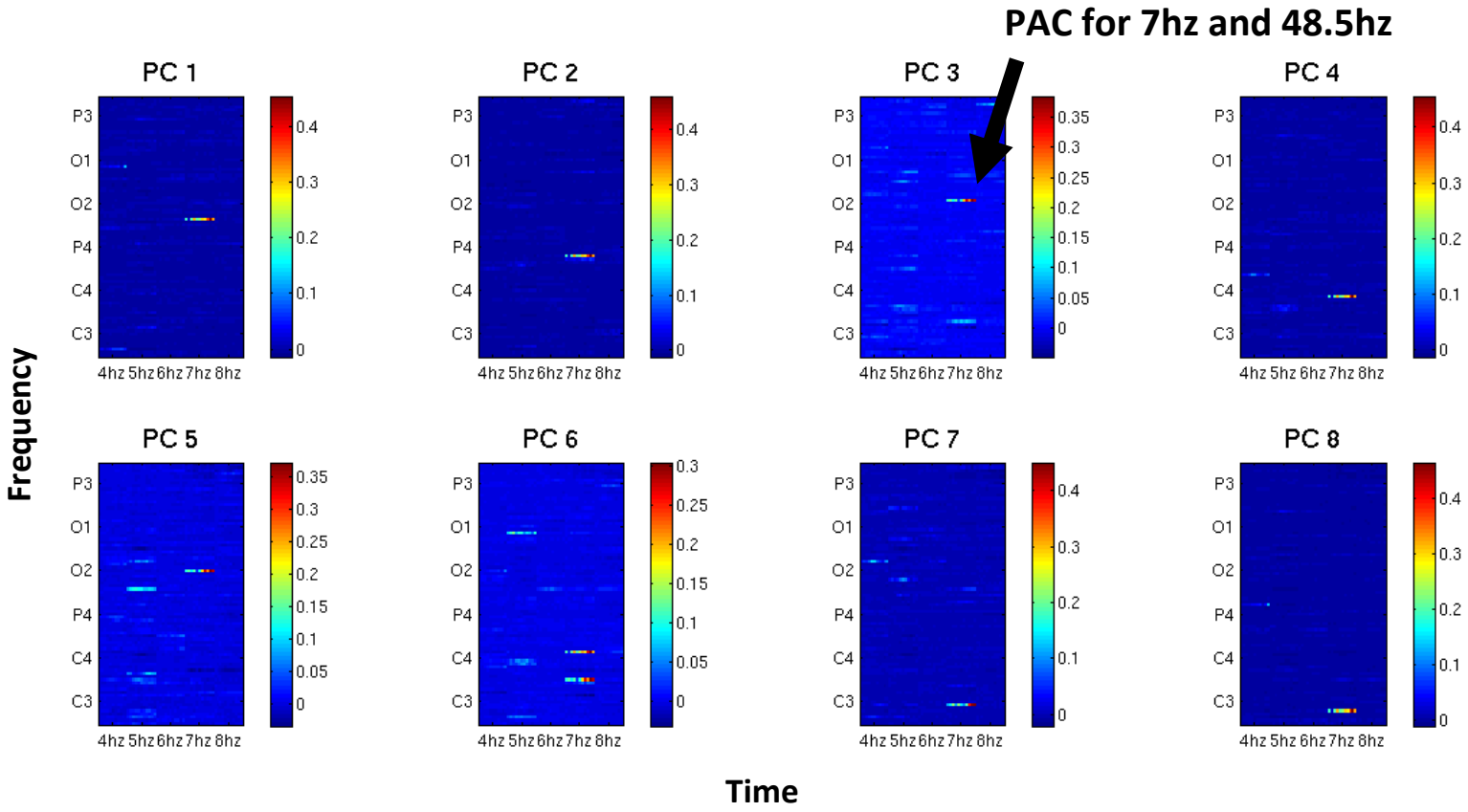

Figure 11. PCA for phase-amplitude coupling. Chosen PCA solution for determining PAC windows of interest. Identified regions were relatively specific to a given high-frequency band as paired with a given low frequency for a given electrode and were identified by precision visual inspection; an example is identified above. Time samples were not differentiated on the basis of the PCA solution, but instead entered into ANOVA along with a factor of diagnostic grouping to test for effects.

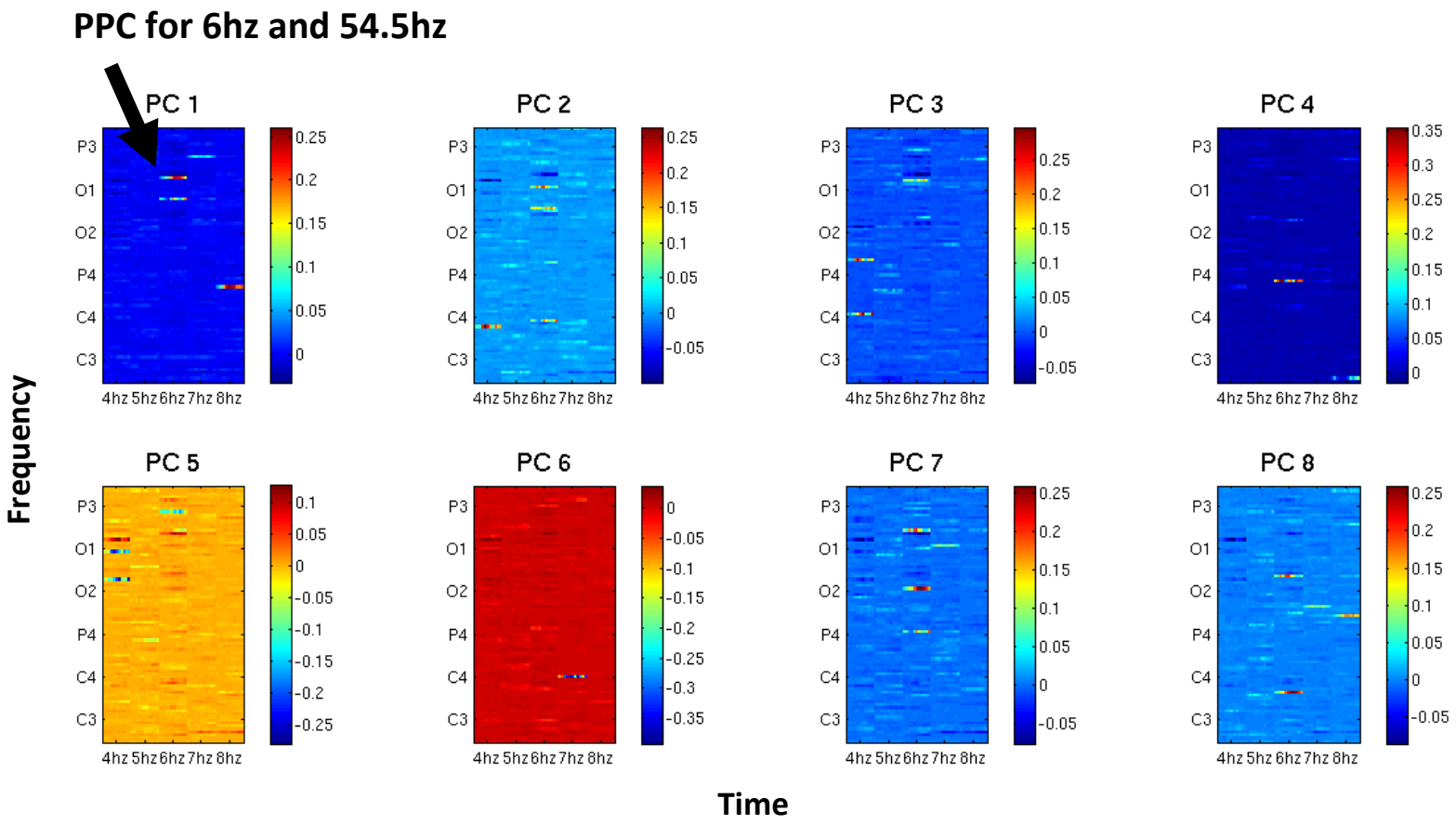

Figure 12. PCA for phase-phase coupling. Chosen PCA solution for determining PPC windows of interest. Identified regions were relatively specific to a given high-frequency band as paired with a given low frequency for a given electrode and were identified by precision visual inspection; an example is identified above. Time samples were not differentiated on the basis of the PCA solution, but instead entered into ANOVA along with a factor of diagnostic grouping to test for effects.

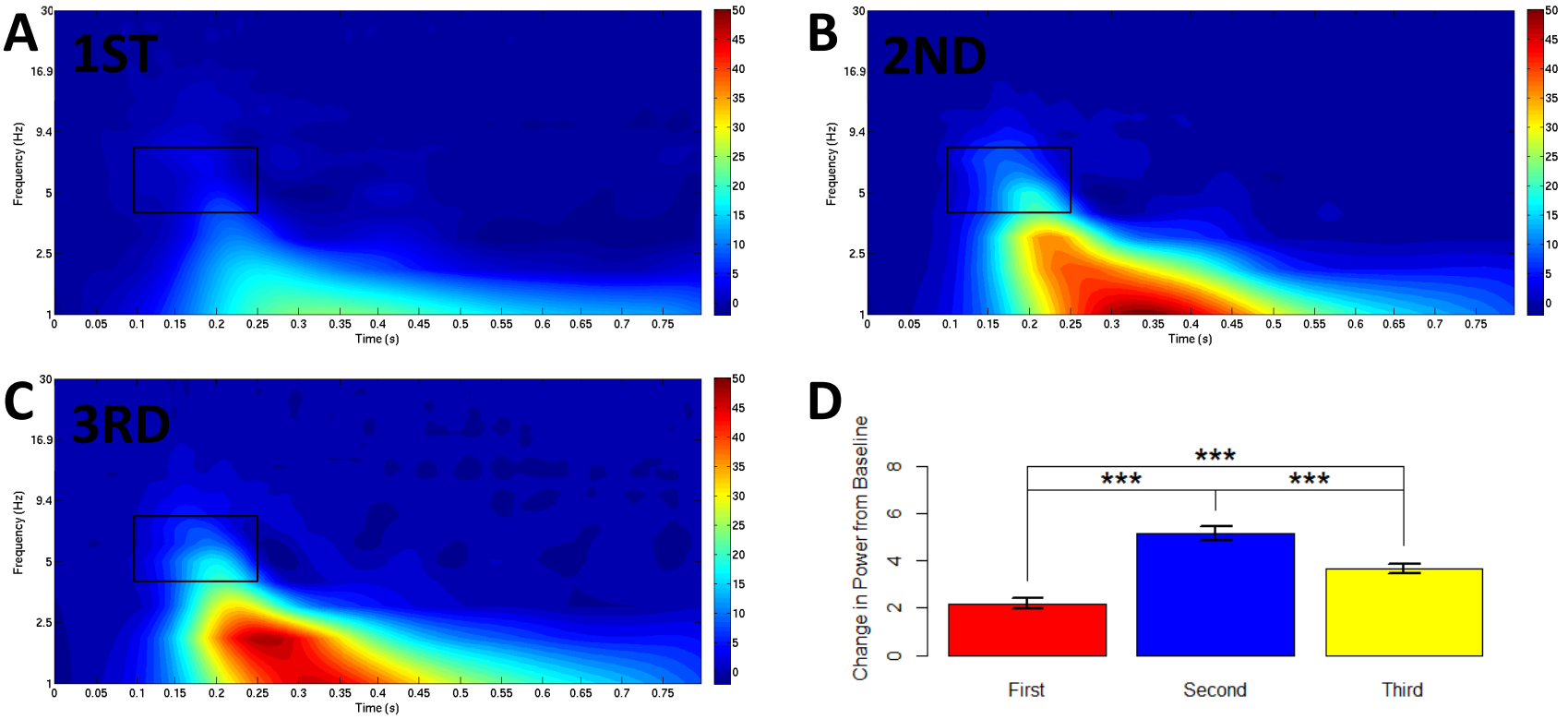

Figure 13. Evoked theta power by WM load. Change in evoked low frequency power from baseline (0ms to 50ms) for all subjects in response to a) first stimuli, b) second stimuli, and c) third stimuli. The target window for evoked theta power (4 to 8hz, 100-250ms post-stimulus) is outlined. Median values for each stimulus are depicted in d); power changes in the target window were greatest to second stimuli and differed for each stimulus by order. $*p < .05$, $**p < .01$, $***p < .001$.

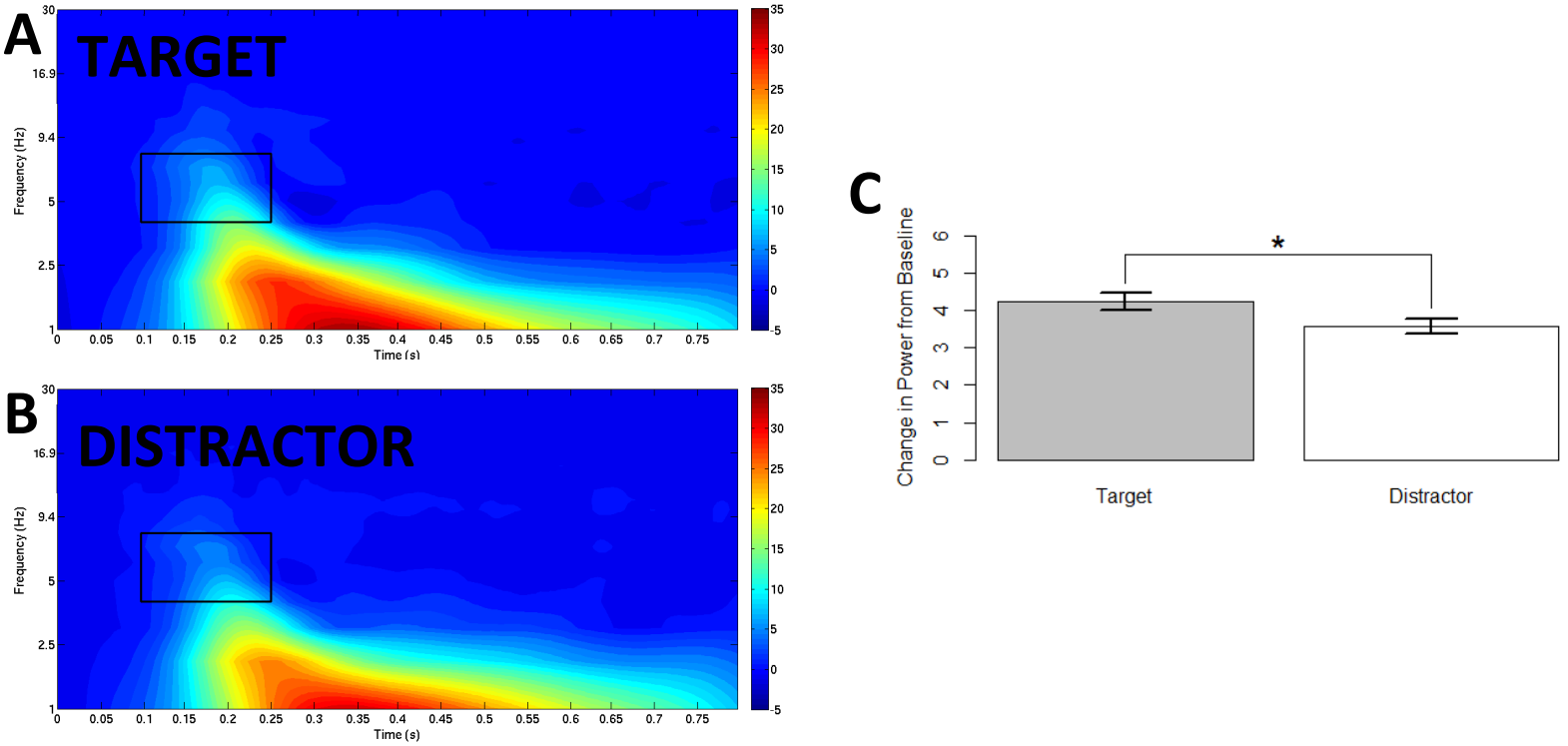

Figure 14. Evoked theta power by stimulus type. Change in evoked low frequency power from baseline (0ms to 50ms) for all subjects in response to a) target stimuli versus b) distractor stimuli. The target window for evoked theta power (4 to 8hz, 150-300ms post-stimulus) is outlined. Median values for each stimulus are depicted in c); power changes in the target window were

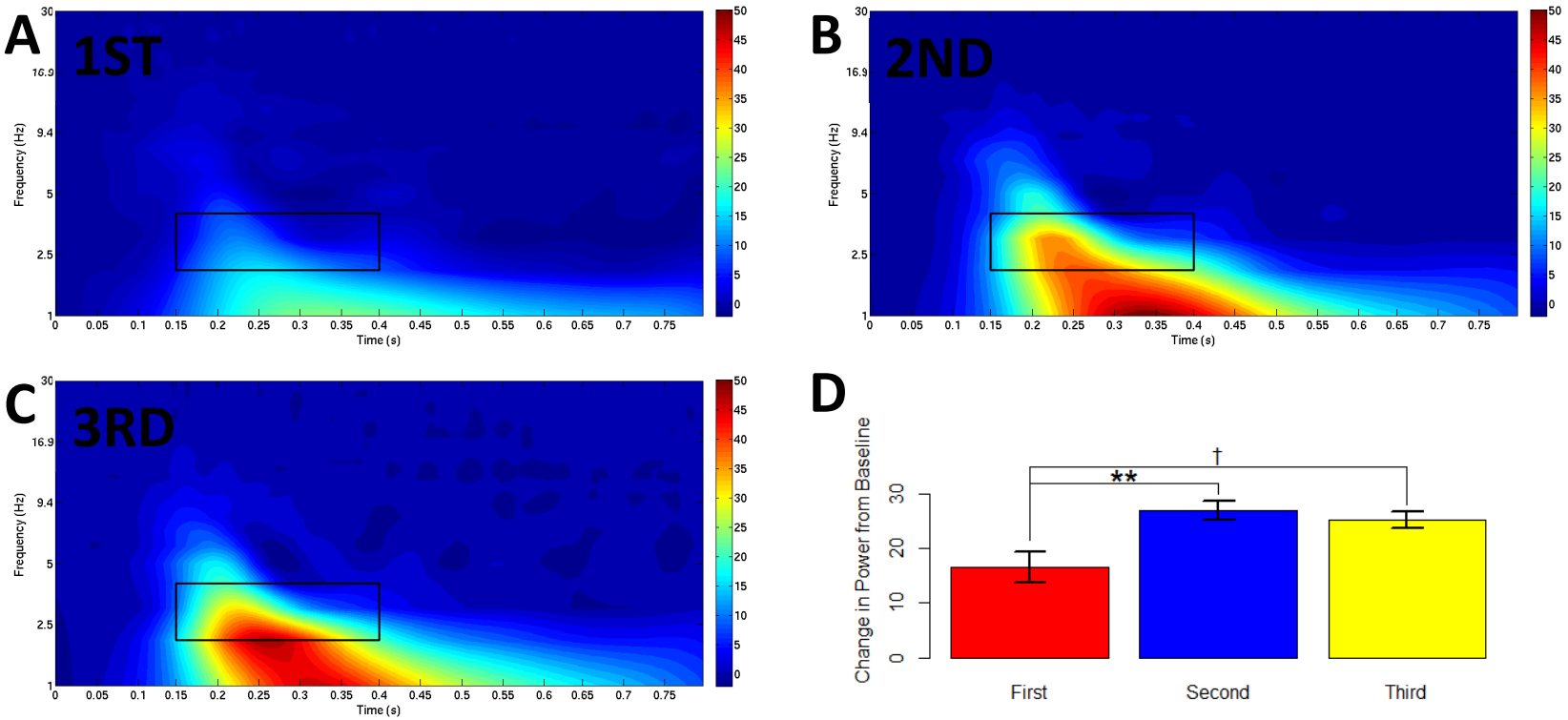

Figure 15. Evoked delta power (2-3hz) by WM load. Change in evoked low frequency power from baseline (0ms to 50ms) for all subjects in response to a) first stimuli, b) second stimuli, and c) third stimuli. The target window for evoked delta power (2 to 3hz, 150-400ms post-stimulus) is outlined. Median values for each stimulus are depicted in d); power increases in the target window were greater to second and third stimuli than to first stimuli. †$p < .10$, *$p < .05$, **$p < .01$, ***$p < .001$.

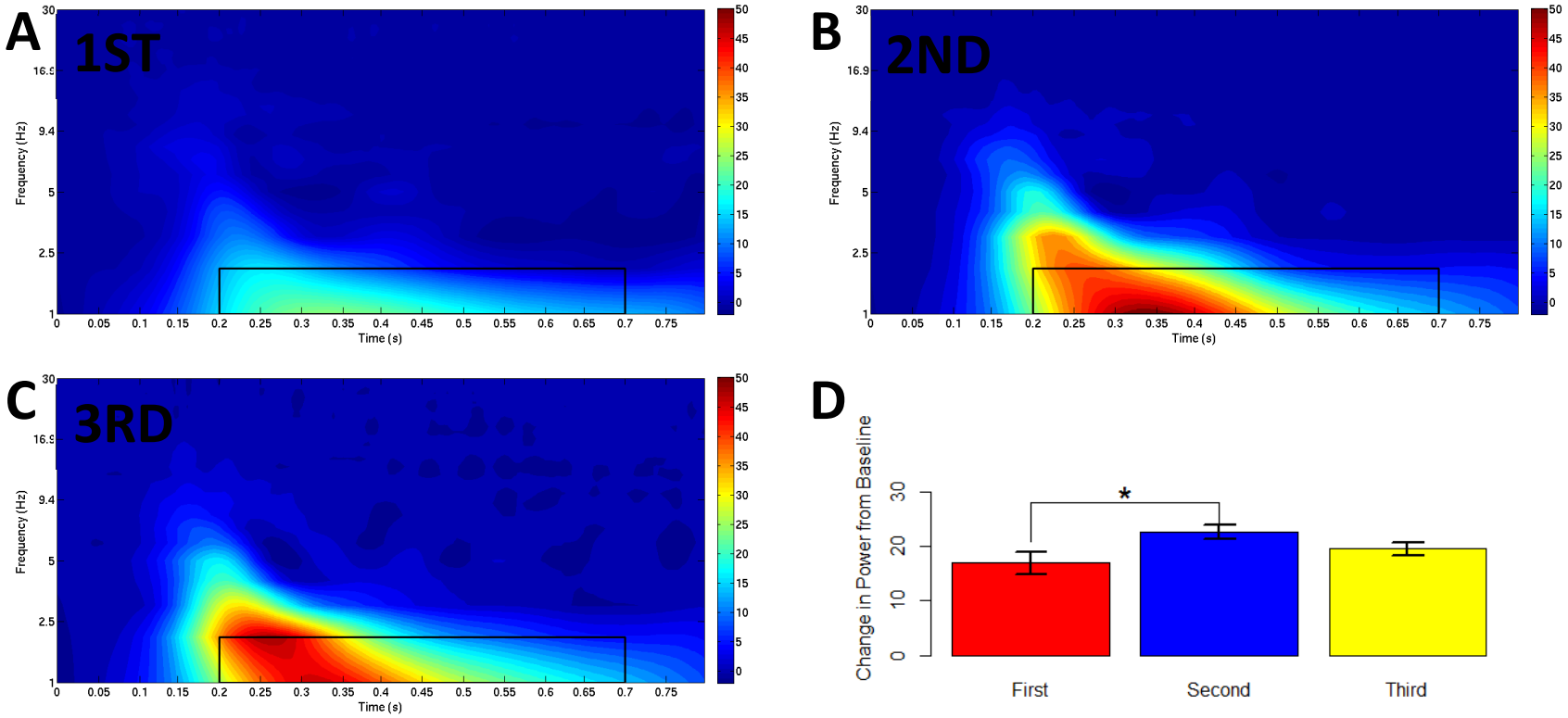

Figure 16. Evoked delta power (1-2hz) by WM load. Change in evoked low frequency power from baseline (0ms to 50ms) for all subjects in response to a) first stimuli, b) second stimuli, and c) third stimuli. The target window for low evoked delta power (1 to 2hz, 200-700ms post-stimulus) is outlined. Median values for each stimulus are depicted in d); power increases in the target window were greater to second stimuli than to first stimuli. $*p < .05$, $**p < .01$, $***p < .001$.

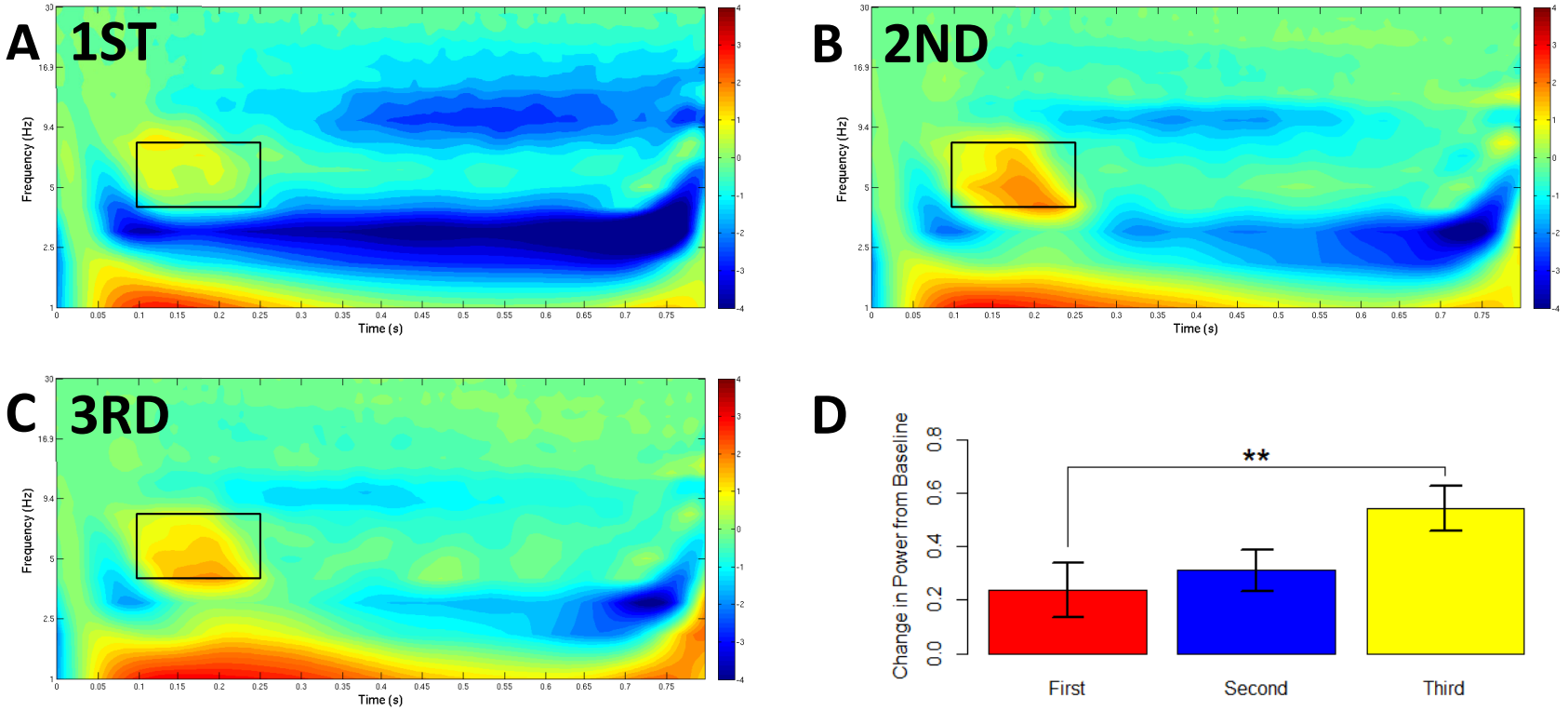

Figure 17. Induced theta power by WM load. Change in induced power in target theta window (4 to 8hz, 100-250ms post-stimulus) from baseline (0ms to 50ms) in response to a) first, b) second, and c) third stimuli for all subjects. Median values are depicted in d). Increases in response to third stimuli were greater than those to first stimuli for the target theta window; median power changes to second stimuli fell in between those to first and third. †$p < .10$, *$p < .05$, **$p < .01$, ***$p < .001$.

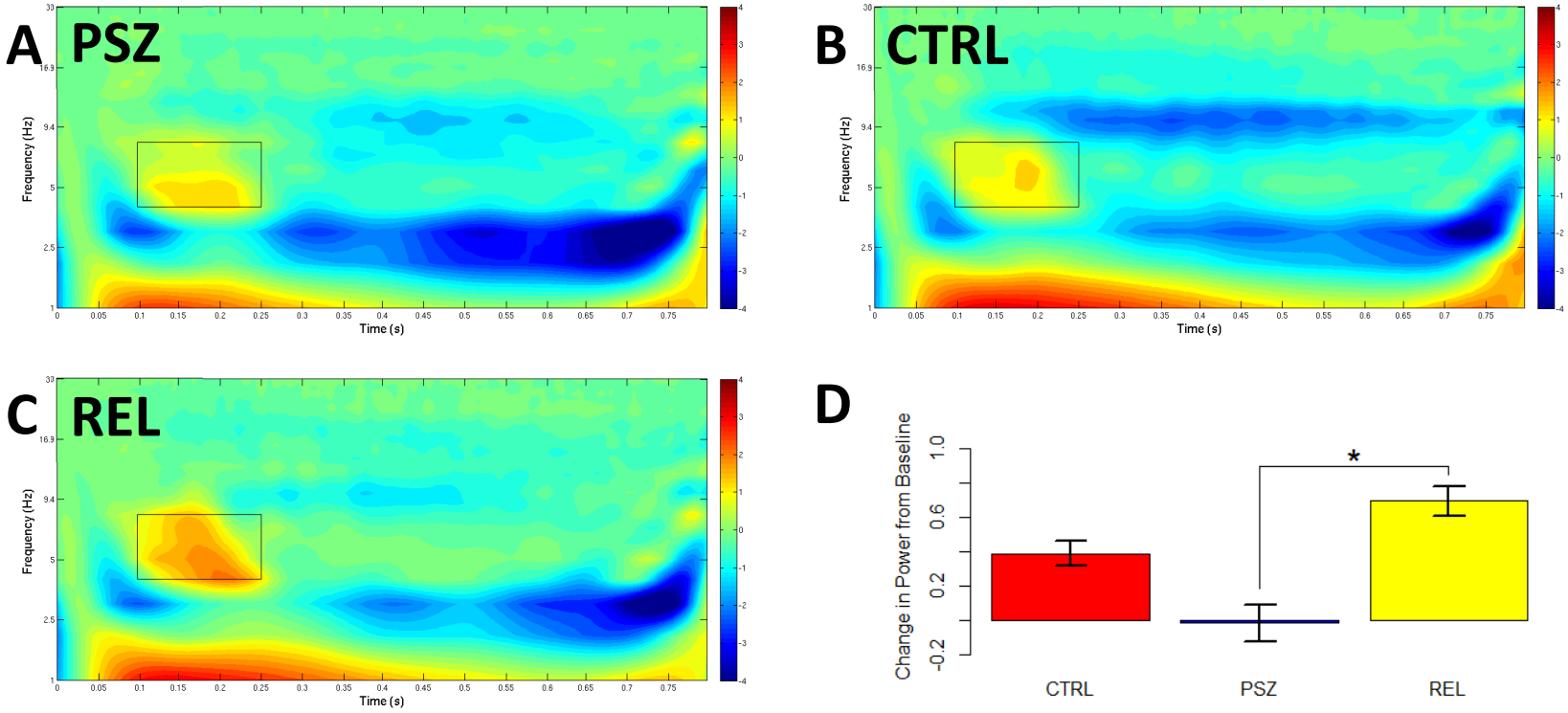

Figure 18. Induced theta power by diagnostic grouping. Change in induced power in target theta window (4 to 8hz, 100-250ms post-stimulus; outlined) from baseline (0ms to 50ms) in response for a) PSZ, b) CTRL, and c) REL. Median values are depicted in d). Increases in theta power from baseline in REL were greater than increases observed in PSZ.
†$p < .10$, *$p < .05$, **$p < .01$, ***$p < .001$.

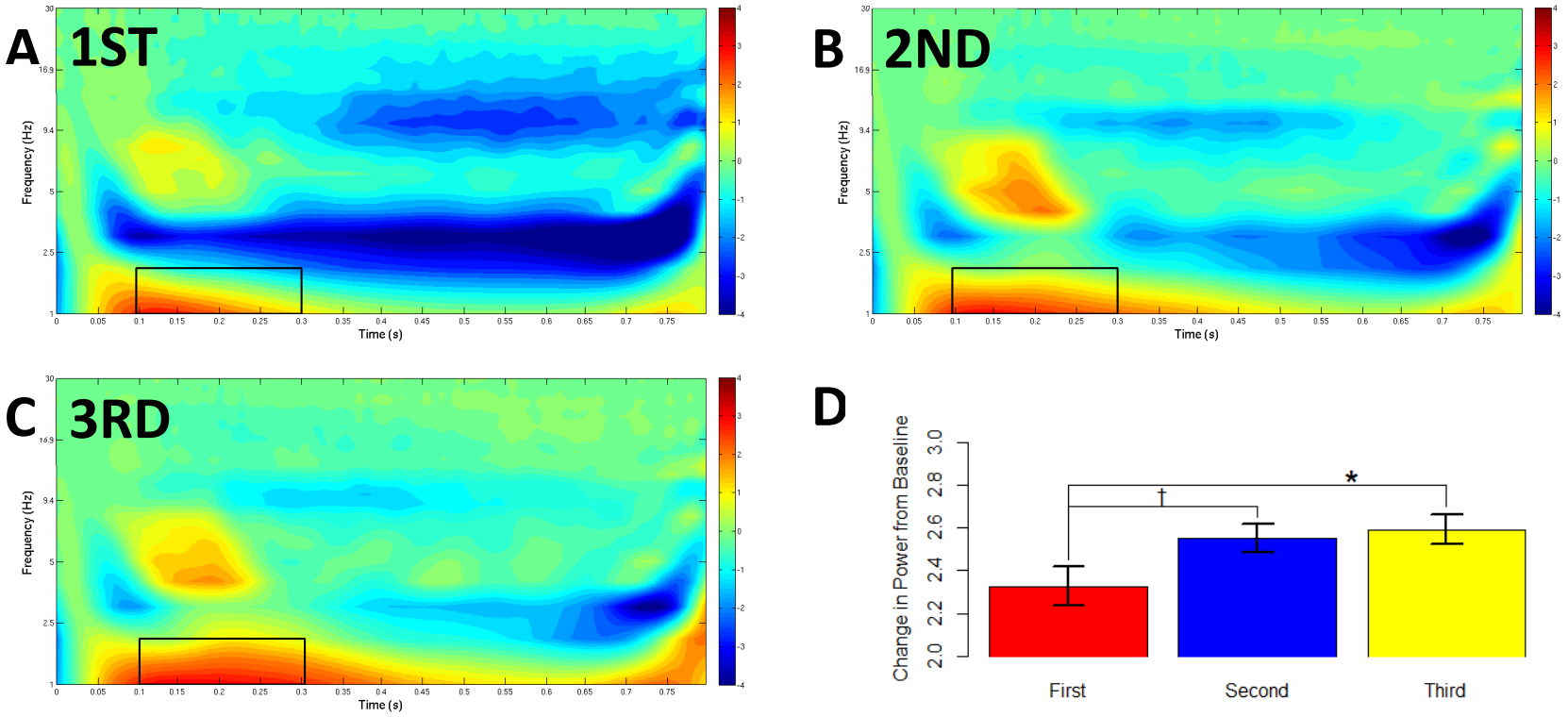

Figure 19. Induced delta power (1-2hz) by WM load. Change in induced power in target delta window (1 to 2hz, 100-400ms post-stimulus) from baseline (0ms to 50ms) in response to a) first, b) second, and c) third stimuli for all subjects. Median values are depicted in d). Increases in induced delta energy in response to third and second stimuli were greater than increases to first stimuli. †$p < .10$, *$p < .05$, **$p < .01$, ***$p < .001$.

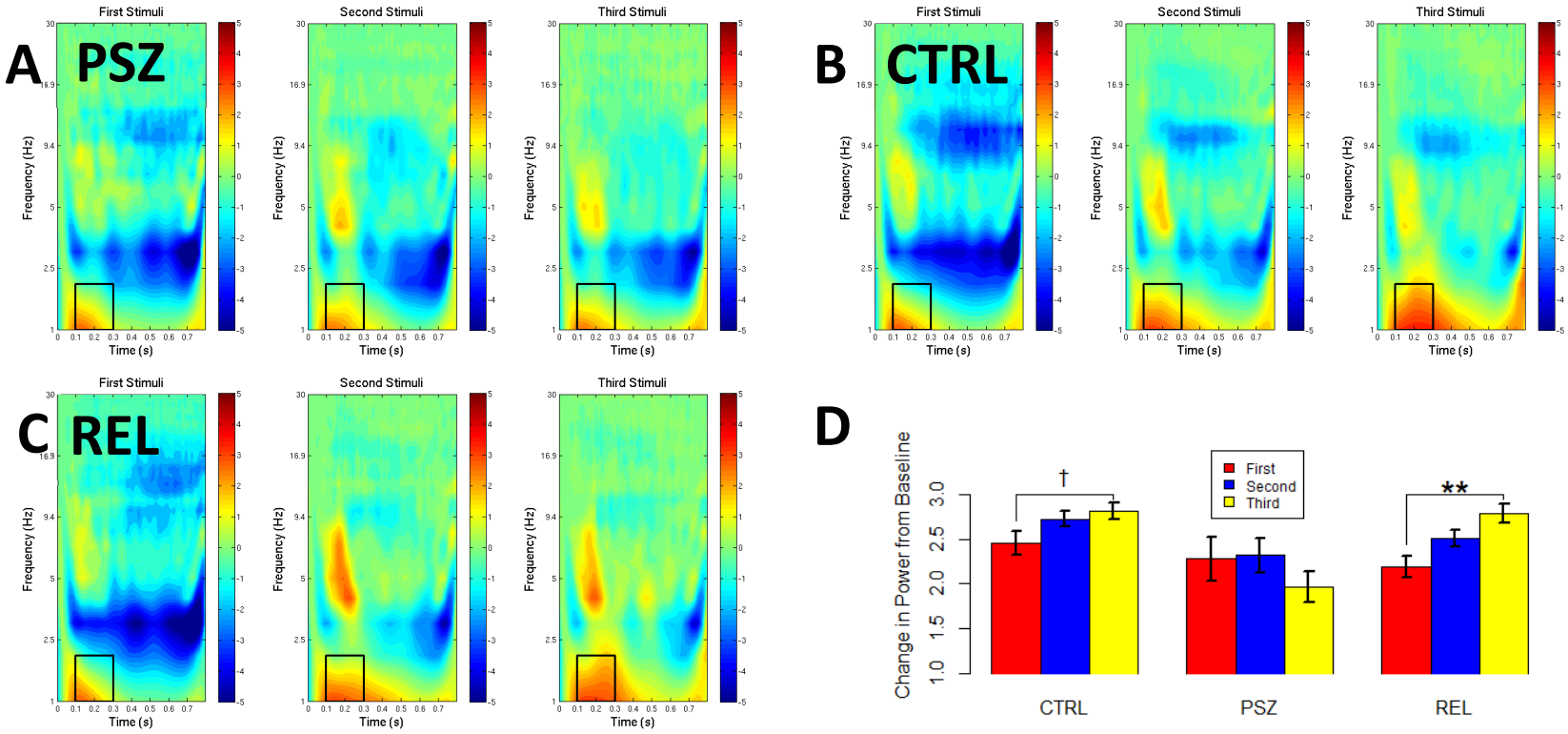

Figure 20. Induced delta power (1-2hz) – diagnostic grouping by WM load. Change in induced power in target delta window (1 to 2hz, 100-300ms post-stimulus) from baseline (0ms to 50ms) for all a) PSZ, b) CTRL, and c) REL in response to first, second and third stimuli. Median values are depicted in d). CTRL and REL showed greater increases in median power in response to third stimuli as compared to first; PSZ showed no differences between the three stimuli in time. †$p < .10$, *$p < .05$, **$p < .01$, ***$p < .001$.

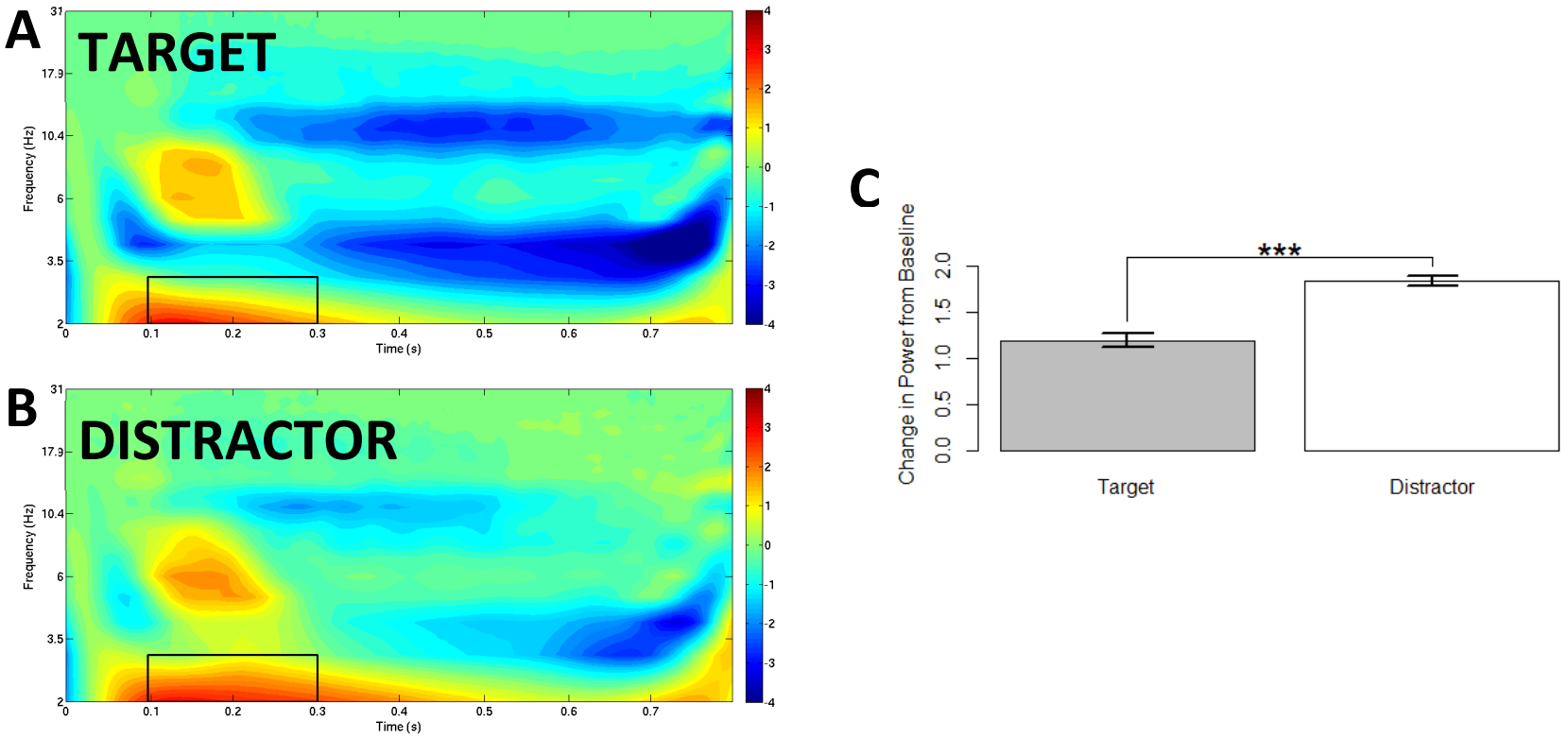

Figure 21. Induced delta power (2-3hz) by stimulus type. Change in induced delta frequency power (2-3hz, 150-450ms post-stimulus; outlined) from baseline (0ms to 50ms) for all subjects in response to a) target stimuli versus b) distractor stimuli. Median values for each stimulus are depicted in c); power increases in the target window were greater to distractor stimuli than to target stimuli. †$p < .10$, *$p < .05$,

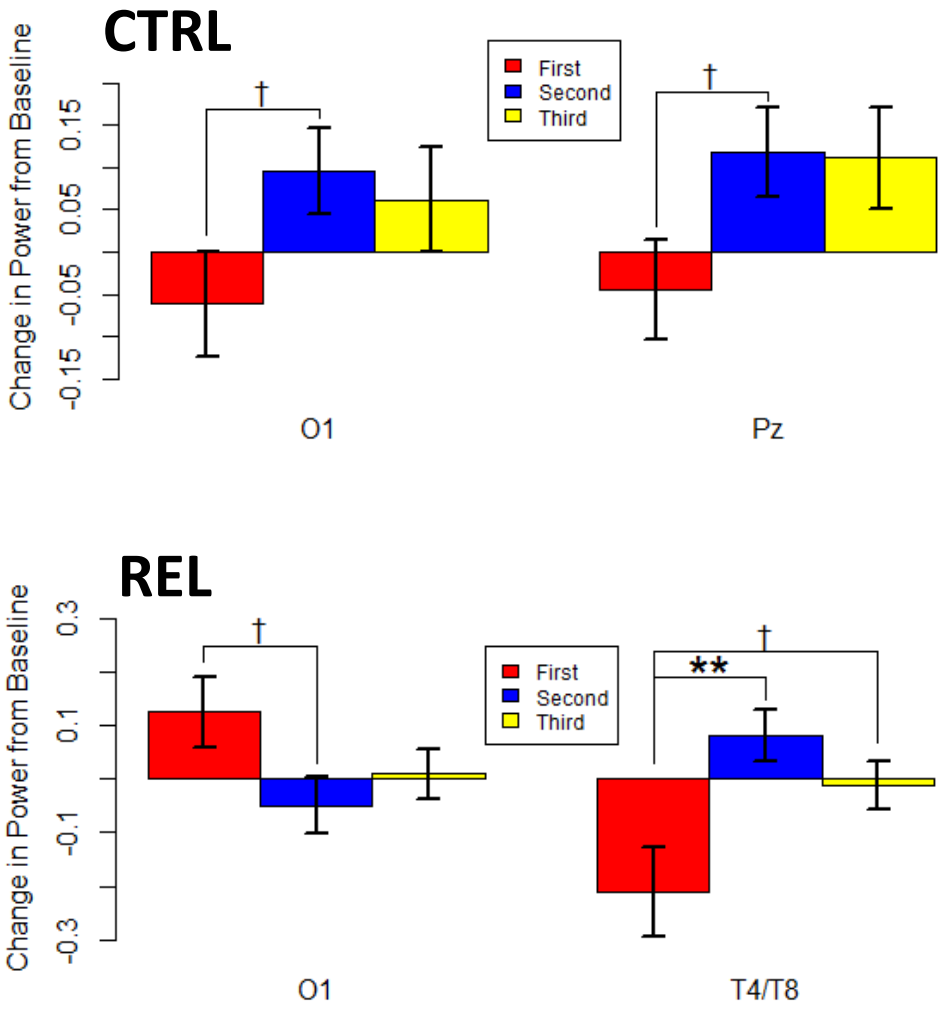

Figure 22. Induced gamma power (64-81hz) – diagnostic grouping by electrode site. Electrode sites showing effects of order on induced gamma-band (64-81hz, 425-775ms post-stimulus) power for CTRL and REL. No effect of order was observed for PSZ. CTRL showed marginal increases from 1st to 2nd stimuli at O1 and Pz. REL showed a decrease in power from 1st to 2nd stimuli at O1, and increases from 1st to both 2nd and 3rd stimuli at T4/T8. †$p < .10$, *$p < .05$, **$p < .01$, ***$p < .001$.

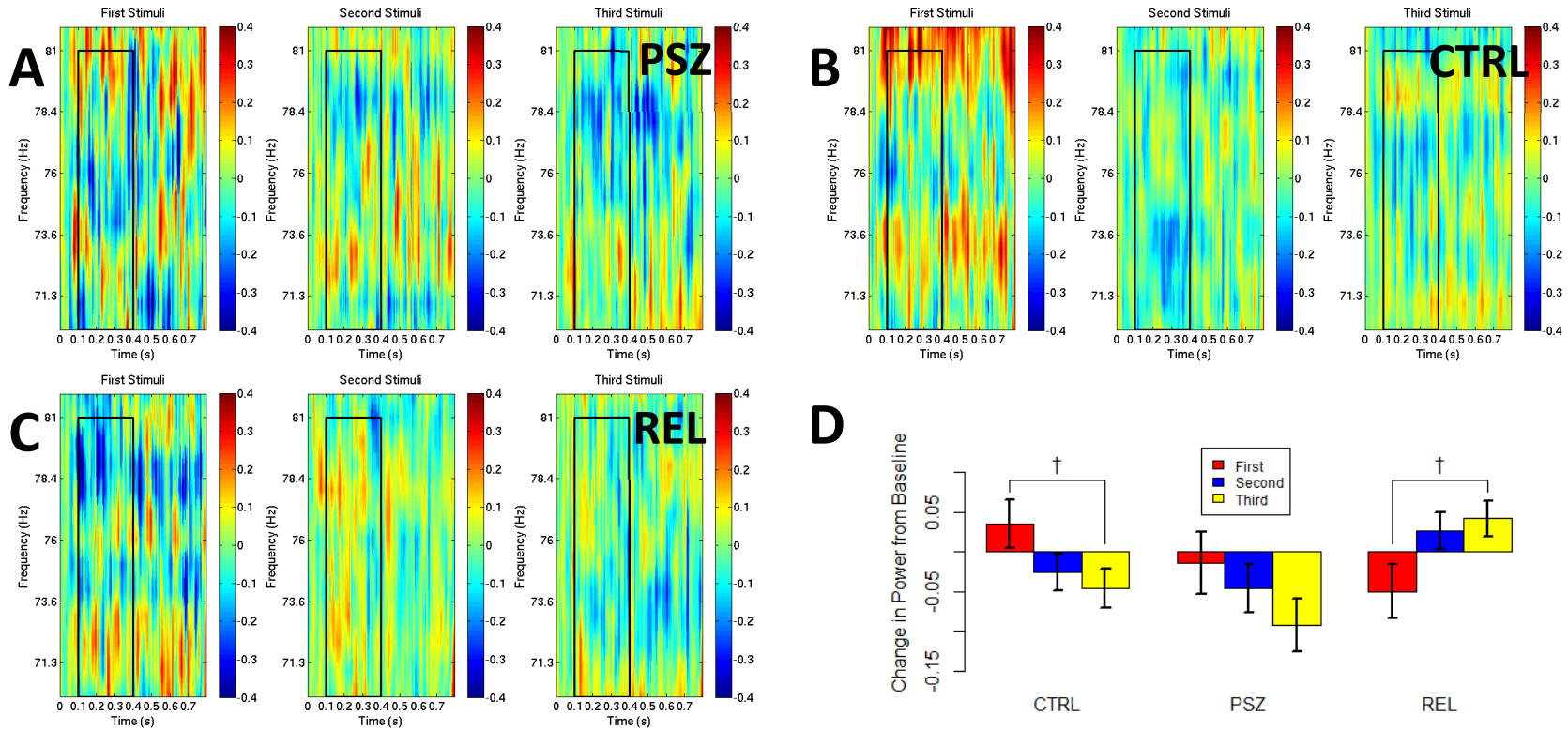

Figure 23. Induced gamma power (71-81hz) – diagnostic grouping by WM load. Change in induced power from baseline (0ms to 50ms) in 71 to 81hz, 100-400ms post-stimulus gamma window for all a) PSZ, b) CTRL, and c) REL in response to first, second and third stimuli. Median values are depicted in d). CTRL and REL showed differences in median power between third stimuli as compared to first; differences observed between the three stimuli in time did not achieve significance for PSZ.
†$p < .10$, *$p < .05$, **$p < .01$, ***$p < .001$.

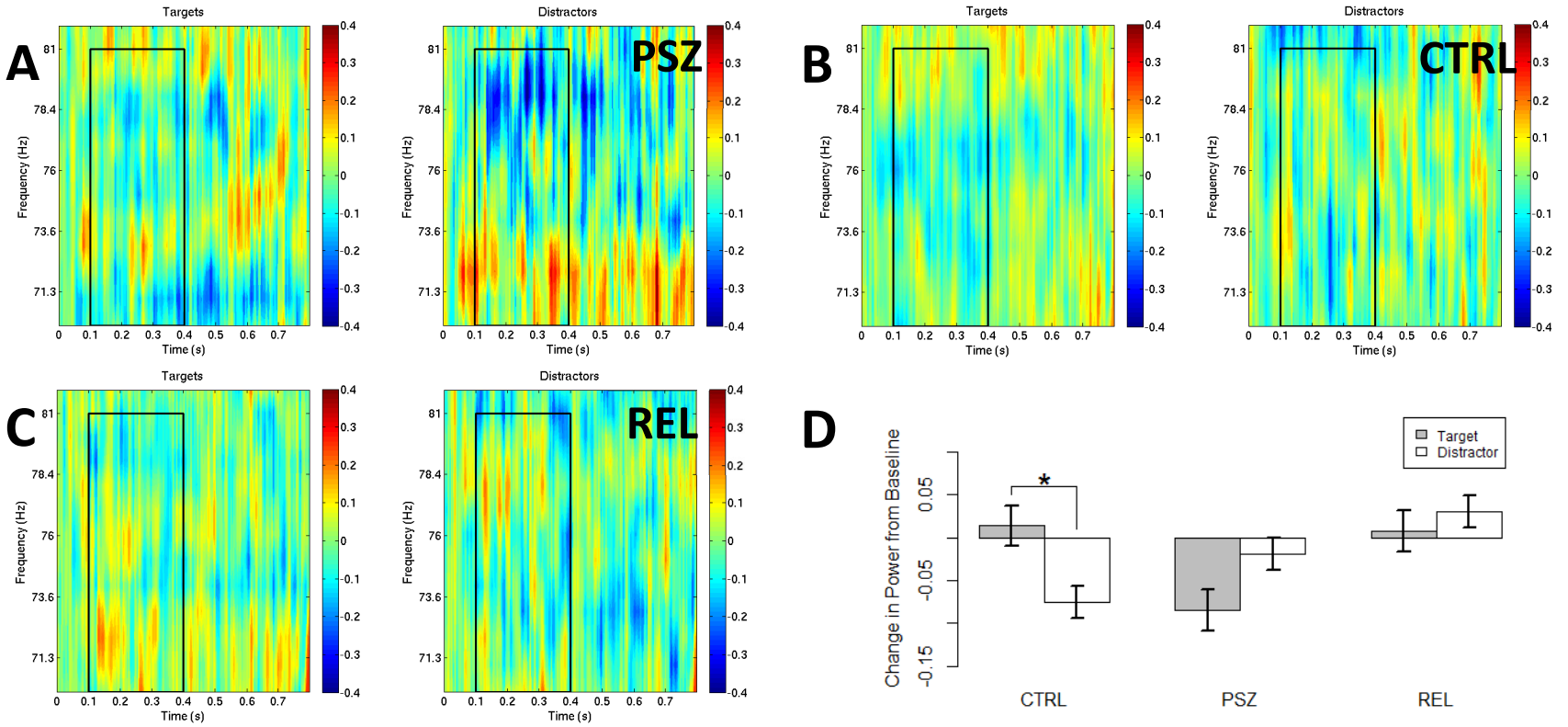

Figure 24. Induced gamma power (71-81hz) – diagnostic grouping by stimulus type. Change in induced power from baseline (0ms to 50ms) in 71 to 81hz, 100-400ms post-stimulus gamma window for all a) PSZ, b) CTRL, and c) REL in response to target and distractor stimuli. Median values are depicted in d). CTRL alone showed differences in median power between target and distractor stimuli. †$p <$ .10, *$p <$ .05, **$p <$ .01, ***$p <$ .001.

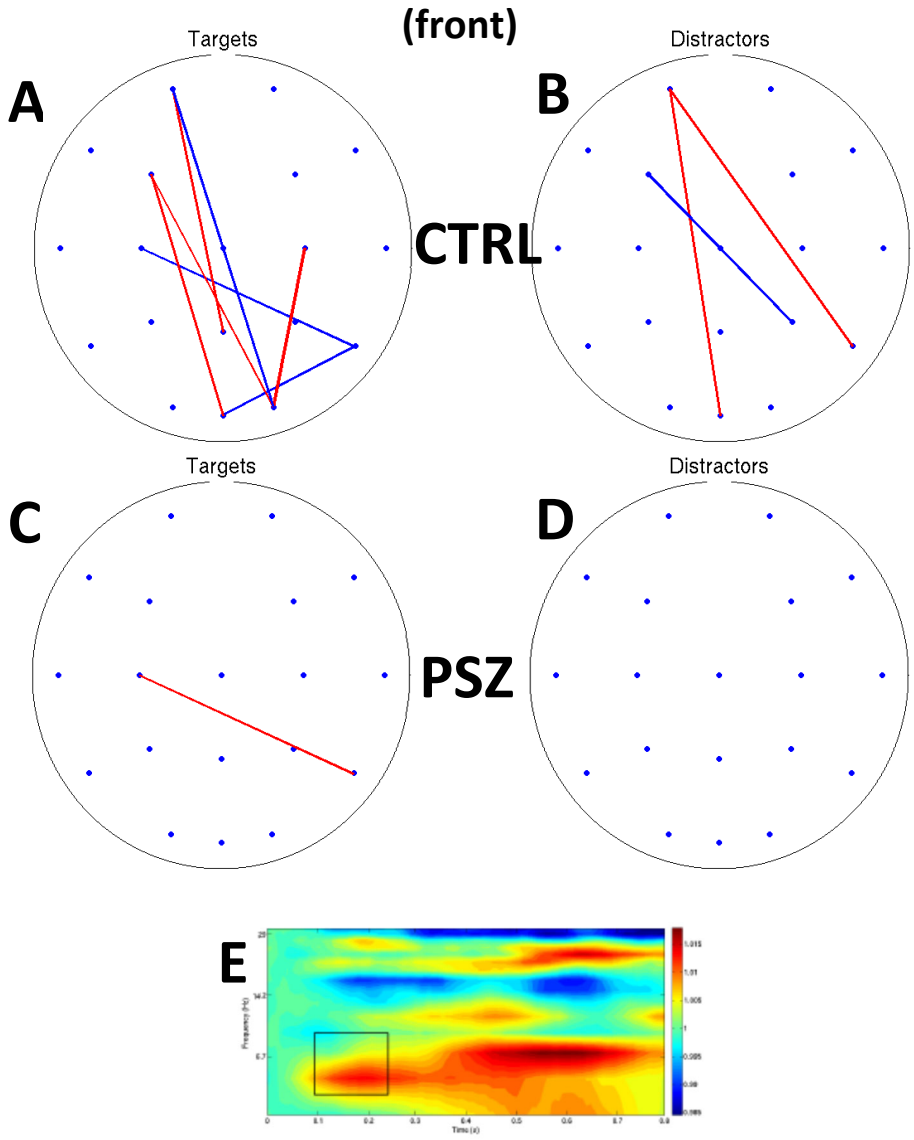

Figure 25. Theta-band IPSC. Electrode pairs showing theta-band (4-8hz, 100-250ms post-stimulus) intersite phase clustering (e.g., phase-locking) values with $p < .10$ for a) target and b) distractor stimuli in CTRL. Those pairs that demonstrated synchrony for CTRL were also examined in PSZ and REL, and electrodes pairs within this subset demonstrating synchrony are shown for PSZ in c) and d) (target and distractor stimuli, respectively). The time-frequency window of analysis is depicted in e). For the subset of the CTRL electrode pairs examined, PSZ showed synchrony changes for a single pair of electrodes in response to target stimuli. REL showed no synchrony changes in the subset of examined electrode pairs. Red lines represent synchrony increases as compared to baseline; blue lines represent synchrony decreases.

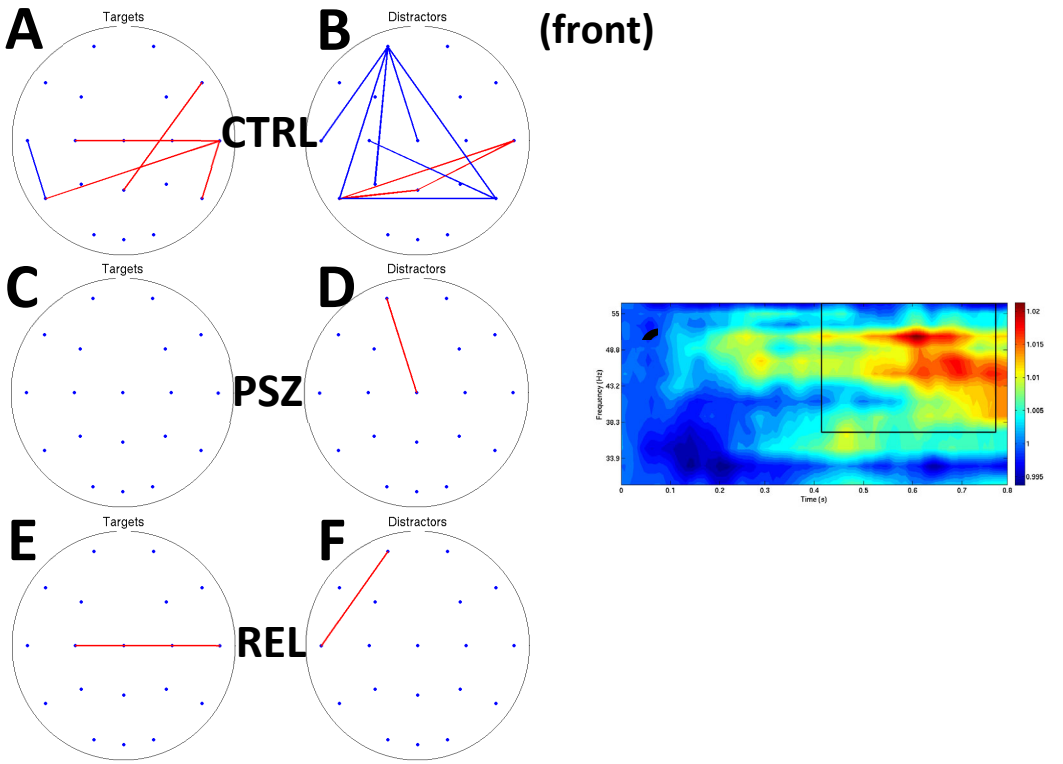

Figure 26. Gamma-band (36-56hz) IPSC. Electrode pairs showing gamma-band (36-56hz, 425-775ms post-stimulus) intersite phase clustering (e.g., phase-locking) values with $p < .10$ for a) target and b) distractor stimuli in CTRL. Those pairs that demonstrated synchrony for CTRL were also examined in PSZ and REL, and electrodes pairs within this subset demonstrating synchrony are shown for PSZ in c) and d) and for REL in e) and f) (target and distractor stimuli, respectively). The time-frequency window of analysis is depicted in g). For the subset of the CTRL electrode pairs examined, PSZ showed synchrony changes in one pair only for distractor stimuli, while REL showed changes in a single pair for both stimulus types. Red lines represent synchrony increases as compared to baseline; blue lines represent synchrony decreases.

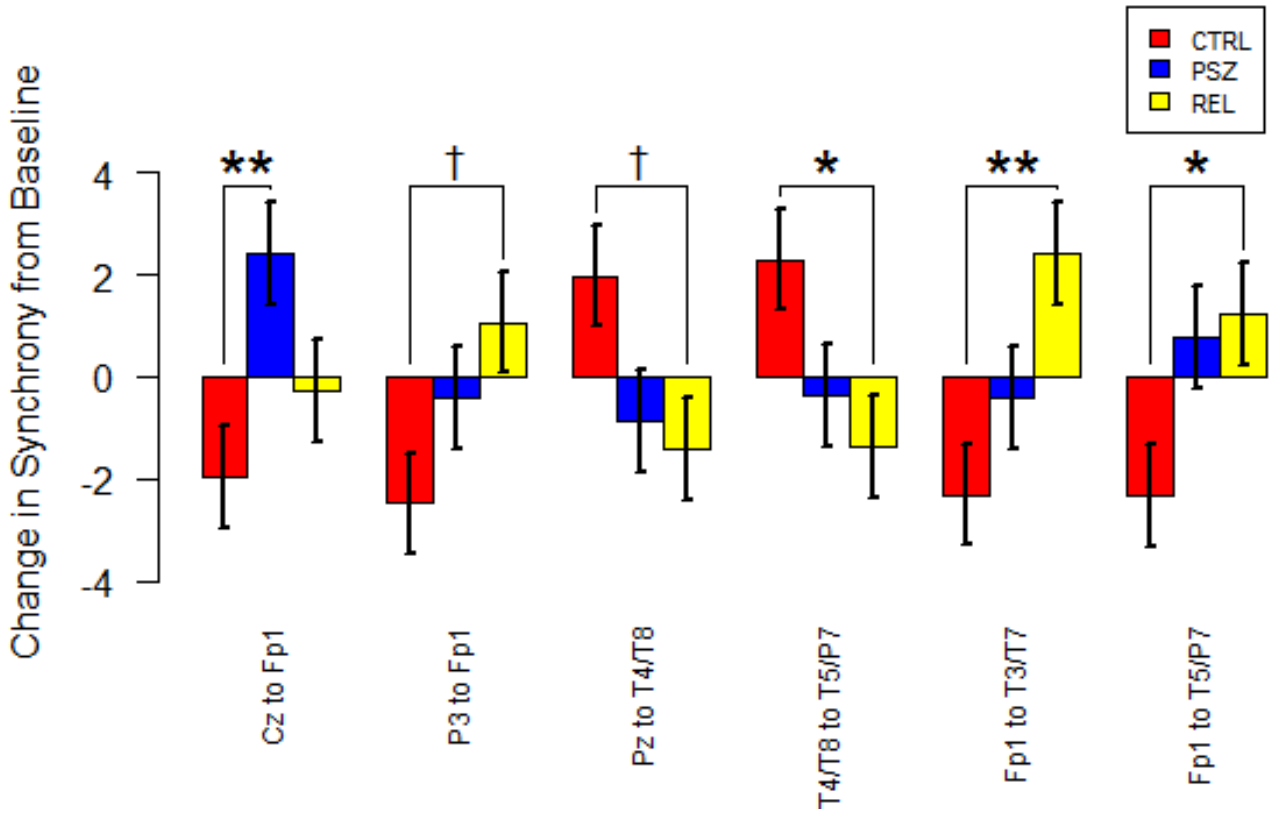

Figure 27. Electrodes with group differences in gamma-band (36-56hz) IPSC. Electrode pairings in for which differences between diagnostic groupings were observed for gamma-band (36-56hz, 425-775ms post-stimulus) intersite phase clustering (e.g., phase-locking) values in response to distractor stimuli. For pairings involving Fp1, CTRL consistently showed decreases in synchrony from baseline, as opposed to increases in PSZ or REL. †$p < .10$, *$p < .05$, **$p < .01$, ***$p < .001$.

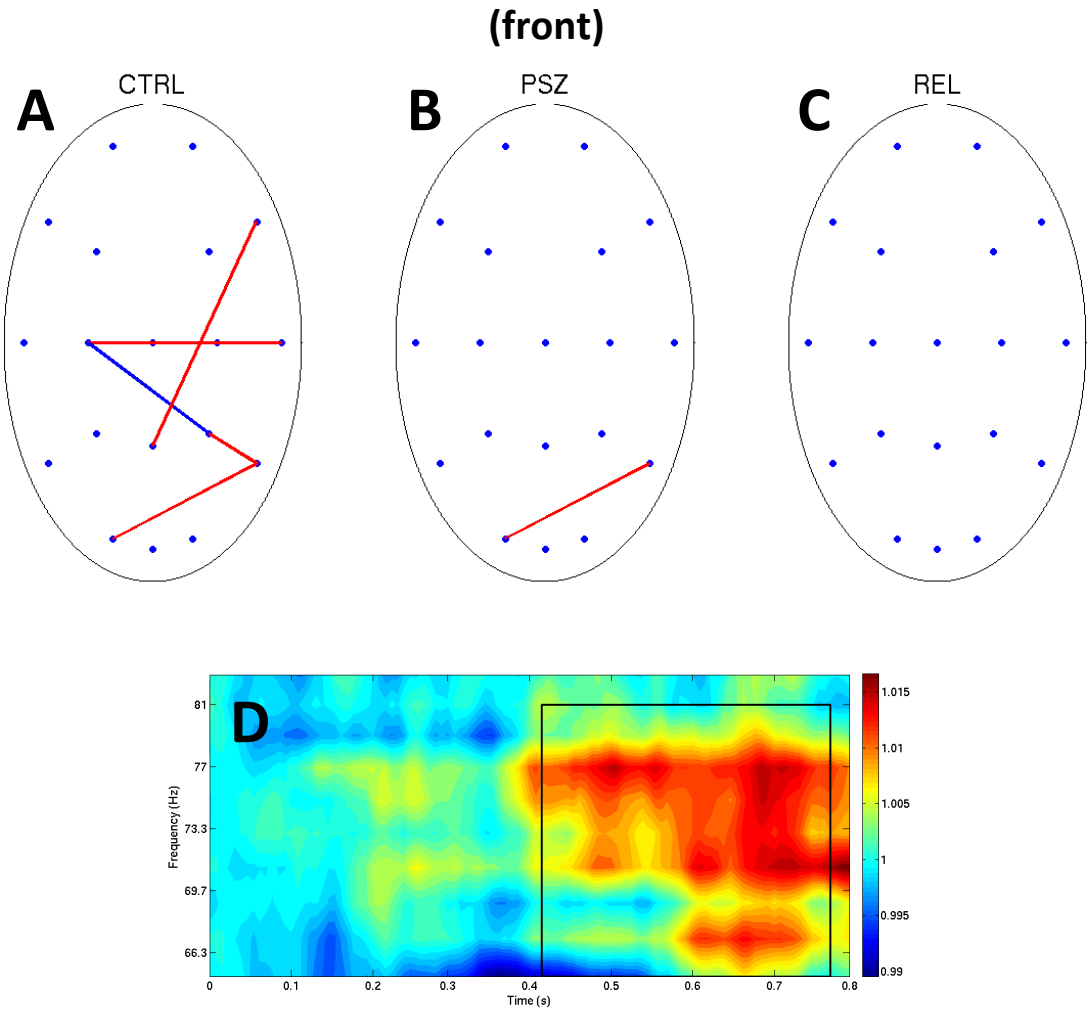

Figure 28. Gamma-band (64-81hz) IPSC. Electrode pairings in a) CTRL, b) PSZ and c) REL showing gamma-band (64-81hz, 425-775ms post-stimulus) intersite phase clustering (e.g., phase-locking) values with $p < .10$ for distractor stimuli. Time-frequency window of interest depicted in d). All depicted relationships represent synchrony increases from baseline. REL had no values below this threshold for those electrode pairs that showed synchrony changes for CTRL.

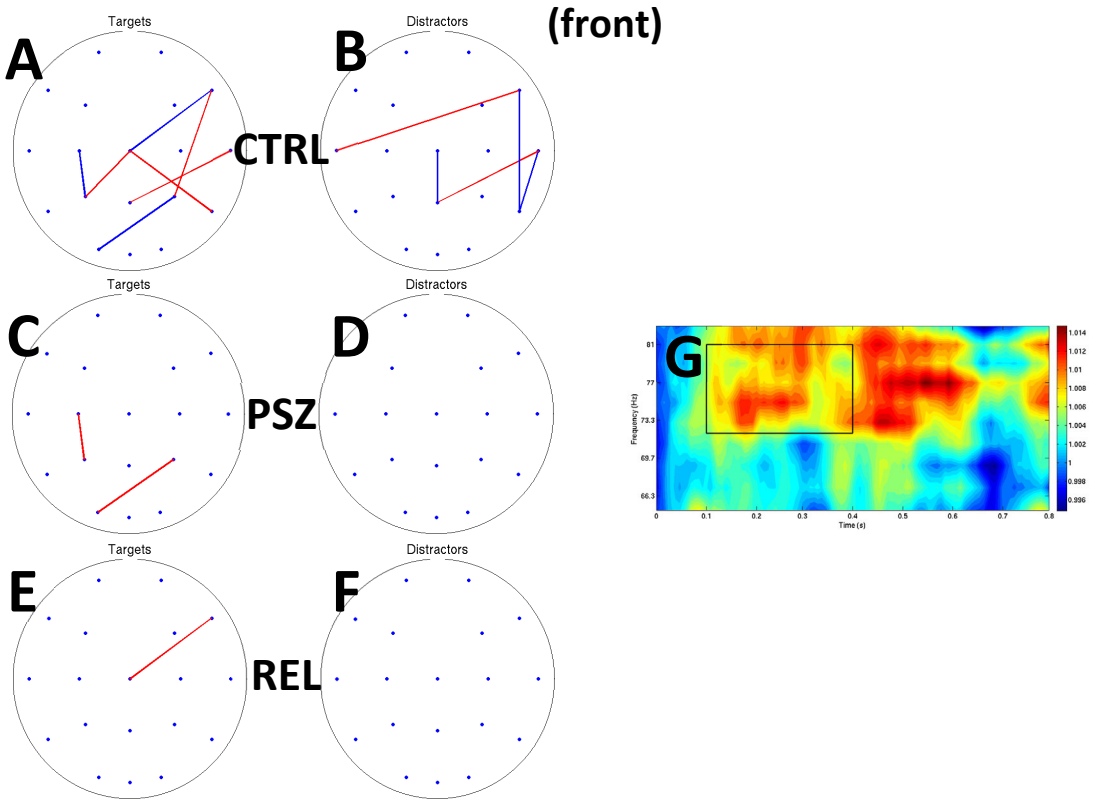

Figure 29. Gamma-band (71-81hz) IPSC. Electrode pairs showing gamma-band (71-81hz, 100-400ms post-stimulus) intersite phase clustering (e.g., phase-locking) values with $p < .10$ for a) target and b) distractor stimuli in CTRL. Those pairs that demonstrated synchrony for CTRL were also examined in PSZ and REL, and electrodes pairs within this subset demonstrating synchrony are shown for PSZ in c) and d) and for REL in e) and f) (target and distractor stimuli, respectively). The time-frequency window of interest is depicted in g). For the subset of the CTRL electrode pairs examined, PSZ and REL showed synchrony changes to target stimuli but not distractors. Red lines represent synchrony increases as compared to baseline; blue lines represent synchrony decreases.

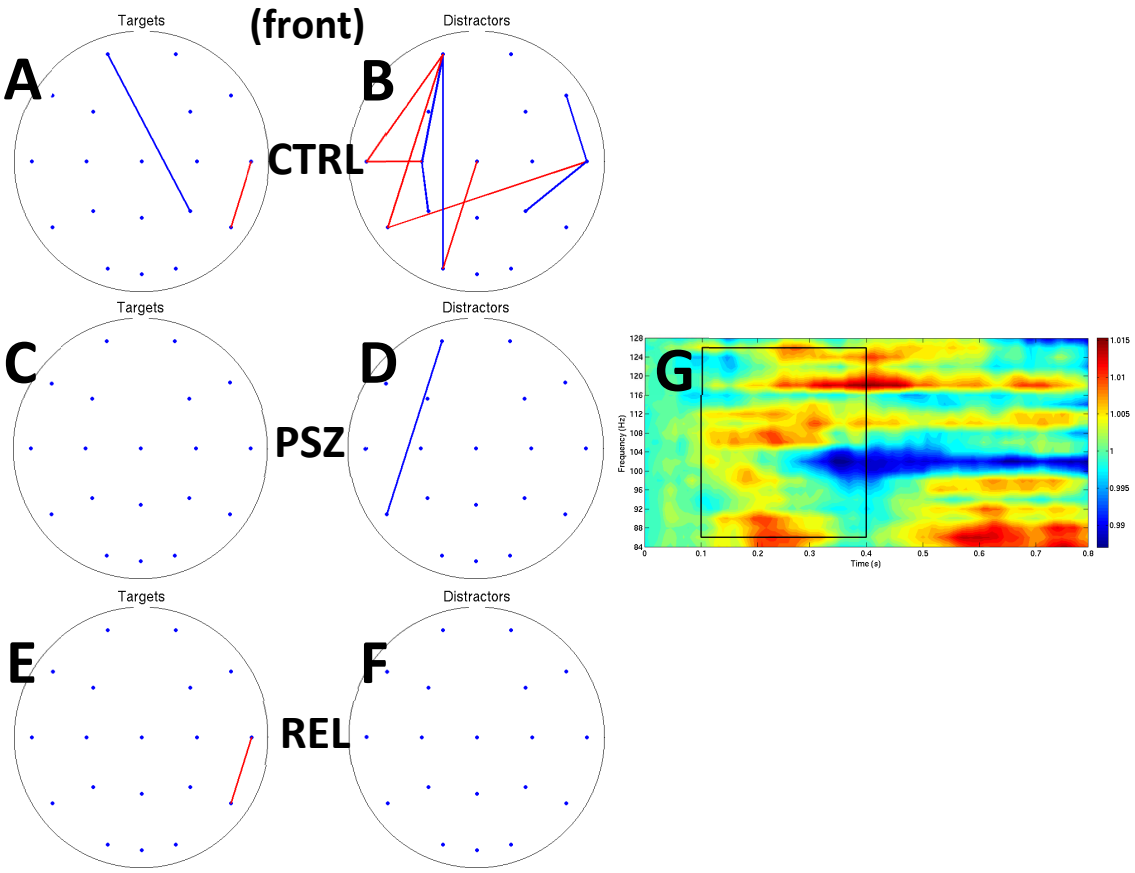

Figure 30. Gamma band (86-126hz) IPSC. Electrode pairs showing gamma-band (86-126hz, 100-400ms post-stimulus) intersite phase clustering (e.g., phase-locking) values with $p < .10$ for a) target and b) distractor stimuli in CTRL. Those pairs that demonstrated synchrony for CTRL were also examined in PSZ and REL, and electrodes pairs within this subset demonstrating synchrony are shown for PSZ in c) and d) and for REL in e) and f) (target and distractor stimuli, respectively). The time-frequency window of interest is depicted in g). For the subset of the CTRL electrode pairs examined, PSZ showed synchrony changes for a single pair of electrodes in response to distractor stimuli, while REL showed synchrony changes for a single pair in response to targets. Red lines represent synchrony increases as compared to baseline; blue lines represent synchrony decreases.

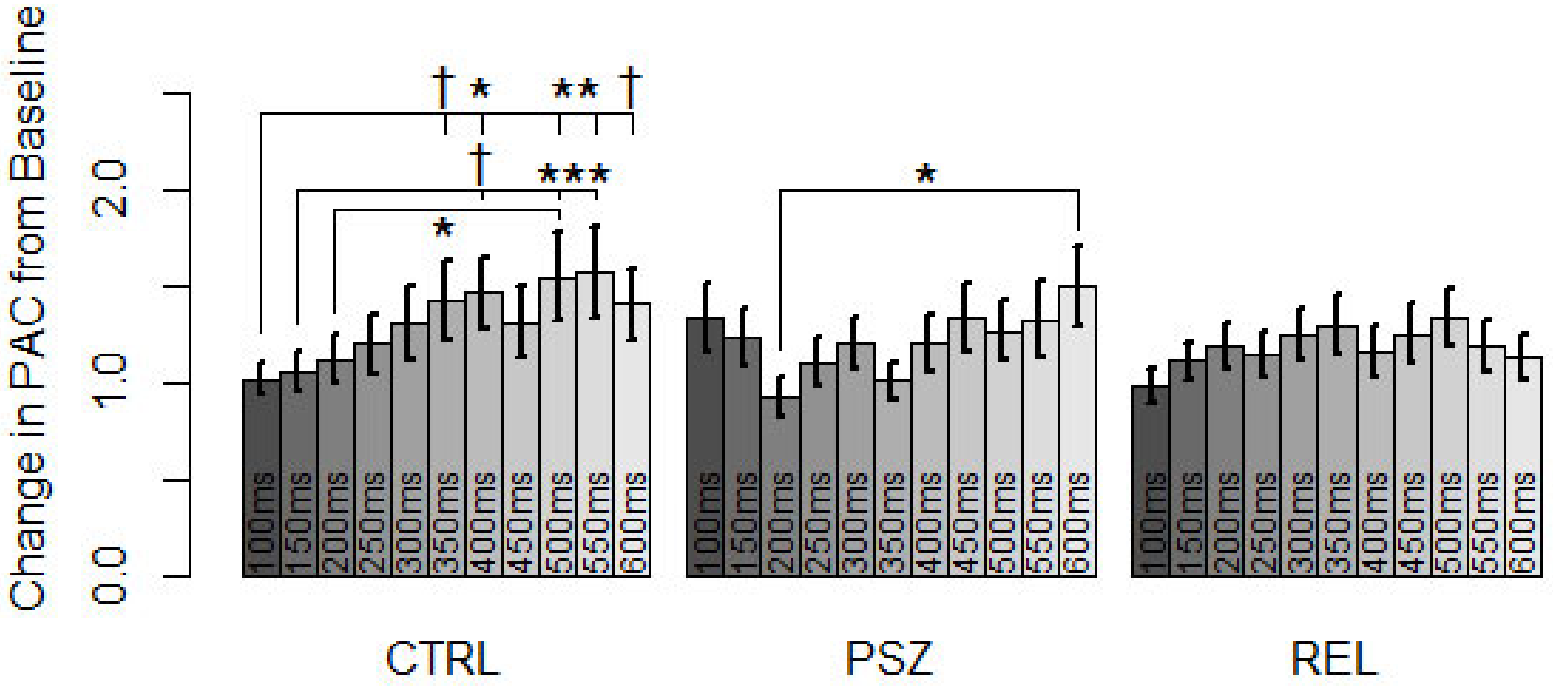

Figure 31. PAC – 7hz and 42.5hz – time by diagnostic grouping. PAC values between 7hz and 42.5hz at electrode O2 at different time samples for CTRL, PSZ and REL. CTRL showed the same general trend of increasing PAC values with time that was observed across all groups for other electrodes/frequency pairings. PSZ showed minimal increase in PAC with time, and EL showed no effect of time on PAC values whatsoever. †$p < .10$, *$p < .05$, **$p < .01$, ***$p < .001$.

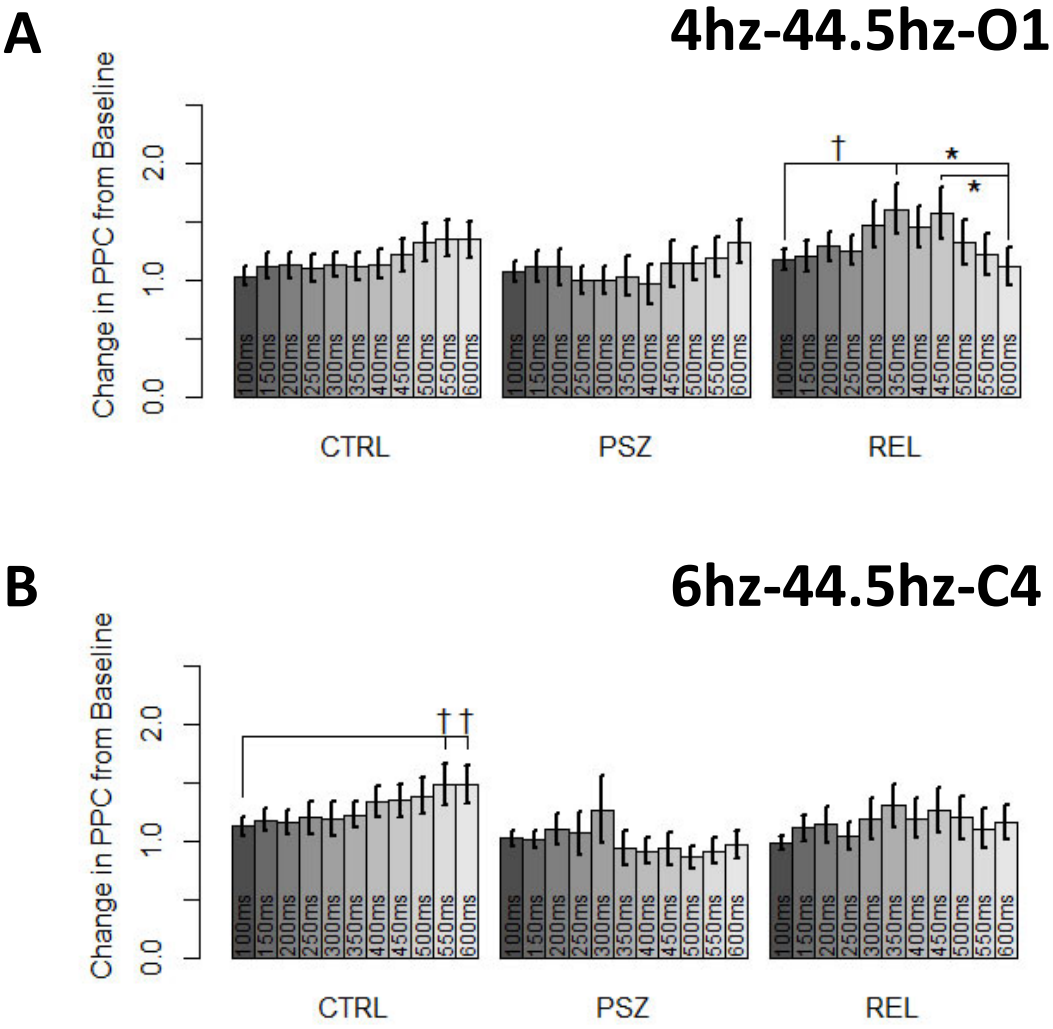

Figure 32.PPC – 4hz to 44.5hz and 6hz to 44.5hz. Interaction effects between diagnostic grouping and time sample on PPC between a) 4hz and 44.5hz at electrode O1, and b) 6hz and 44.5hz at electrode C4 for CTRL, PSZ and REL. REL alone showed an effect of time on PPC between 4hz and 44.5hz at O1, with peak values occurring mid-epoch. For PPC between 6hz and 44.5hz at C4, CTRL alone showed a slight effect of time, with later values being slightly greater than PPC at the earliest time point.
†$p < .10$, *$p < .05$, **$p < .01$, ***$p < .001$.

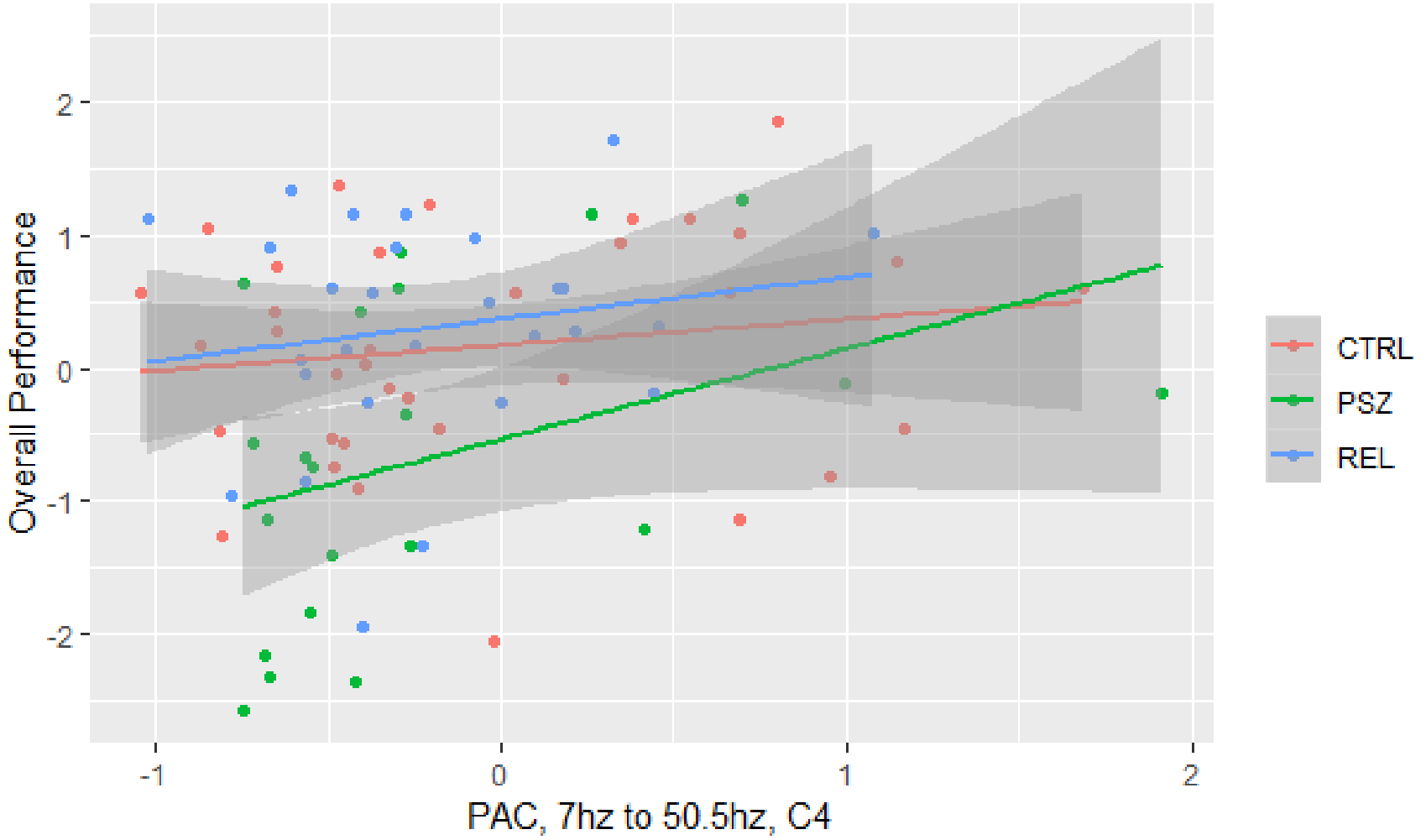

Figure 33. PAC predicts task performance in PSZ. Relationship between overall WM task performance changes in mean PAC values between 7hz and 50.5hz at electrode C4 for CTRL, PSZ and REL. Change in PAC for this pairing and site were predictive for PSZ alone.

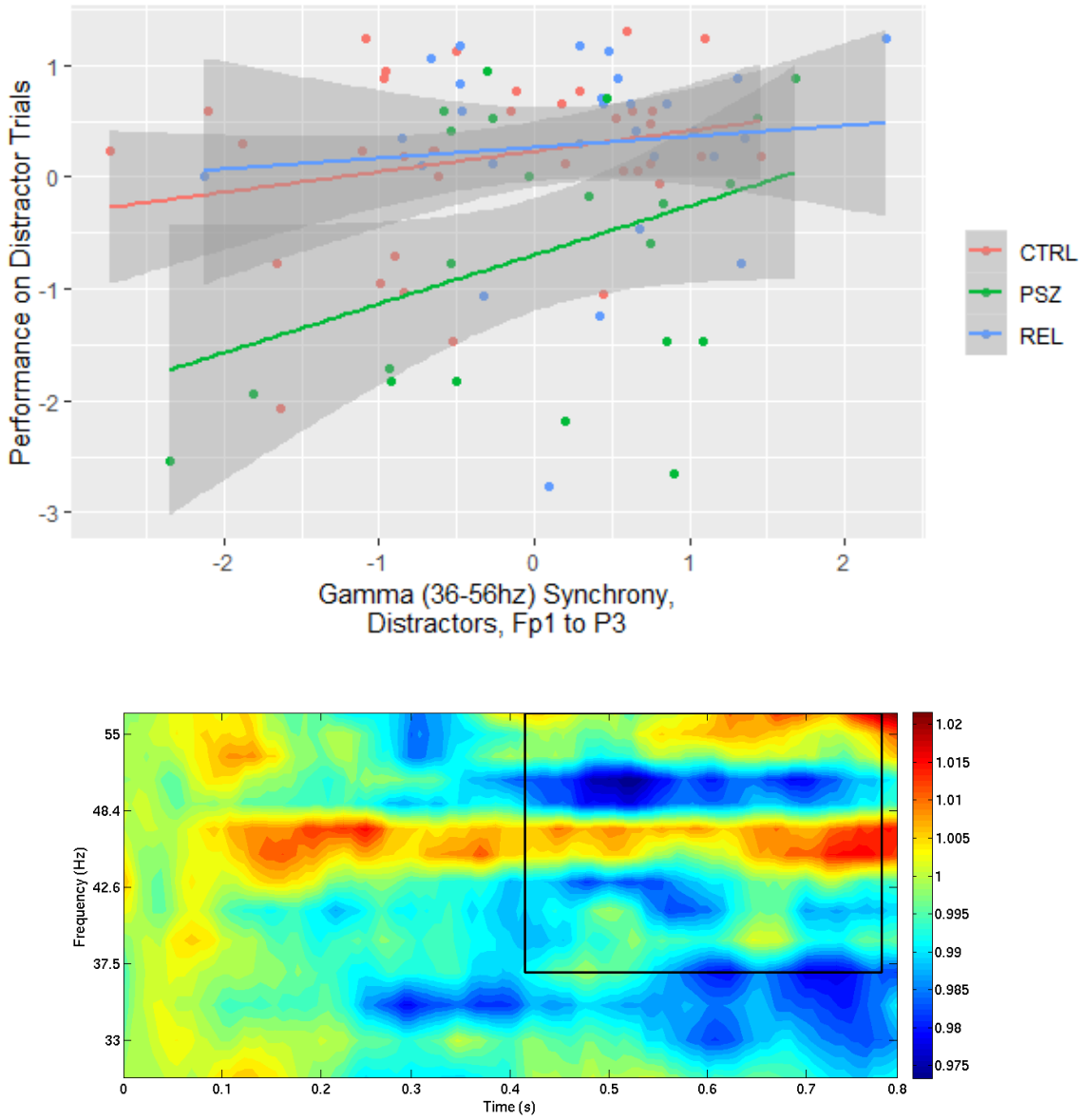

Figure 34. Gamma (36-56hz) IPSC predicts task performance in PSZ. Relationship between WM task performance on distractor trials and changes in gamma (36-56hz) phase synchrony in response to distractors between electrodes Fp1 and P3 for CTRL, PSZ and REL. Change in synchrony for this time-frequency window and electrode pair was predictive for PSZ alone and is depicted in the bottom panel.